Development of Dielectric Resonator Antenna (DRA)

K. W. Leung
State Key Laboratory of Millimeter Waves &
Department of Electronic Engineering,
City University of Hong Kong

Presented to the IEEE LI Section Antenna and Propagation Society on Monday October 8th 2012

Outline

I. Introduction

II. Circularly Polarized DRA Using a Parasitic Strip

III. Frequency Tuning Technique

IV. Omnidirectional Circularly Polarized DRAs

V. Dualband & Wideband DRAs

VI. Dualfunction DRAs

What is Dielectric Resonator Antenna (DRA) ?

- The DRA is an antenna that makes use of a radiating mode of a dielectric resonator (DR).

- It is a 3-dimensional device of any shape,
  e.g., hemispherical, cylindrical, rectangular, triangular, etc.

- Resonance frequency determined by the its dimensions and dielectric constant ε_r.

Some DRAs :

Advantages of the DRA

- Low cost
- Low loss (no conductor loss)
- Small size and light weight
- Reasonable bandwidth (~10% for ε_r ~10)
- Easy of excitation
- High radiation efficiency (generally > 95%)

Excitation schemes

(i) Microstrip line feed

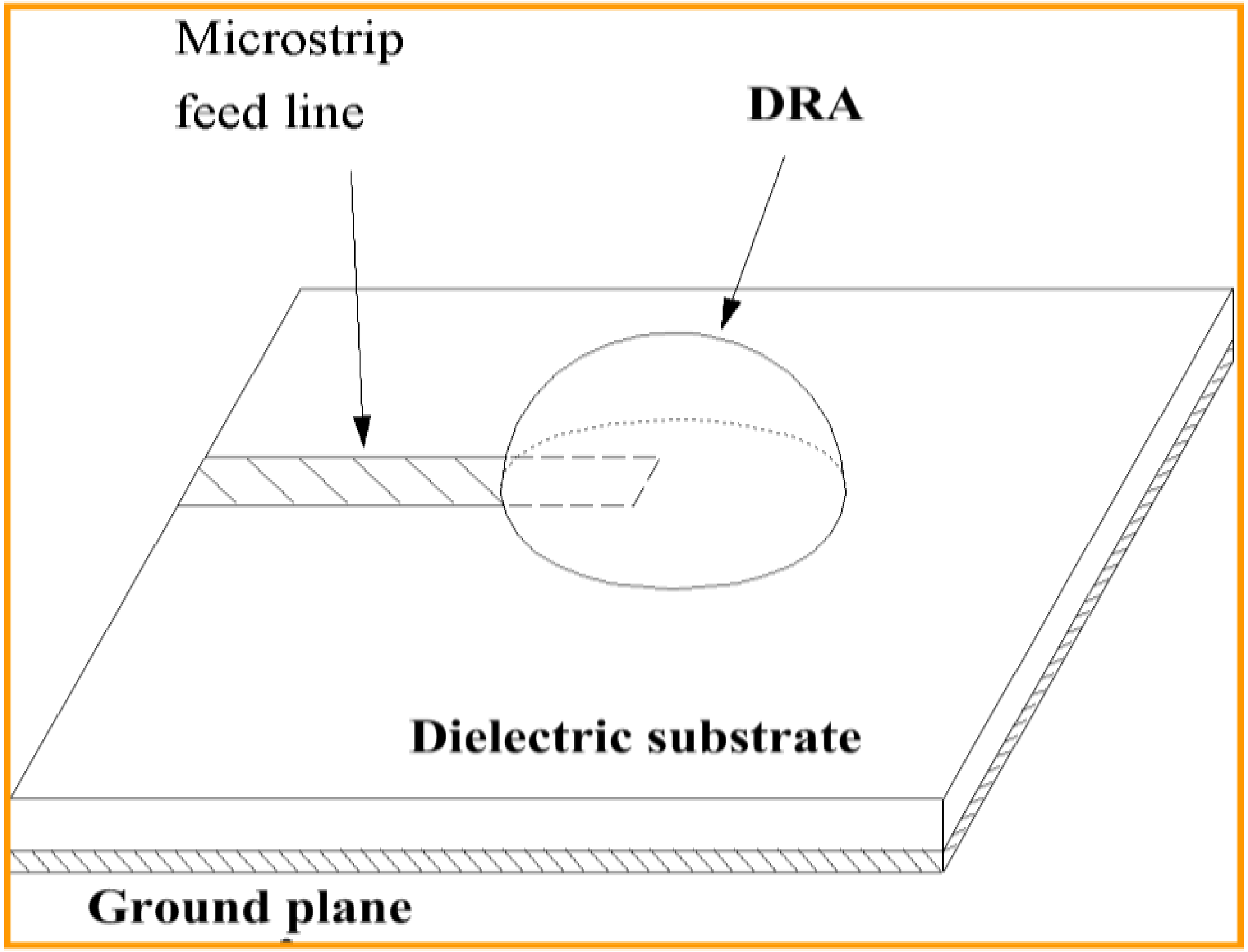

Excitation schemes

(ii) Aperture-couple feed

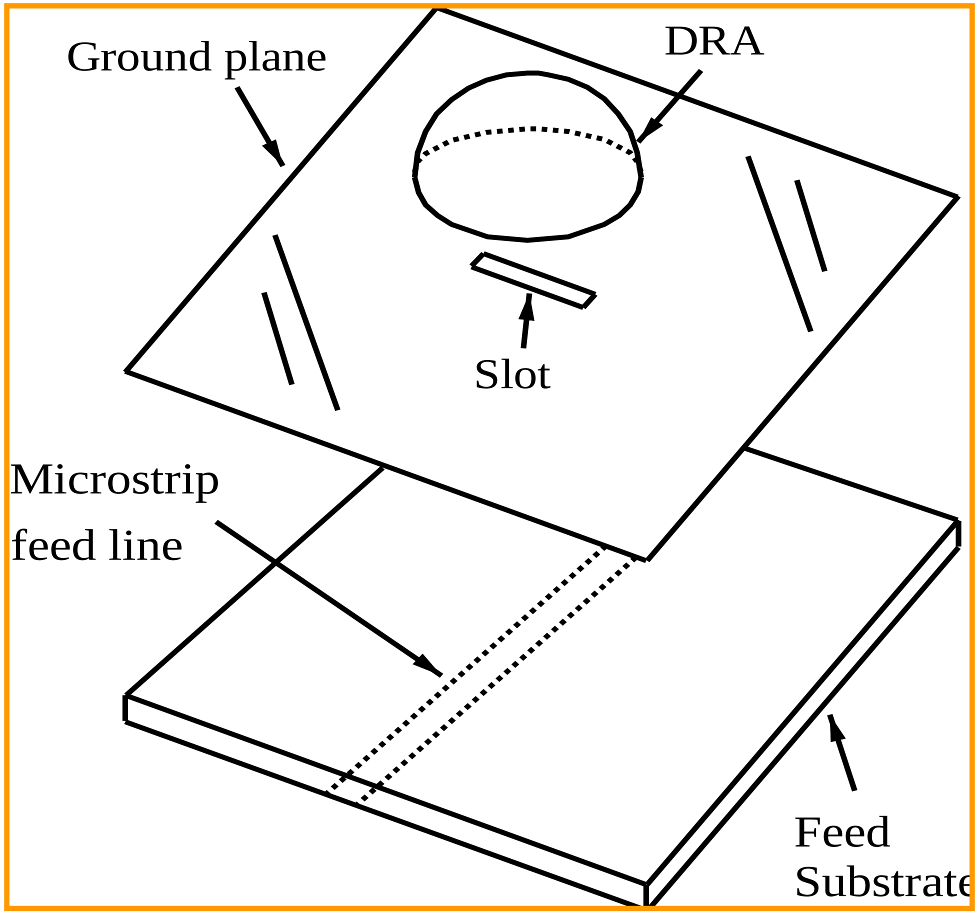

Excitation schemes

(iii) Coaxial feed

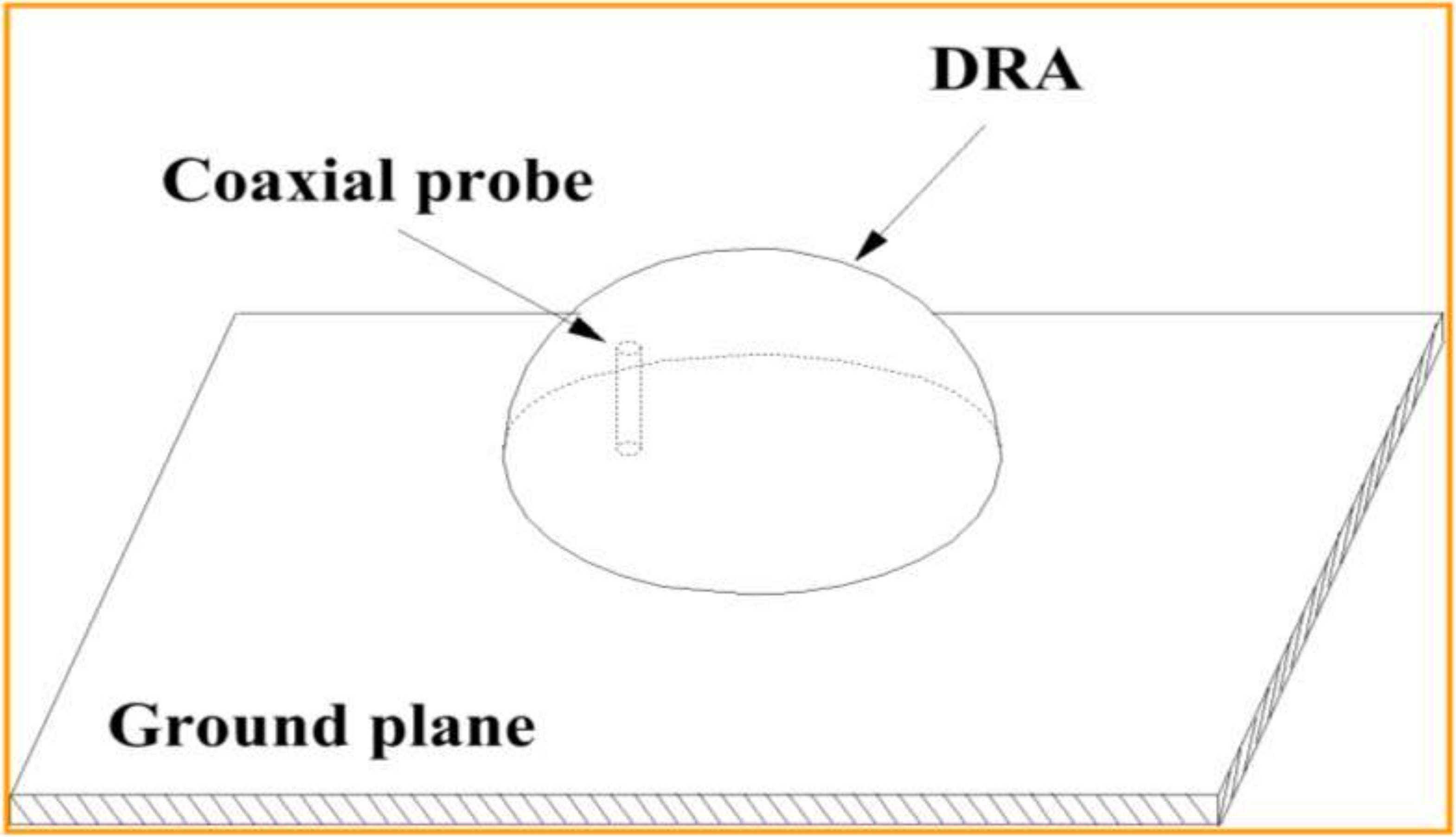

Coaxial feed

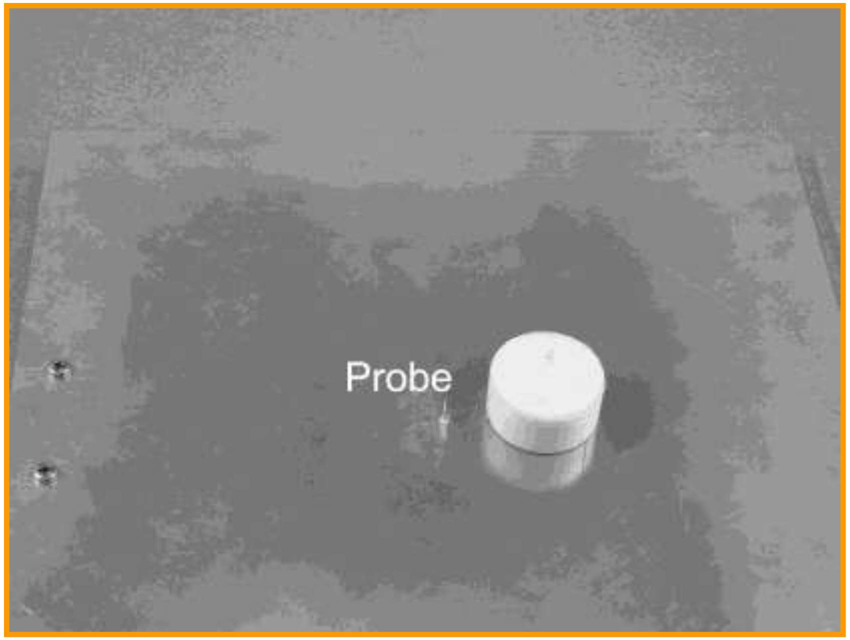

Top view

Bottom view

Aperture-coupled feed

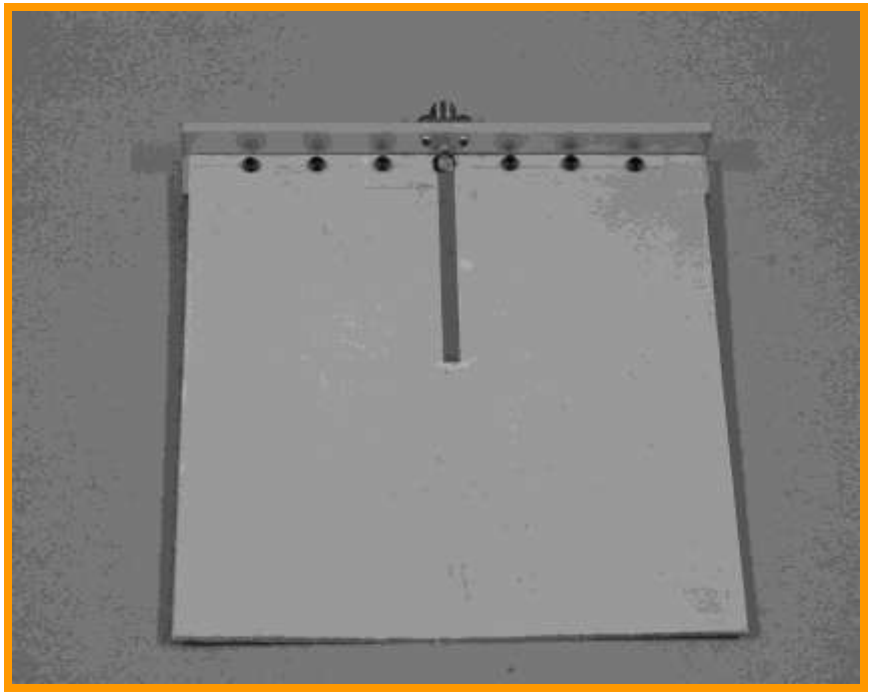

Bottom view

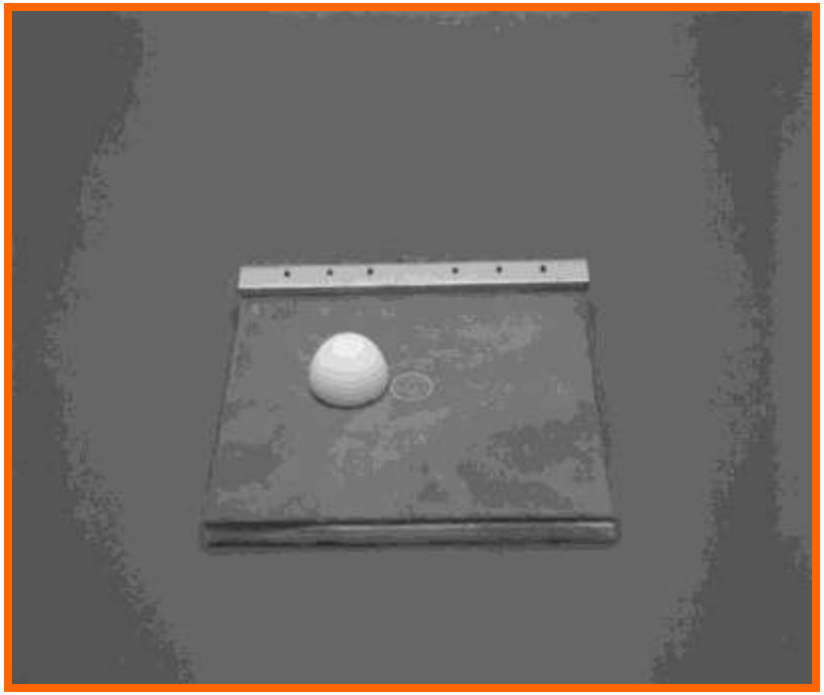

Top view

Corporate feedline for DRA array

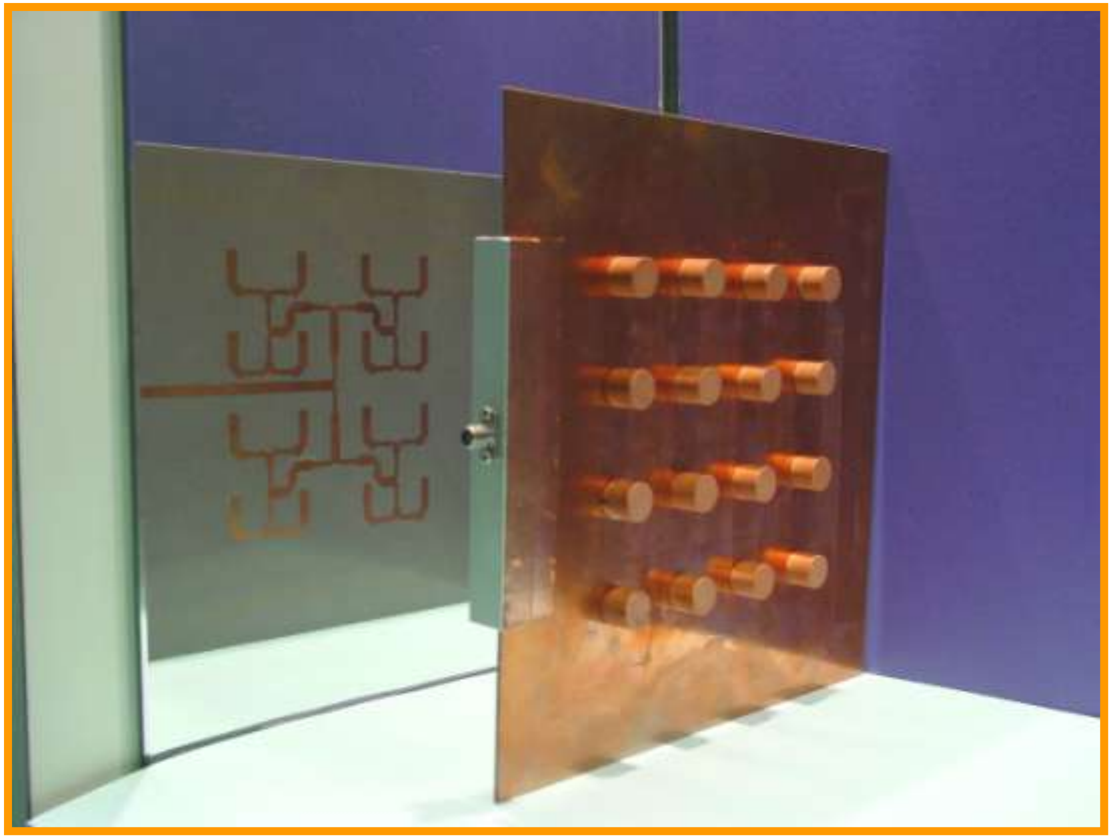

Slot-fed DRA array using corporate microstrip feed network

Conformal-Strip Method

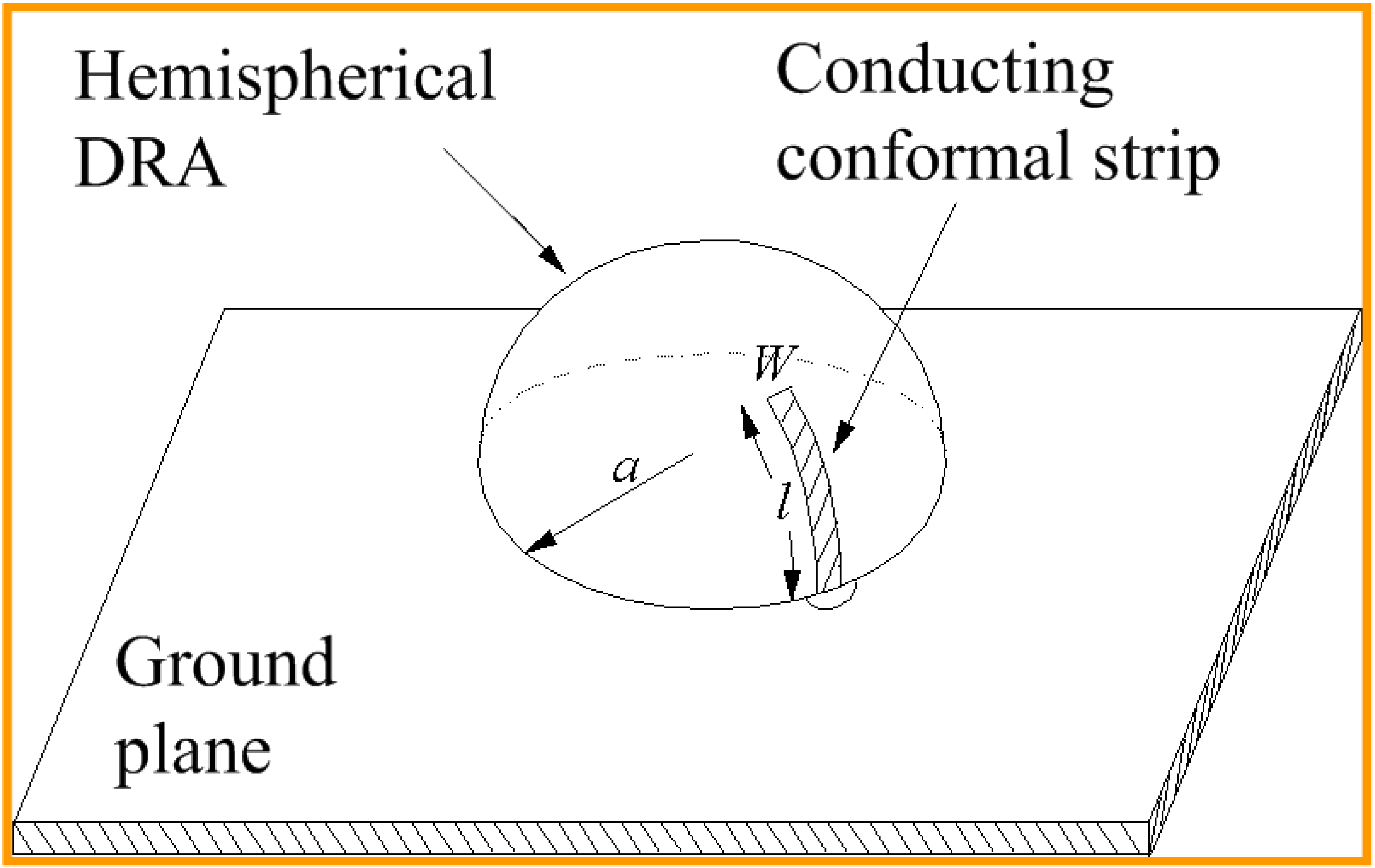

Rectangular Dielectric Resonator Antennas

Proposed Antenna Geometry

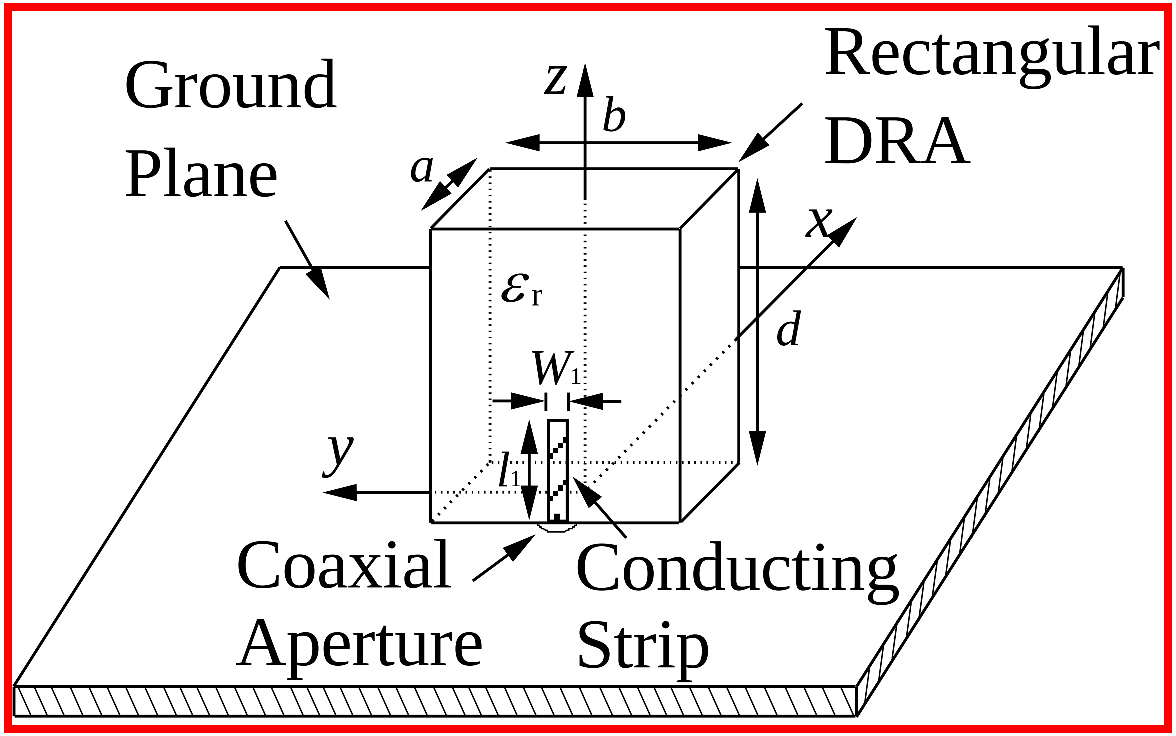

a (mm)	b (mm)	d (mm)	l_1 (mm)	W_1 (mm)	ε_r
14.3	25.4	26.1	10	1	9.8

Analytical Solution

- Dielectric Waveguide Model (DWM)

Resonant frequency of $TE_{mnl}(y)$ mode

$$f_0 = \frac{c}{2\pi\sqrt{\varepsilon_r}}\sqrt{k_x^2 + k_y^2 + k_z^2}$$

$$k_x = \frac{m\pi}{a}, k_y = \frac{n\pi}{b}, k_z = \frac{l\pi}{2d}$$

$$k_x^2 + k_y^2 + k_z^2 = \varepsilon_r k_0^2$$

Numerical Solution

- Finite-Difference Time-Domain (FDTD) method

Advantages

- Very simple
- High modeling capability for general EM structures
- No spurious modes nor large matrix manipulation
- Provide a very wideband frequency response

Disadvantages

- Time consuming, powerful computer required

Source model and extraction of S parameters

Baseband Gaussian pulse

$$E_z = \exp[-(\Delta t \cdot n - 3T)^2 / T^2]$$ T : pulse width

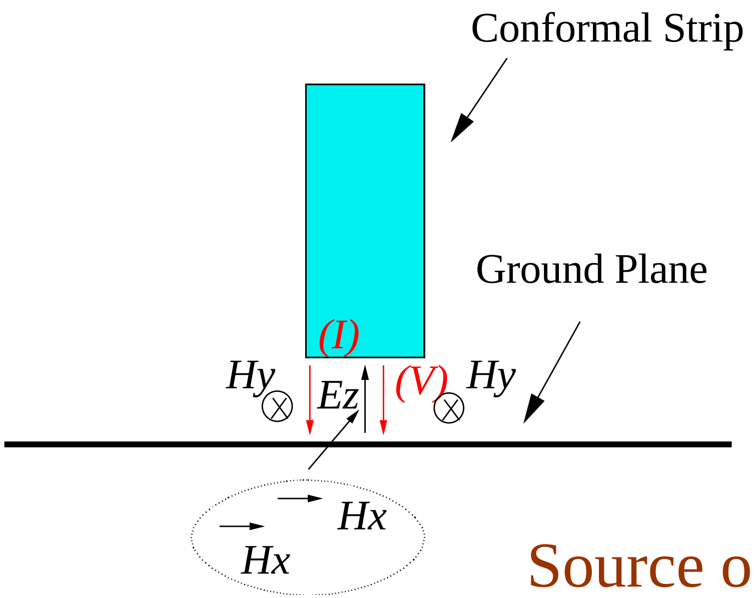

$$Z_{in} = \frac{FFT[V(t)]}{FFT[I(t)]}$$

$$S_{11} = \frac{Z_{in} - Z_0}{Z_{in} + Z_0}$$

Source occupies only one grid

Parameters

Uniform Cartesian grids

$\Delta x = 0.715$ mm, $\Delta y = 0.508$ mm, $\Delta z = 0.5$ mm

T = 0.083ns, $t_0 = 3T$

10-cell-thick PML with polynomial spatial scaling
($m = 4$ and $\kappa_{max} = 1$)

total grid size : $80\Delta x \quad 110\Delta y \quad 112\Delta z$

total time steps : 10000

Input Impedance/S_{11}

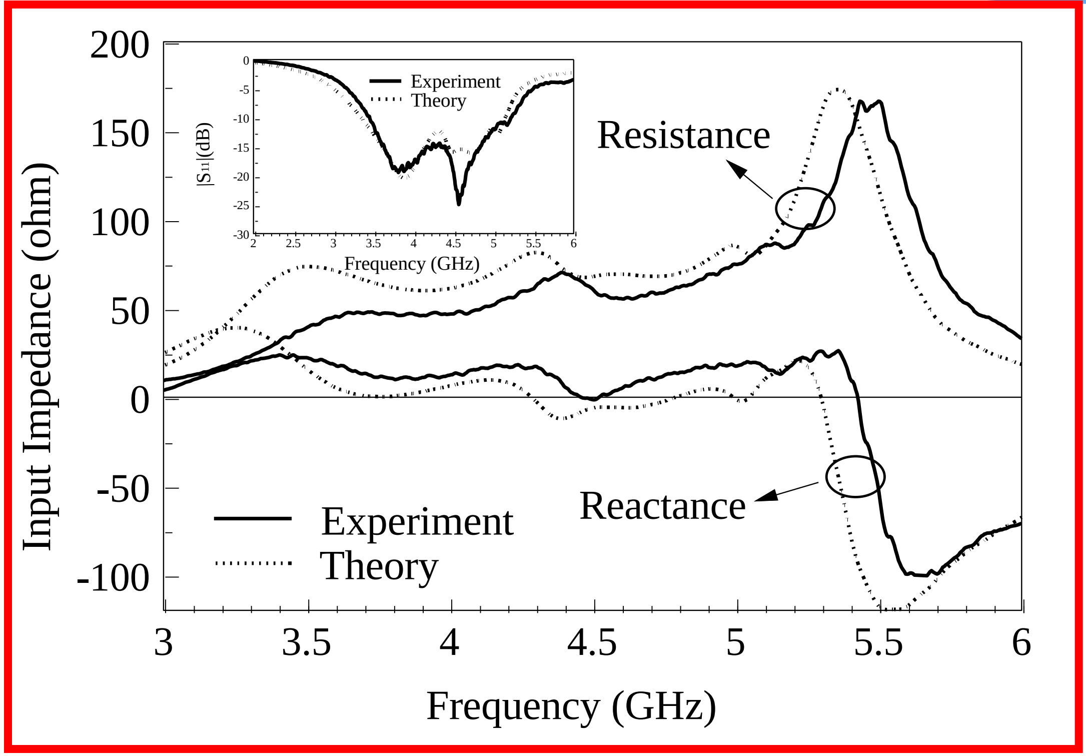

- Reasonable agreement.
- Wide Bandwidth of ~ 43%.
- Dual resonant $\mathbf{TE_{111}}^{y}$ and $\mathbf{TE_{113}}^{y}$ modes are excited.

Comparison between Theory and Measurement

Resonant Modes	Measured resonant frequencies	Calculated resonant frequencies (FDTD)		Predicted resonant frequencies (DWM)	
	f_{mea} (GHz)	f_{FDTD} (GHz)	error (%)	f_{DWM} (GHz)	error (%)
TE^{y}_{111}	3.81	3.90	2.3	3.95	3.6
TE^{y}_{112}	N/A	N/A	N/A	4.26	N/A
TE^{y}_{113}	4.57	4.60	0.7	4.7	1.7

- Reasonable agreement.

Field Distribution --- TE_{111}^{y}

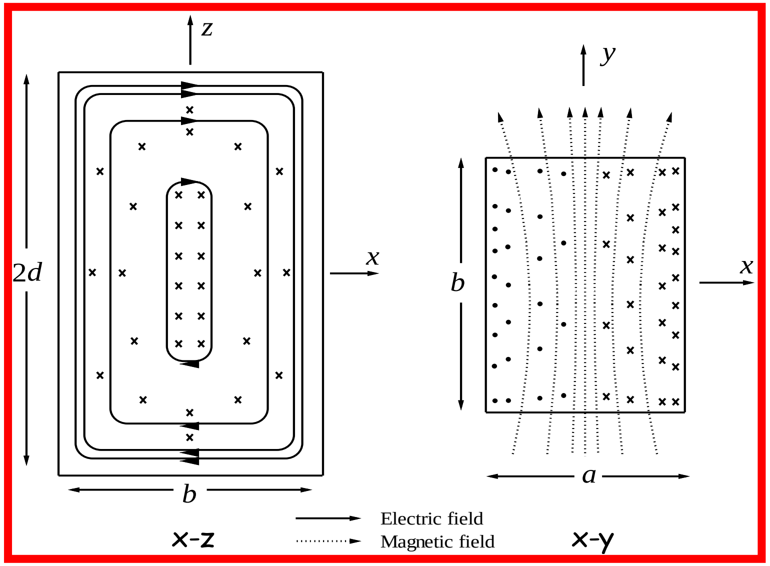

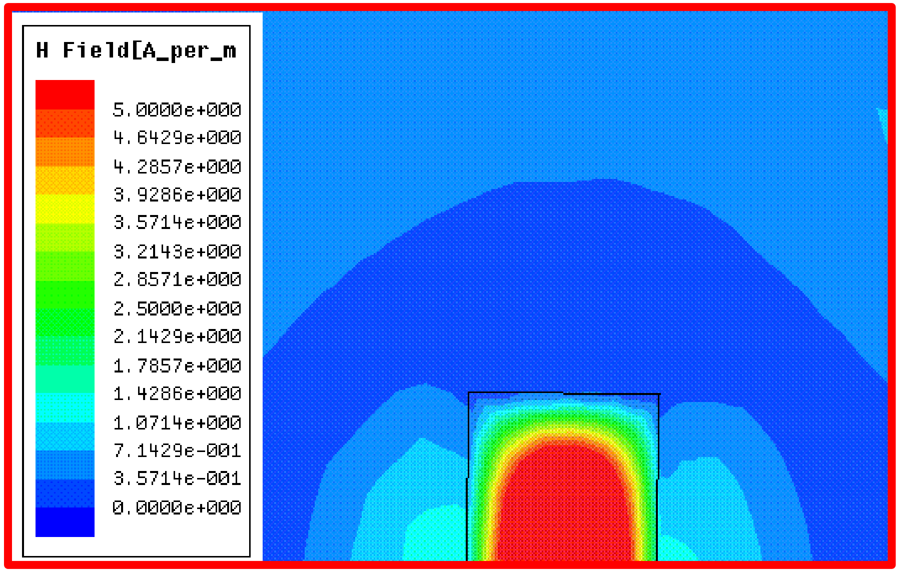

Imaged DRA (gound plane removed)

With gound plane

Field Distribution --- TE_{112}^{y}

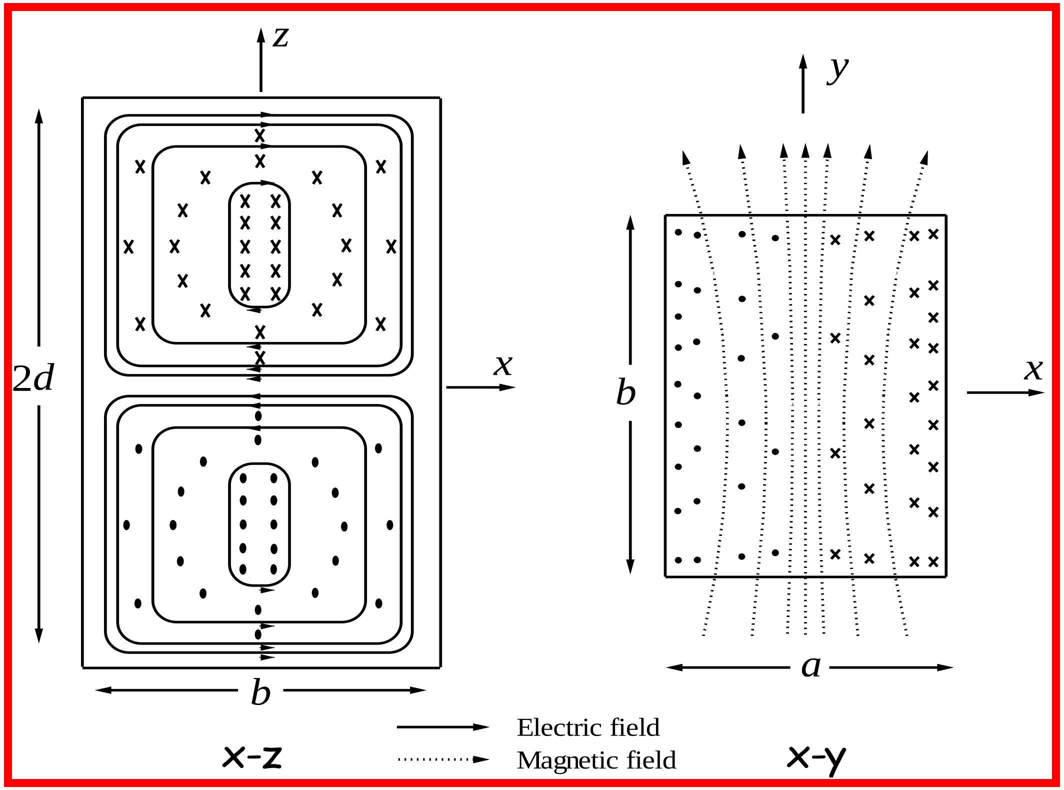

Imaged DRA (gound plane removed)

Field Distribution --- TE_{113}^{y}

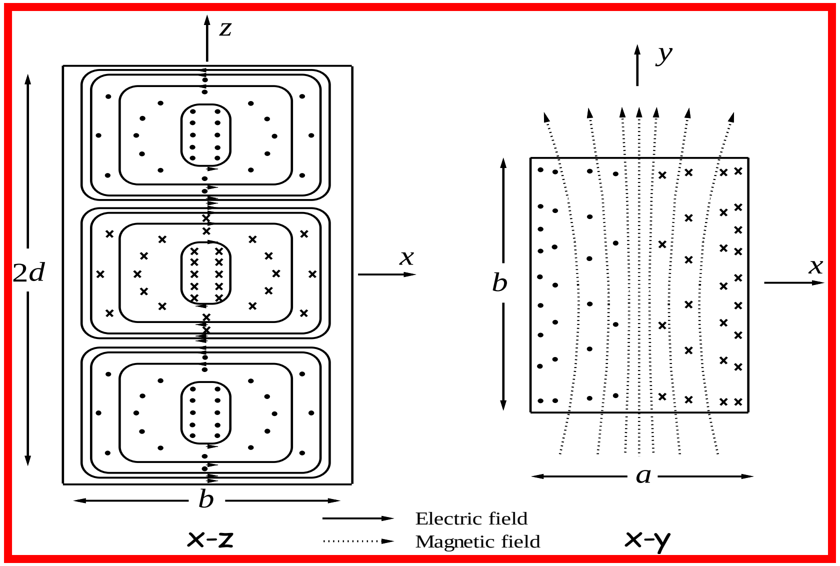

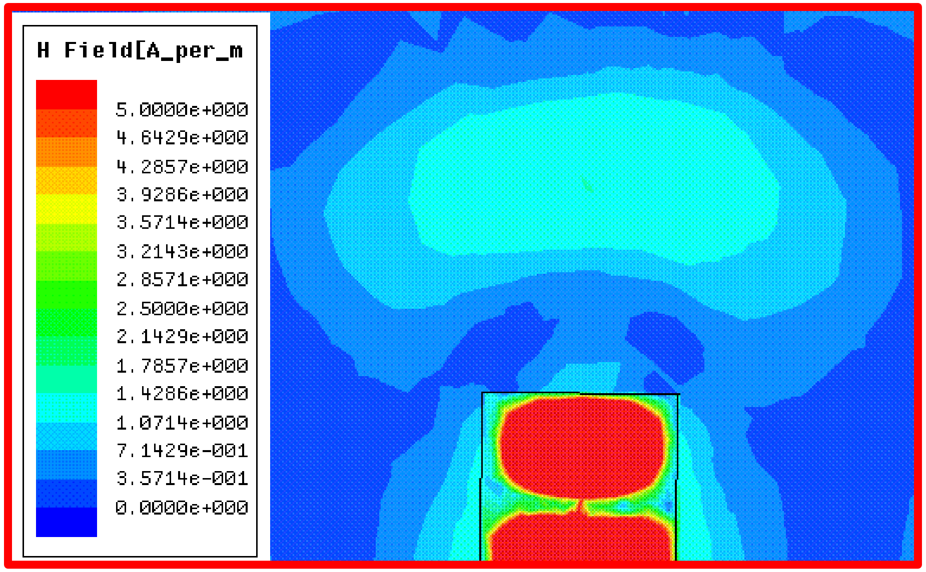

Imaged DRA (gound plane removed)

With gound plane

Radiation Patterns

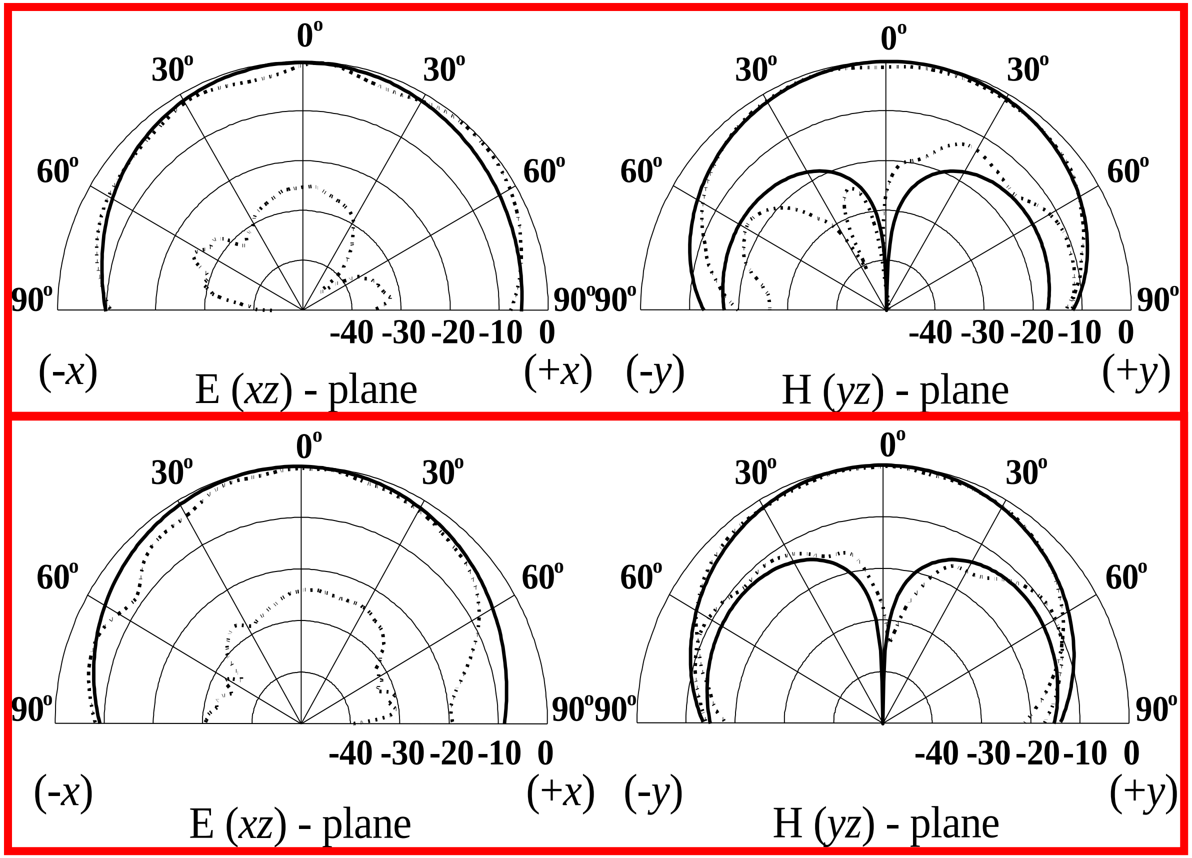

f = 3.5 GHz

f = 4.3 GHz

- Broadside radiation patterns are observed.
- Measured E-plane crosspolarized fields mainly caused by finite ground plane diffraction.

III. Circularly Polarized Design using a Parasitic Strip

Proposed Antenna Geometry

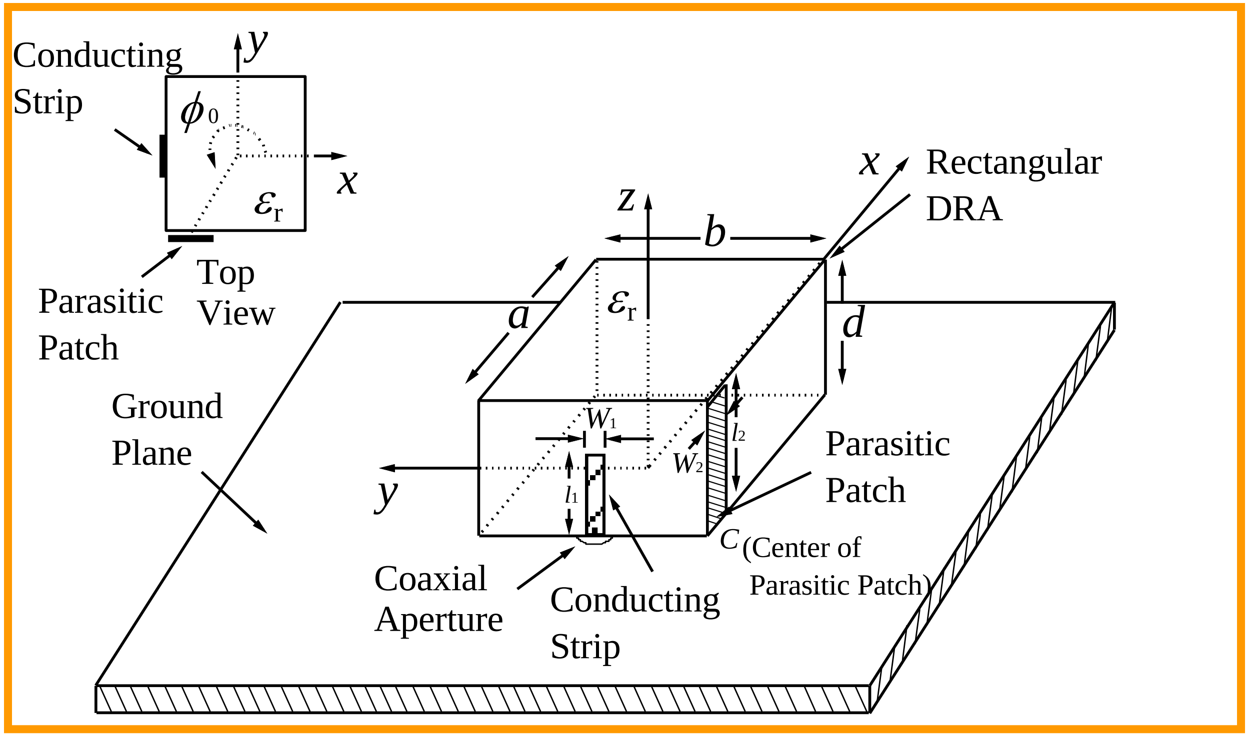

a (mm)	b (mm)	d (mm)	l_1 (mm)	W_1 (mm)	l_2 (mm)	W_2 (mm)	ϕ_0 (degree)	ε_r
24	23.5	12.34	10	1	12	1	225.6	9.5

Input Impedance/S_{11}

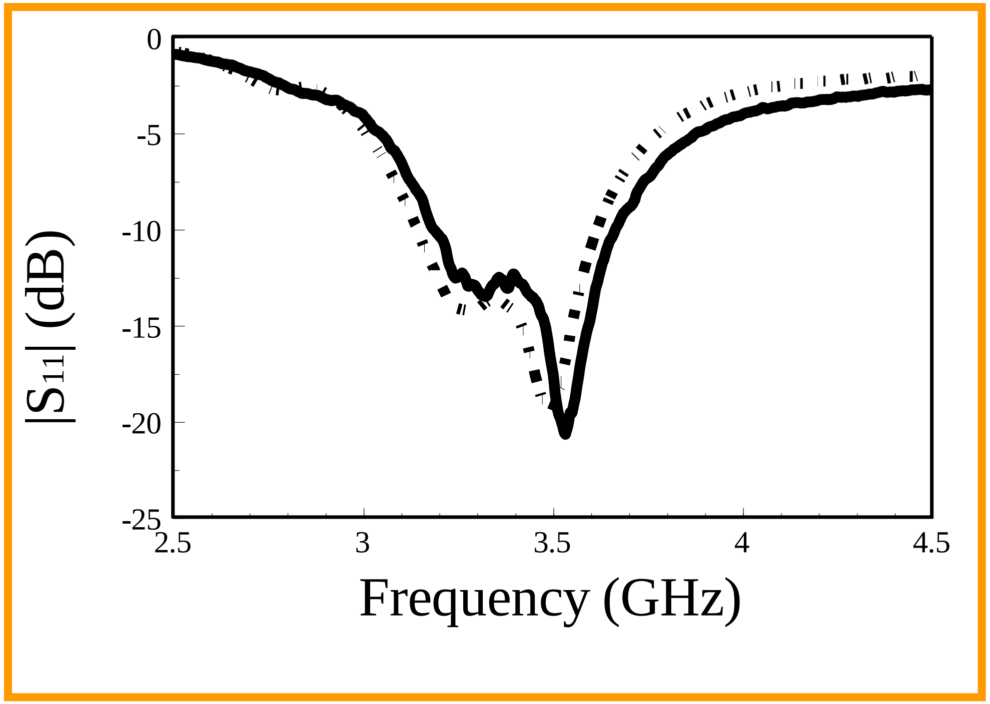

- Reasonable agreement.
- Bandwidth ~ 14%.
- Two nearly-degenerate TE_{111}(y) modes are excited.
  ⇒ CP operation

Axial Ratio in the boresight direction

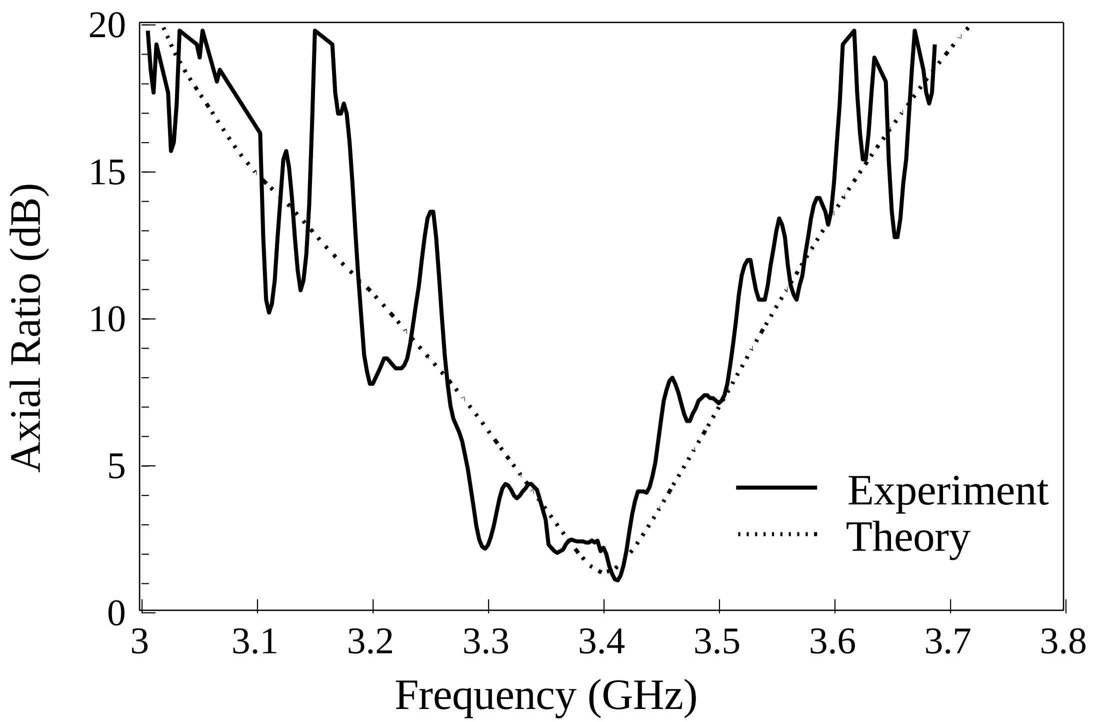

3-dB AR bandwidth is ~ 2.7%, which is a typical value for a singly-fed CP DRA.

The H field of the DRA without and with parasitic strip (Top view)

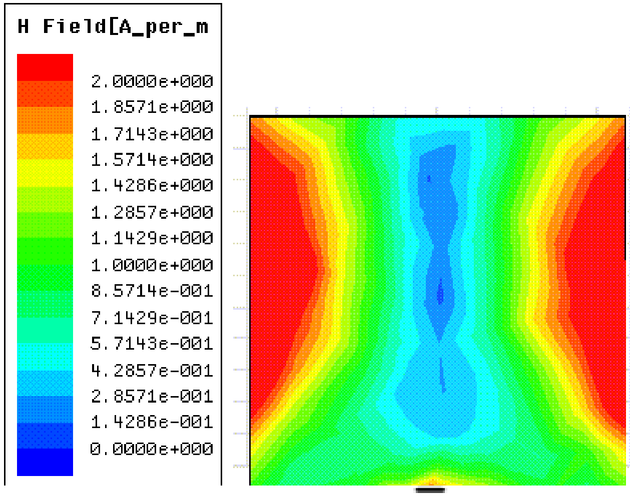

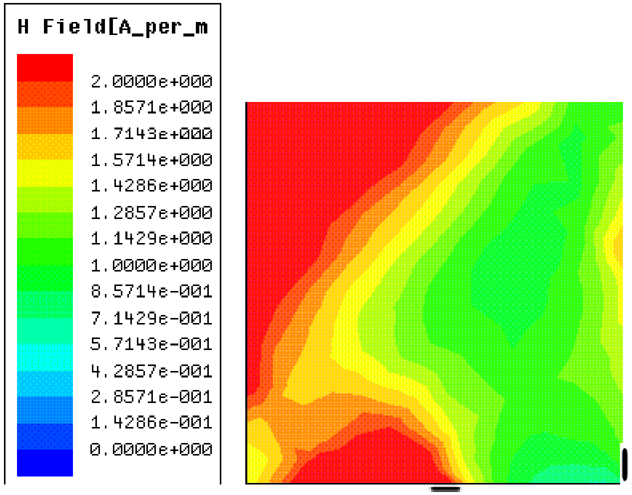

Without parasitic strip - LP field

With parasitic strip - CP field

3.4 GHz

3.4 GHz

Radiation Patterns (*f* = 3.4GHz,)

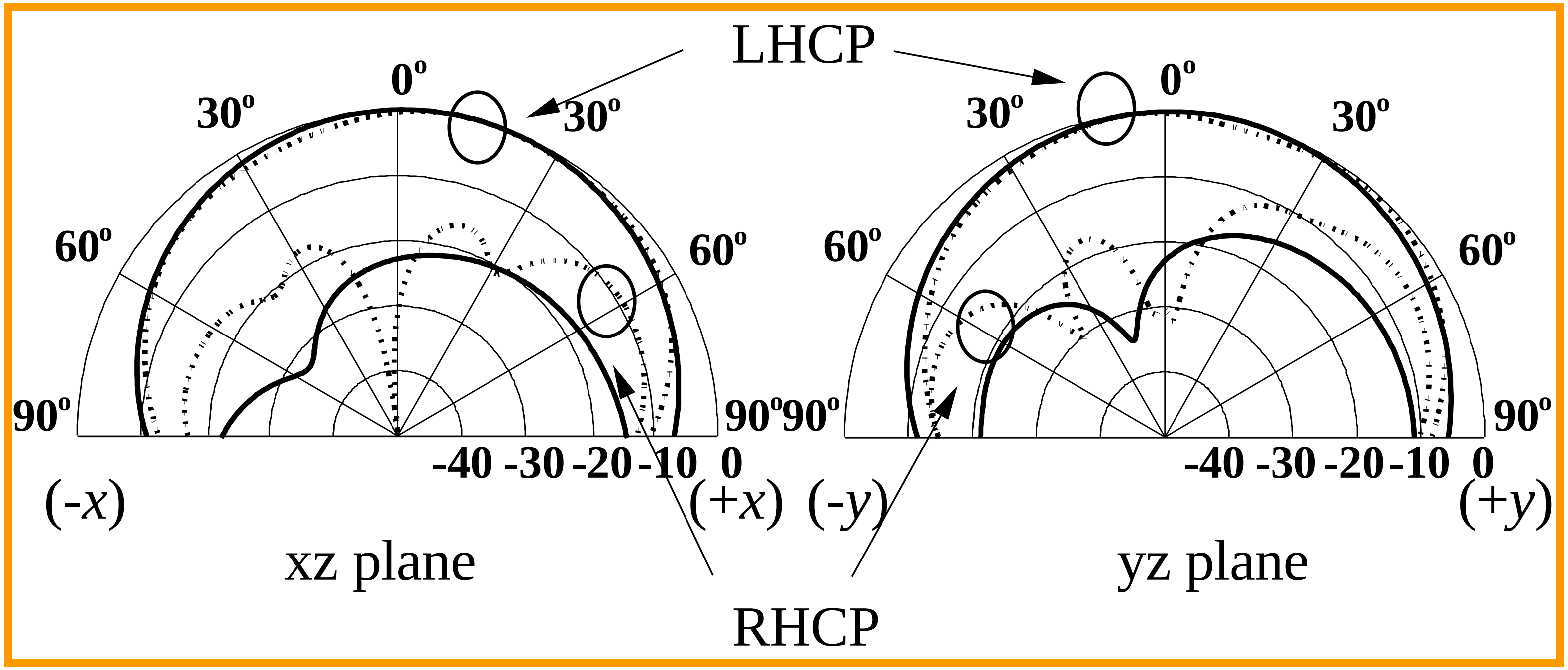

- A broadside radiation mode is observed.
- For each radiation plane, the LHCP field is more than 20dB stronger than the RHCP field.
- The maximum gain is 5.7 dBic (not shown here).

Effects of feeding strip length l_1

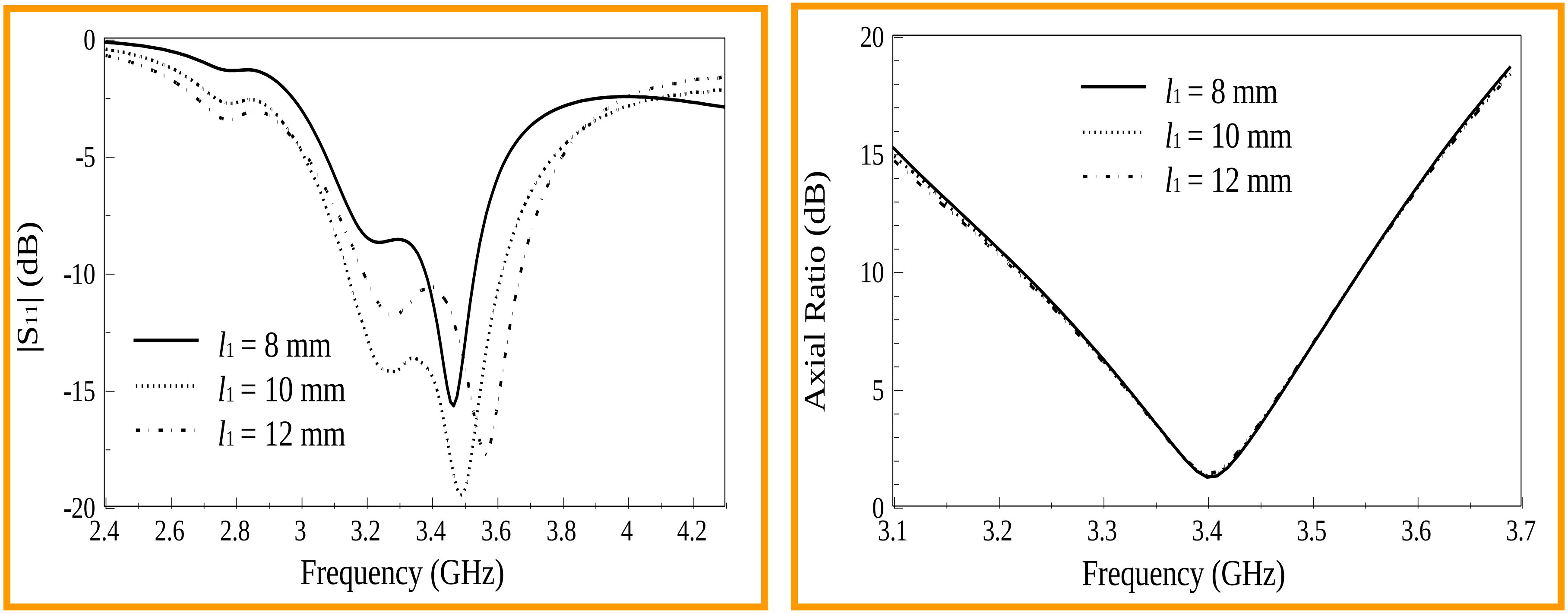

- Input impedance changes substantially with l_1.
- AR is almost unchanged for different l_1.
- l_1 can be adjusted to match the impedance without changing AR.

II. Frequency Tuning Technique

Backgruond

- The DRA for a paticular frequency may not be available from the comericial market.

- Fabrication tolerances cause errors between measured and calculated resonant frequencies.

- Frequency tuning methods:
  (i) loading-disk; and
  (ii) parasitic slot.

Frequency Tuning Technique
- using a loading disk

The slot-coupled DRA with a conducting loading cap

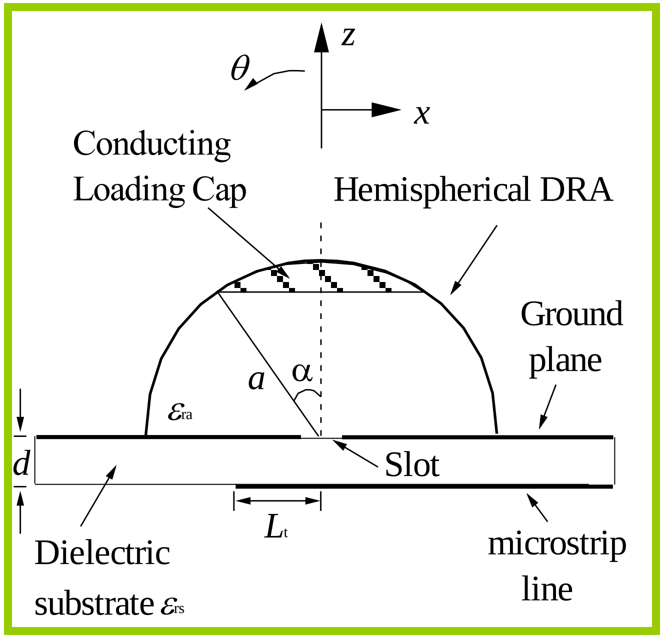

Side view

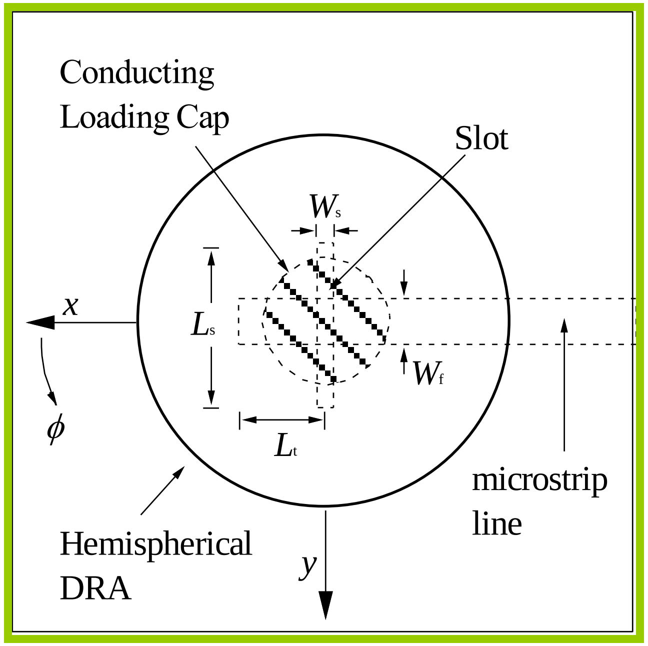

Top view

- **Hemispherical DRA: radius a = 12.5 mm, dielectric constant ε_r = 9.5.**
- **Coupling slot : length L_s , width W_s**
- **Open-circuit stub: length L_t**
- **Grounded dielectric slab: ε_{rs} = 2.33, height d = 1.57 mm**
- **Microstrip feedline: width W_f = 4.7 mm**

Calculated and measured return losses (L_s = 12 mm and W_s = 1 mm)

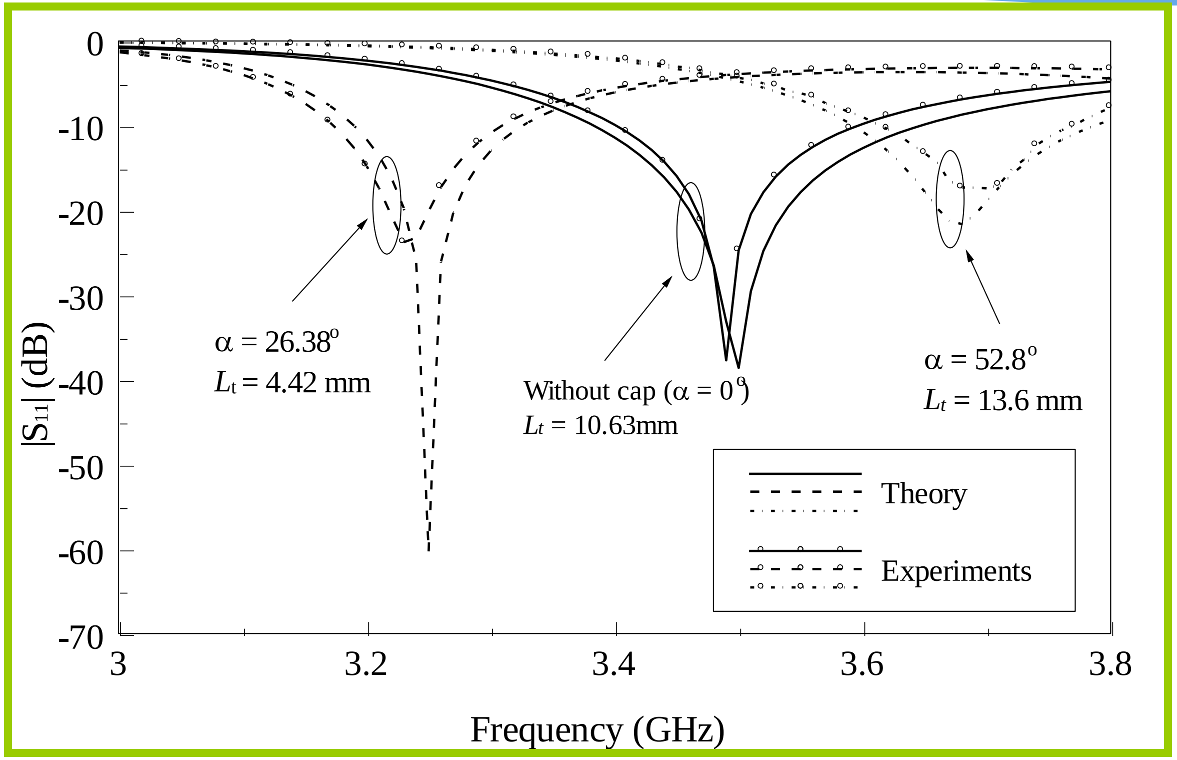

Resonance frequency:

- 3.52 GHz without any conducting cap ($\alpha = 0^0$), with L_t = 4.42 mm
- 3.25 GHz ($\alpha = 26.38^o$ and L_t = 4.42 mm)
- 3.68 GHz ($\alpha = 52.8^o$ and L_t = 13.6 mm)

Calculated and measured radiation patterns

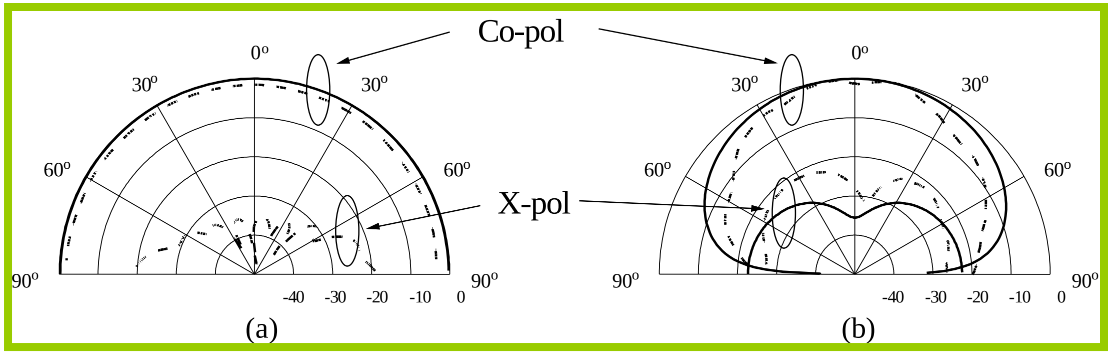

3.25 GHz (α = 26.38° and L_t = 4.42 mm)

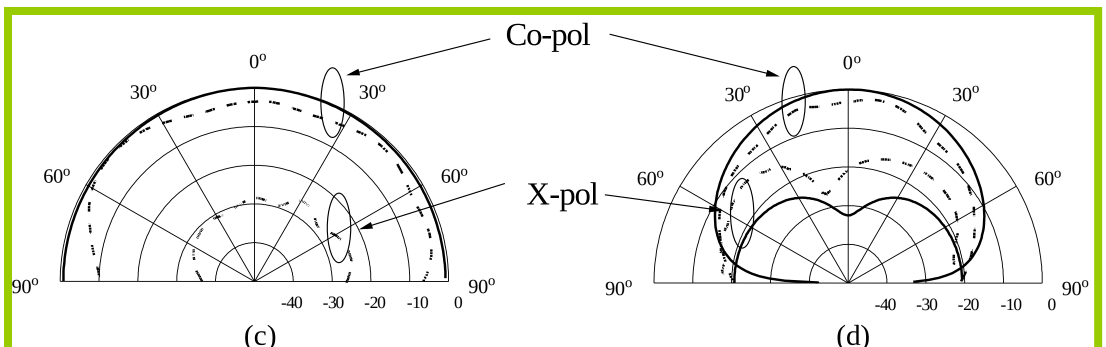

3.58 GHz (α = 52.8° and L_t = 13.6 mm)

- **Reasonable agreement between theory and experiment.**
- **The effect of loading cap on field pattern is not significant.**

Calculated α and L_t for having a good return loss (minimum $|S_{11}| < -20$dB)

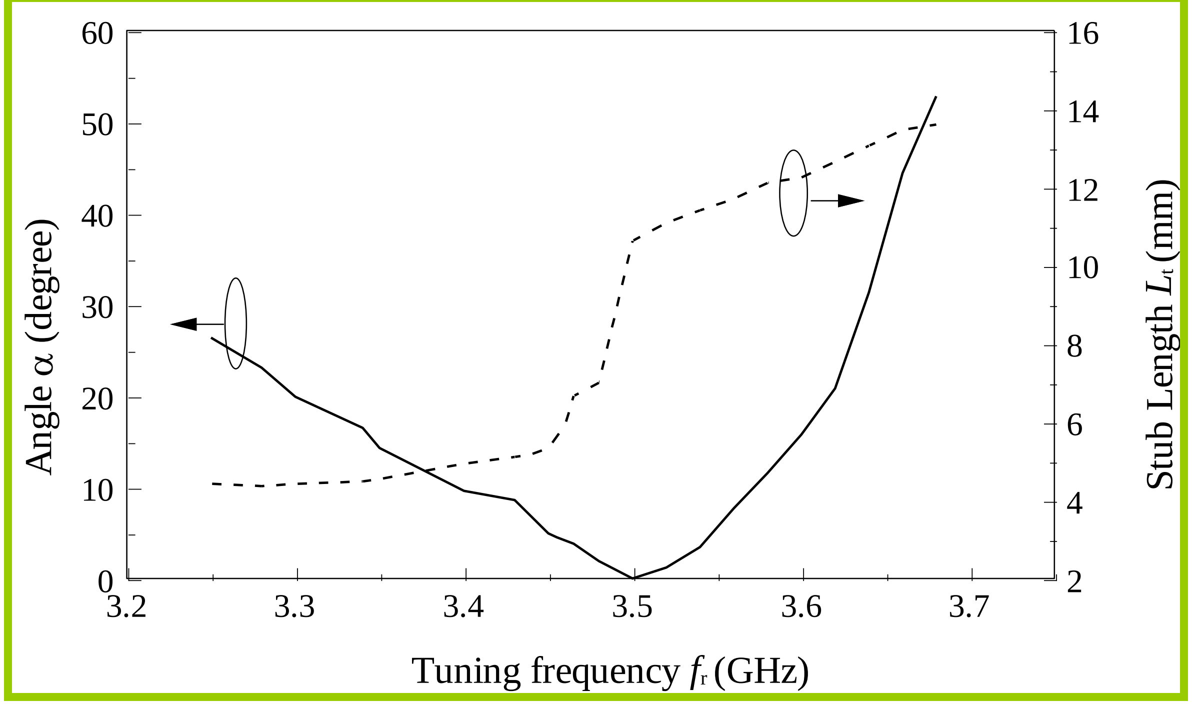

The resonant frequency can be tuned by varying α and L_t

- α decreases from 26.38° to 0° (3.25 < f_r < 3.5 GHz)
- α increases from 0° to 52.8° (3.5 < f_r < 3.78 GHz)

Impedance bandwidth

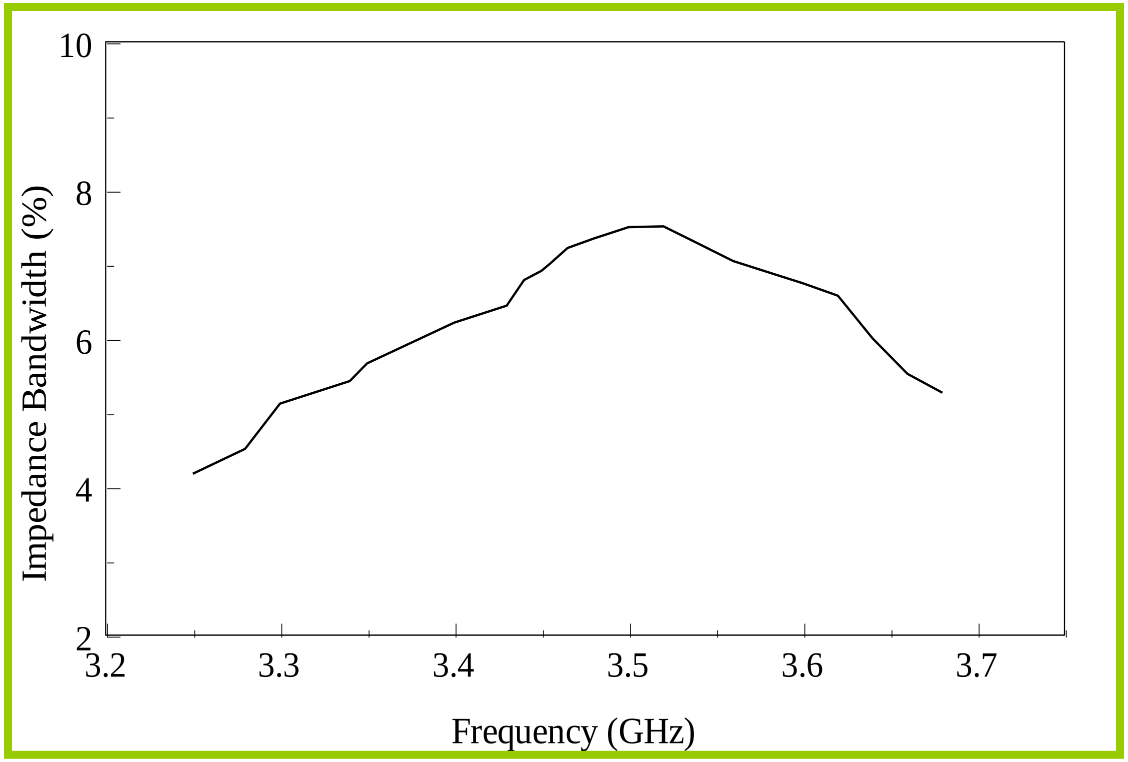

- The bandwidth decreases after a loading cap is added.

Frequency Tuning Technique
- using a parasitic slot

The annular-slot-excited cavity-backed DRA

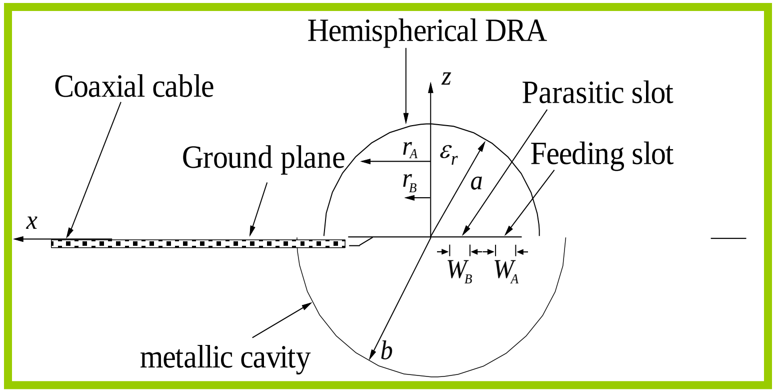

(a) Side view

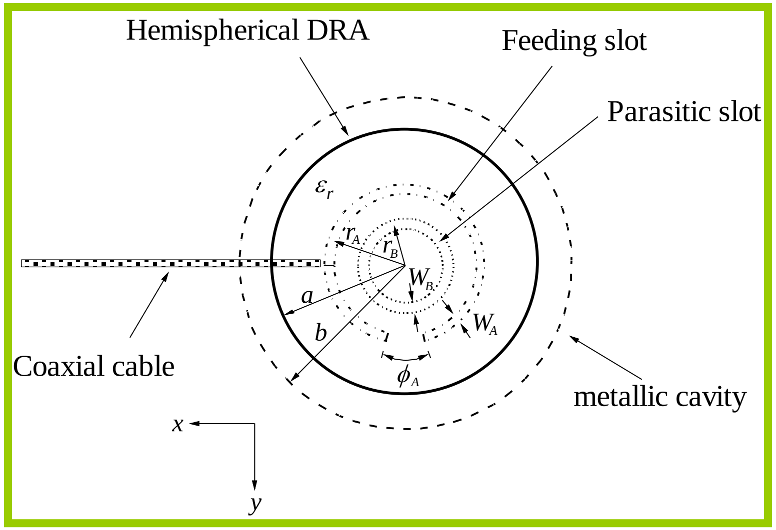

(b) Top view

IV. Omnidirectional Circularly Polarized DRA

Advantages of omnidirectional CP antenna

- Provide larger coverage.

CP DRAs concentrated on broadside-mode designs only.

Design I:

Slotted omnidirectional CP DRA

Antenna configurations

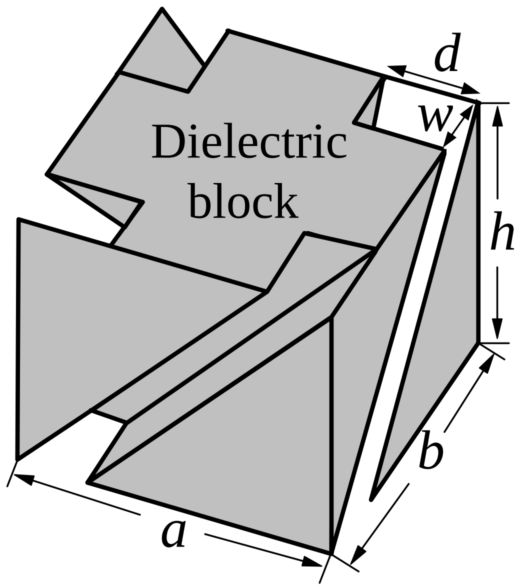

Perspective view

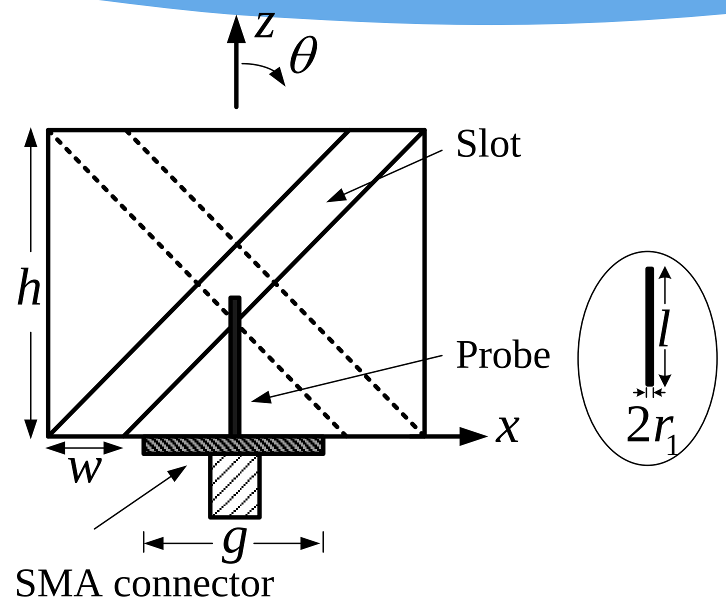

Front view

- Dielectric cube with oblique slots (polarizer) fabricated on its four sidewalls.
- Centrally fed by a coaxial probe extended from a SMA connector, whose flange used as the small ground plane.

Antenna principle

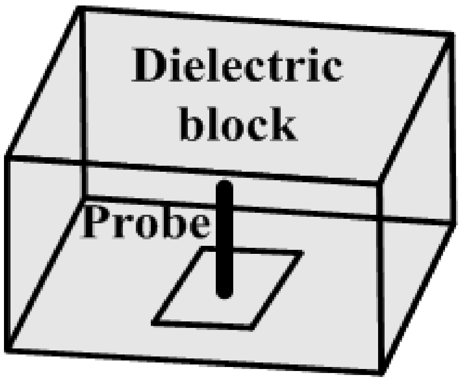

LP omnidirectional DRA

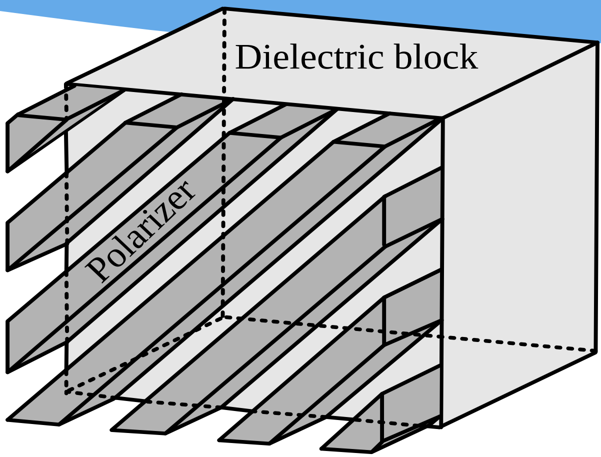

Dielectric block with the wave polarizer

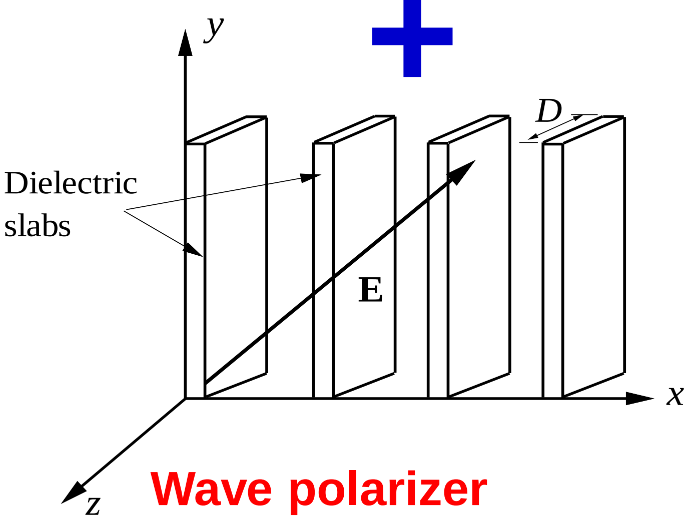

Wave polarizer

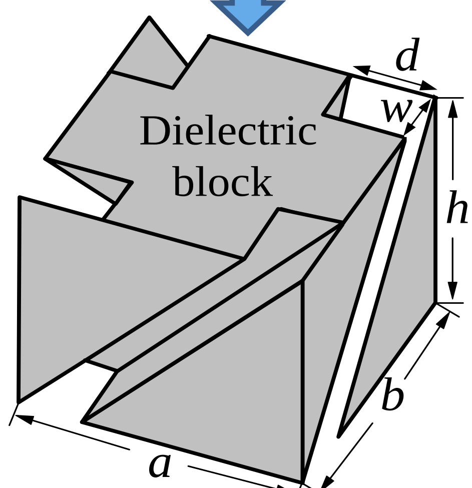

Proposed compact omnidirectional CP DRA

Photographs of the prototype

Prototype for 2.4 GHz WLAN design

Top face and sidewalls

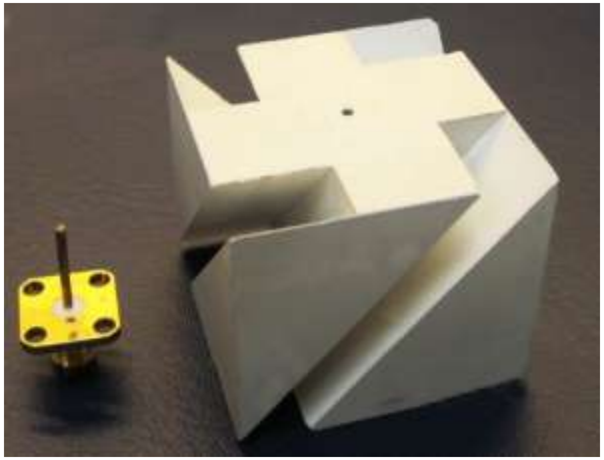

Bottom face

Design parameters

ε_r = 15, a = b = 39.4 mm, h = 33.4 mm, w = 9.4 mm,

d =14.4 mm, r_1 = 0.63 mm, l = 12.4 mm, g = 12.7 mm

Simulated and measured results

Reflection coefficient

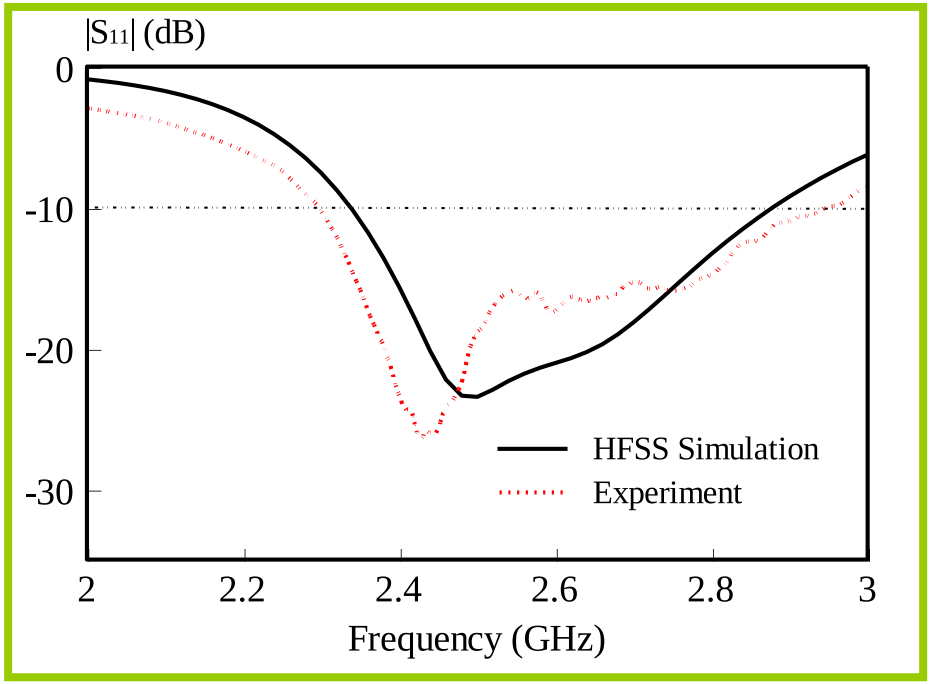

Axial ratio

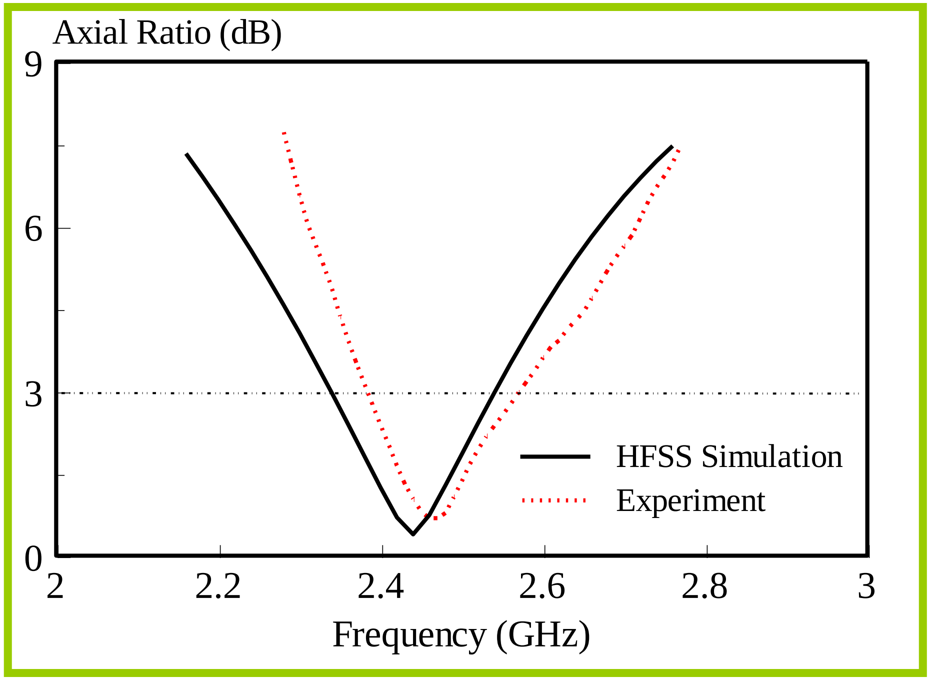

Impedance bandwidth:
Simulated: 20.3% (2.34-2.87 GHz)
Measured: 24.4% (2.30-2.94 GHz)

AR bandwidth:
Simulated: 8.2% (2.34-2.54 GHz)
Measured: 7.3% (2.39-2.57 GHz)

Simulated and measured radiation patterns

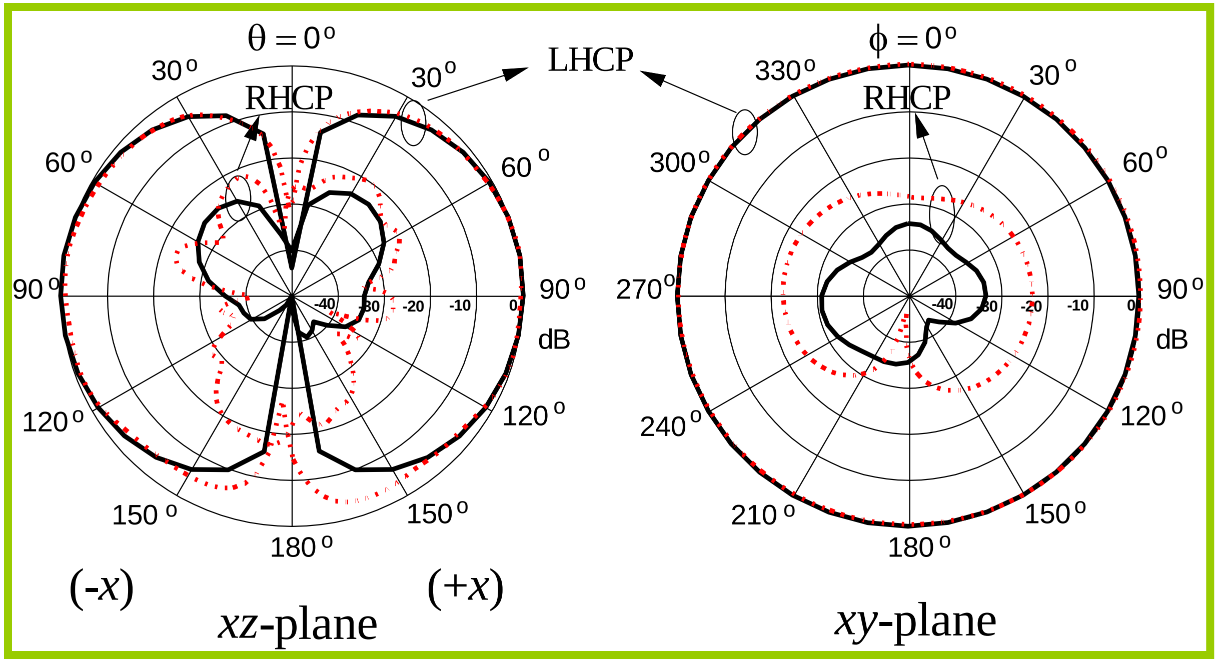

- Very good omnidirectional characteristic
- In the horizontal plane, LHCP fields > RHCP fields by ~20 dB .

Simulated and measured antenna gain

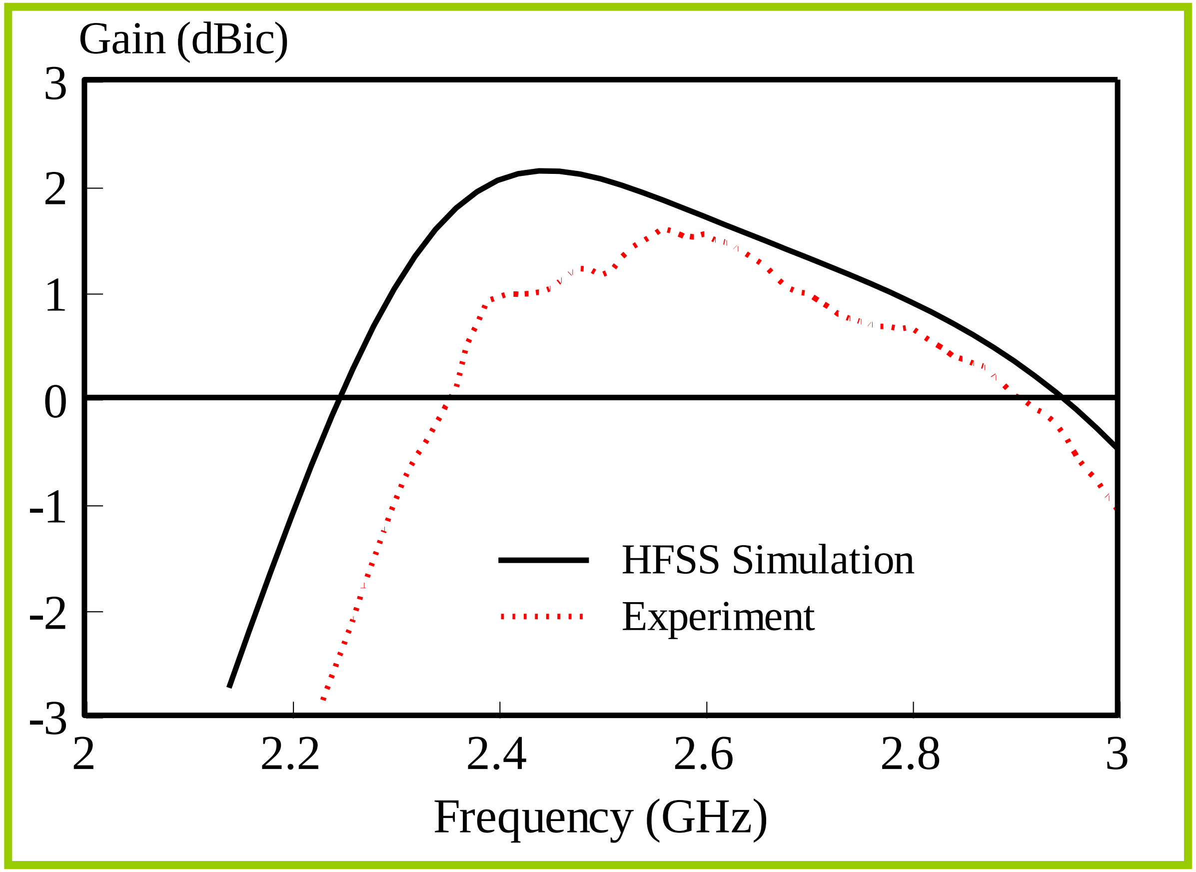

Design II:

Wideband omnidirectional CP antenna with parasitic metallic strips

Antenna configurations

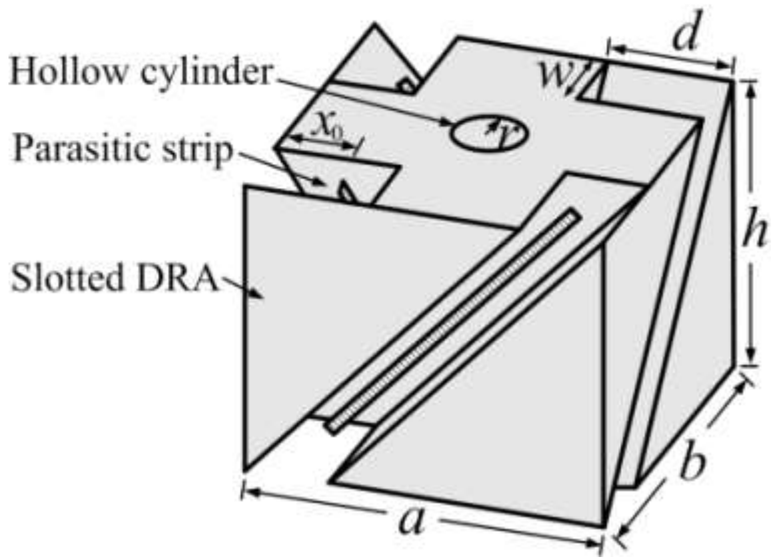

Perspective view

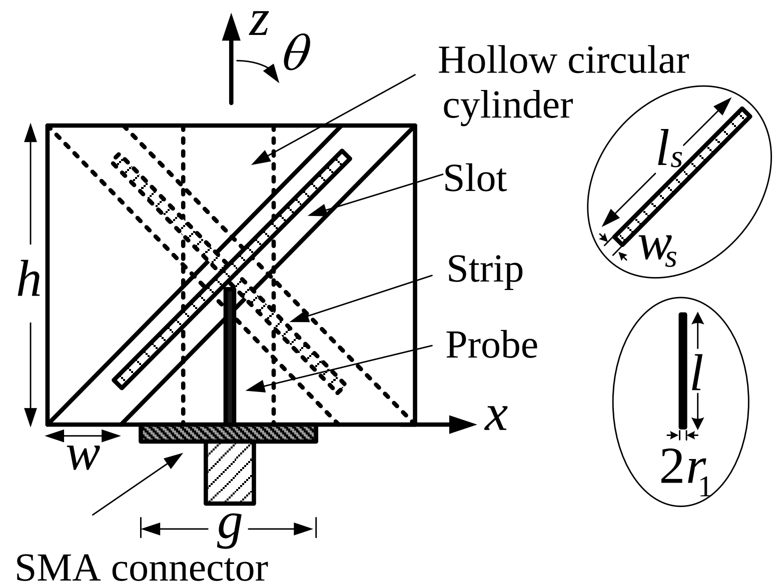

Front view

- Four parasitic metallic strips are embedded in the lateral slots to enhance the AR bandwidth.
- The hollow circular cylinder is introduced to enhance the impedance bandwidth.

Photographs of the prototype

Prototype for 3.4 GHz WiMAX design

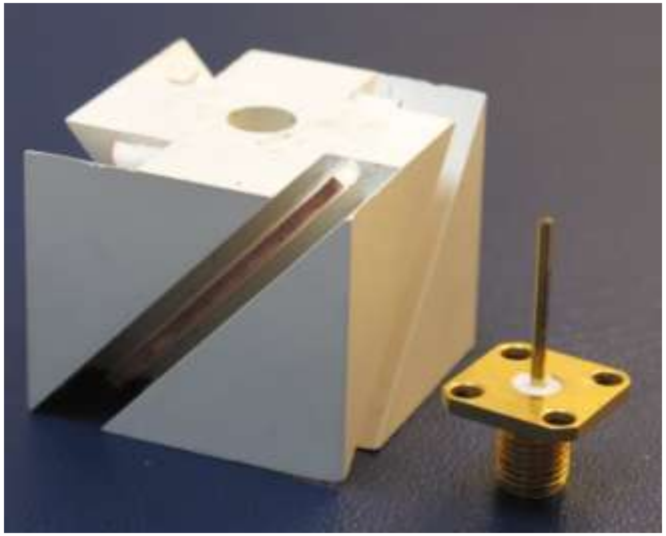

Top face and sidewalls

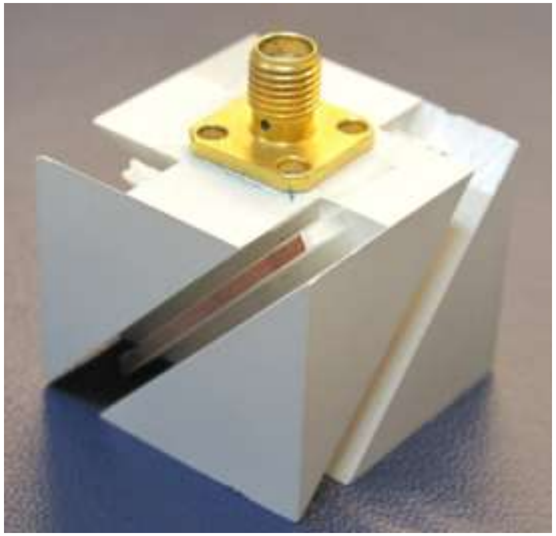

Bottom face

Design parameters

ε_r = 15, a = b = 30 mm, h = 25 mm, r = 3 mm, w = 7 mm, d =10.5 mm
l_s = 30.5 mm, w_s = 1 mm, x_0 = 6.4 mm, r_1 = 0.63 mm, l = 19 mm.

Simulated and measured reflection coefficient and axial ratio

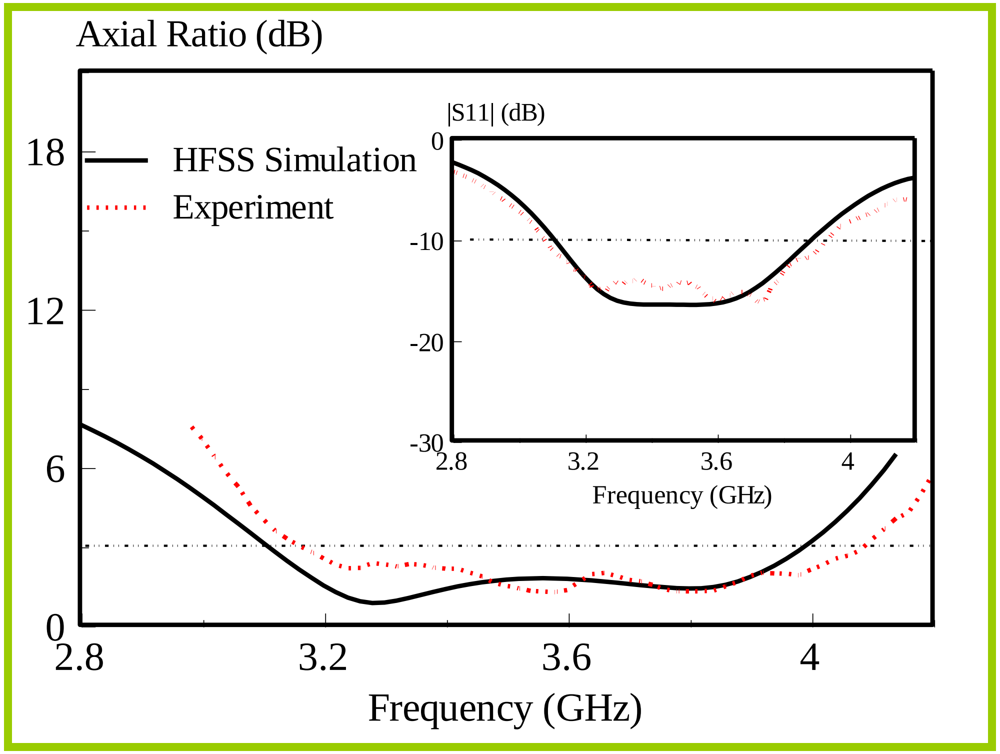

Impedance bandwidth:
Simulated: 22.3% (3.11-3.89 GHz)
Measured: 24.5% (3.08-3.94 GHz)

AR bandwidth:
Simulated: 24.8% (3.11-3.99 GHz)
Measured: 25.4% (3.16-4.08 GHz)

Overlapping bandwidth: 22.0%; bandwidth widened by ~3 times.

Simulated and measured results

Antenna gain

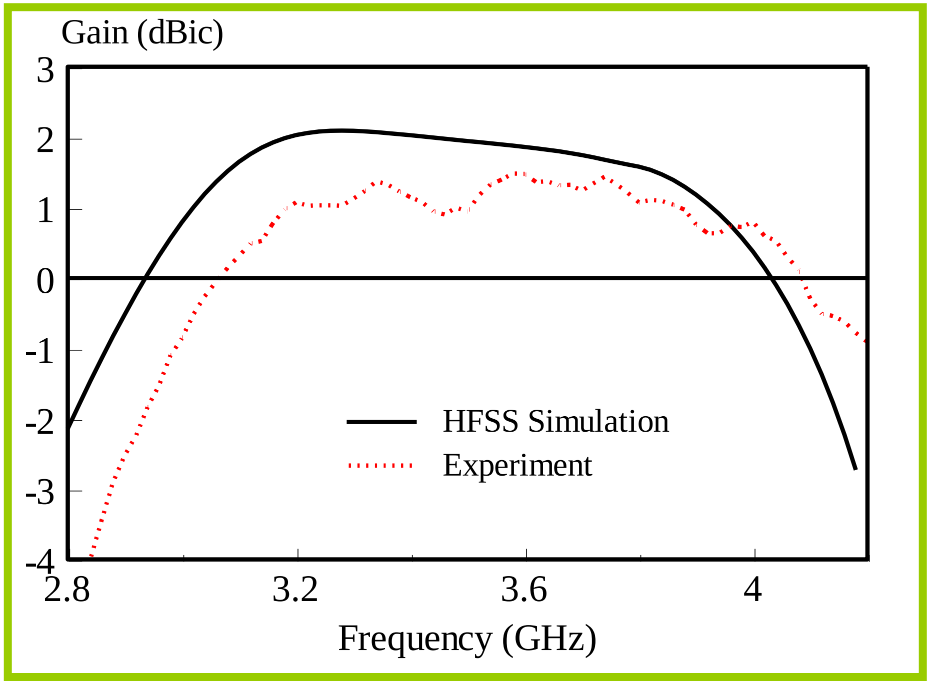

Radiation efficiency

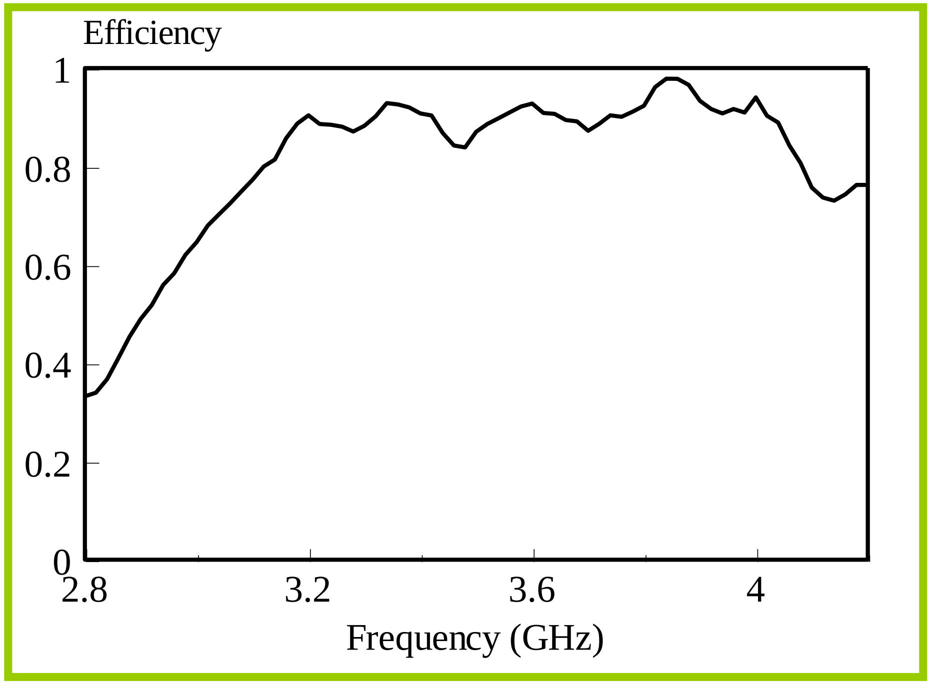

- Measured gain: wider bandwidth.
- Measured antenna efficiency: 84-98% (3.1-3.9 GHz).

Simulated and measured radiation patterns

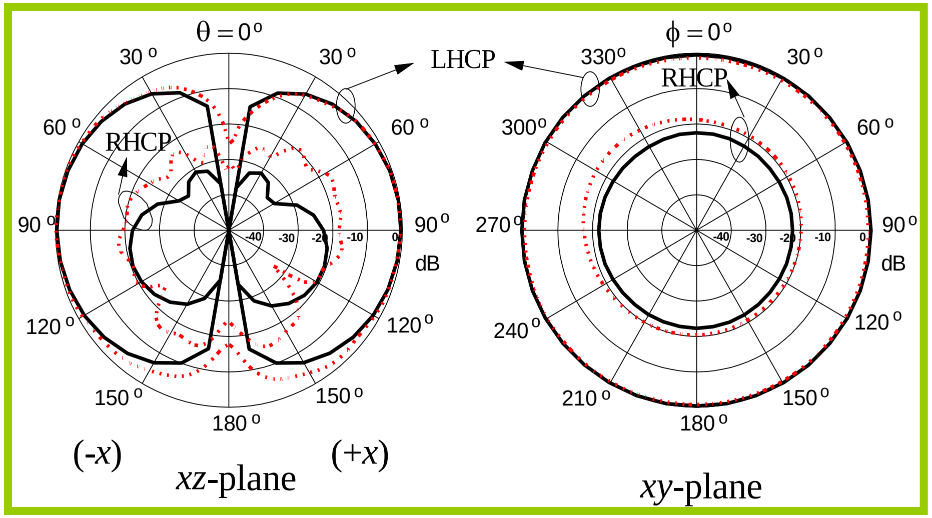

3.4 GHz

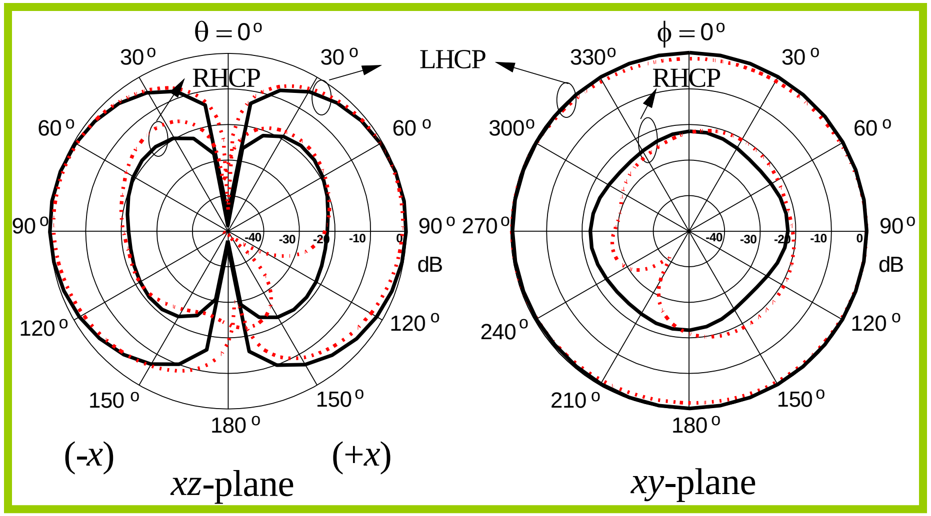

3.8GHz

- LHCP fields > RHCP fields by more than 15 dB in horizontal plane.
- Stable radiation patterns across the entire passband (3.1 – 3.9 GHz).

V. Dualband & Wideband DRAs

(i) Rectangular DRA

Background

- Dualband and wideband antennas are extensively used (e.g., WLAN)
- Multi-element DRA [1]

  - requiring more DR elements and space
- Hybrid slot-DRA [2]

  - coupling slot used as the feed and antenna

  - inflexible in matching the impedance

[1] Petosa, N. Simons, R. Siushansian, A. Ittipiboon and C. Michel, “Design and analysis of multisegmentdielectric resonator antennas,” *IEEE Trans. AP*, vol.48, pp.738-742, 2000.
[2] Buerkle, K. Sarabandi, and H. Mosallaei, “Compact slot and dielectric resonator antenna with dual-resonance, broadband characteristics,” *IEEE Trans. AP* , vol. 53, pp.1020-1027, 1983.

Use of higher-order DRA

- Wideband DRA [1]
- Dualband DRA [2]
- Trial-and-error approach is normally used
- Systematic design approach is desirable

[1] B. Li and K. W. Leung, "Strip-fed rectangular dielectric resonator antennas with/without a parasitic patch," *IEEE Trans. Antennas Propagat.*, vol.53, pp.2200-2207, Jul.2005.
[2] T. H. Chang and J. F. Kiang, "Dual-band split dielectric resonator antenna," *IEEE Trans. Antennas Propagat.*, vol.55, no.11, pp.3155-3162, Nov.2007.

Design Formulas for Dual-Mode rectangular DRA

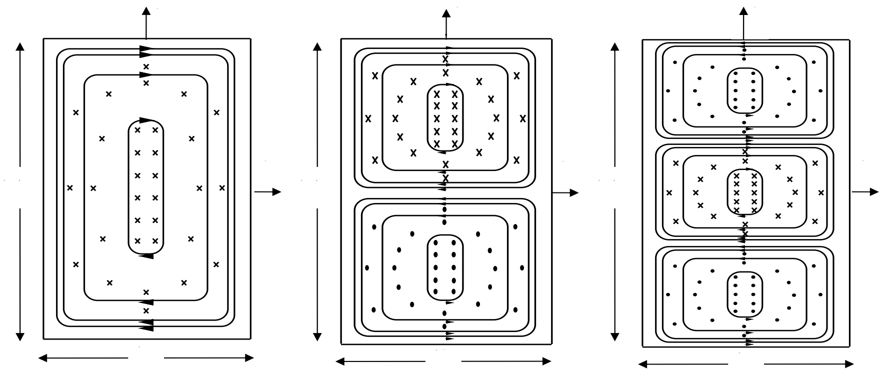

TE^{y}_{111} TE^{y}_{112} TE^{y}_{113}

- The E-field should vanish on the PEC and the TE_{112} mode cannot be excited properly.
- The TE_{111} mode and TE_{113} mode are used in the dual-mode design.

Formula Derivation

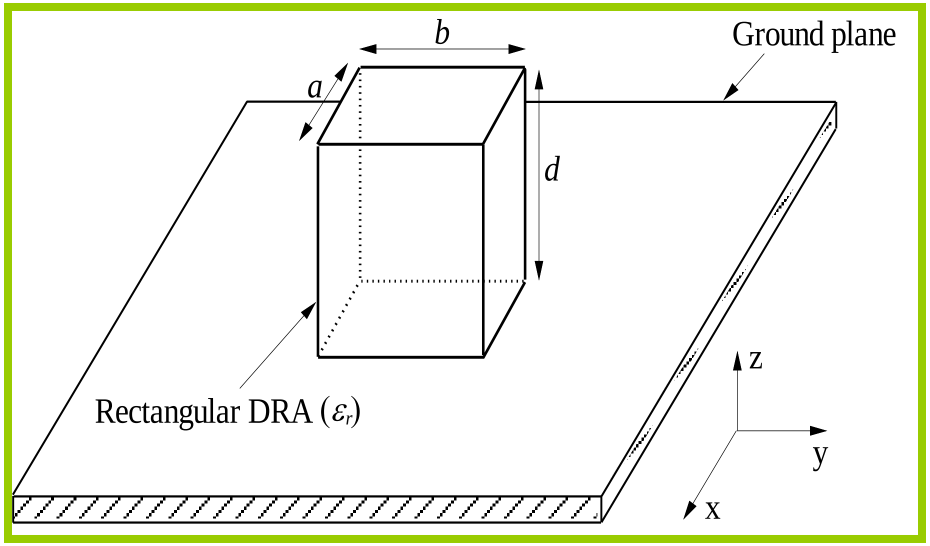

The wavenumbers $k_{x1,\,x2}$ and $k_{z1,\,z2}$ can be written as follows:

$$k_{z2} = \frac{3\pi}{2d}$$

$$k_{z1} = \frac{\pi}{2d}$$

$$k_{x1} = k_{x2} = \frac{\pi}{a}$$

From the DWM model, the frequencies f_1, f_2 are given by:

$$f_{1,2} = \frac{c}{2\pi\sqrt{\varepsilon_r}}\sqrt{k_{x1,x2}^2 + k_{y1,y2}^2 + k_{z1,z2}^2}$$

where

$$k_{y1,y2} = \sqrt{k_{1,2}^2 - k_{x1,x2}^2 - k_{z1,z2}^2} \qquad (*)$$

in which $k_{1,2} = 2\pi\sqrt{\varepsilon_r}\, f_{1,2}/c$ are wavenumbers in the dielectric, with c being the speed of light in vacuum.

Engineering Formulas for the DRA dimensions

$$a = \frac{10.32}{\sqrt{9k_1^2 - k_2^2}} + 10.32^{-(3.96 - \frac{f_2}{f_1})}$$

$$d = \pi\sqrt{\frac{2}{k_2^2 - k_1^2}} + \Delta d$$

$$b = 0.65b_1 + 0.35b_2$$

where

$$\Delta d = \left[0.1393\left(\frac{f_2}{f_1}\right)^4 - 2.3209\left(\frac{f_2}{f_1}\right)^3 + 11.4422\left(\frac{f_2}{f_1}\right)^2 - 23.4984\left(\frac{f_2}{f_1}\right) + 18.4437\right] \times 10^{-3} \quad \text{(m)}$$

$$b_{1,2} = \frac{2}{k_{y1,y2}} \tan^{-1}\sqrt{\left(1 - \frac{1}{\varepsilon_r}\right)\left(\frac{k_{1,2}}{k_{y1,y2}}\right)^2 - 1}$$

Limit of frequency ratio f_2/f_1

From $$a = \frac{10.32}{\sqrt{9k_1^2 - k_2^2}} + 10.32^{-(3.96-\frac{f_2}{f_1})}$$

We have

$$9k_1^2 - k_2^2 d \geq 0 \quad \Rightarrow \quad 3k_1 > k_2 \text{ or } 3f_1 > f_2$$

giving

$$\boldsymbol{f_2/f_1 < 3}$$

which is the theoretical limit that is not known before.

Error analysis

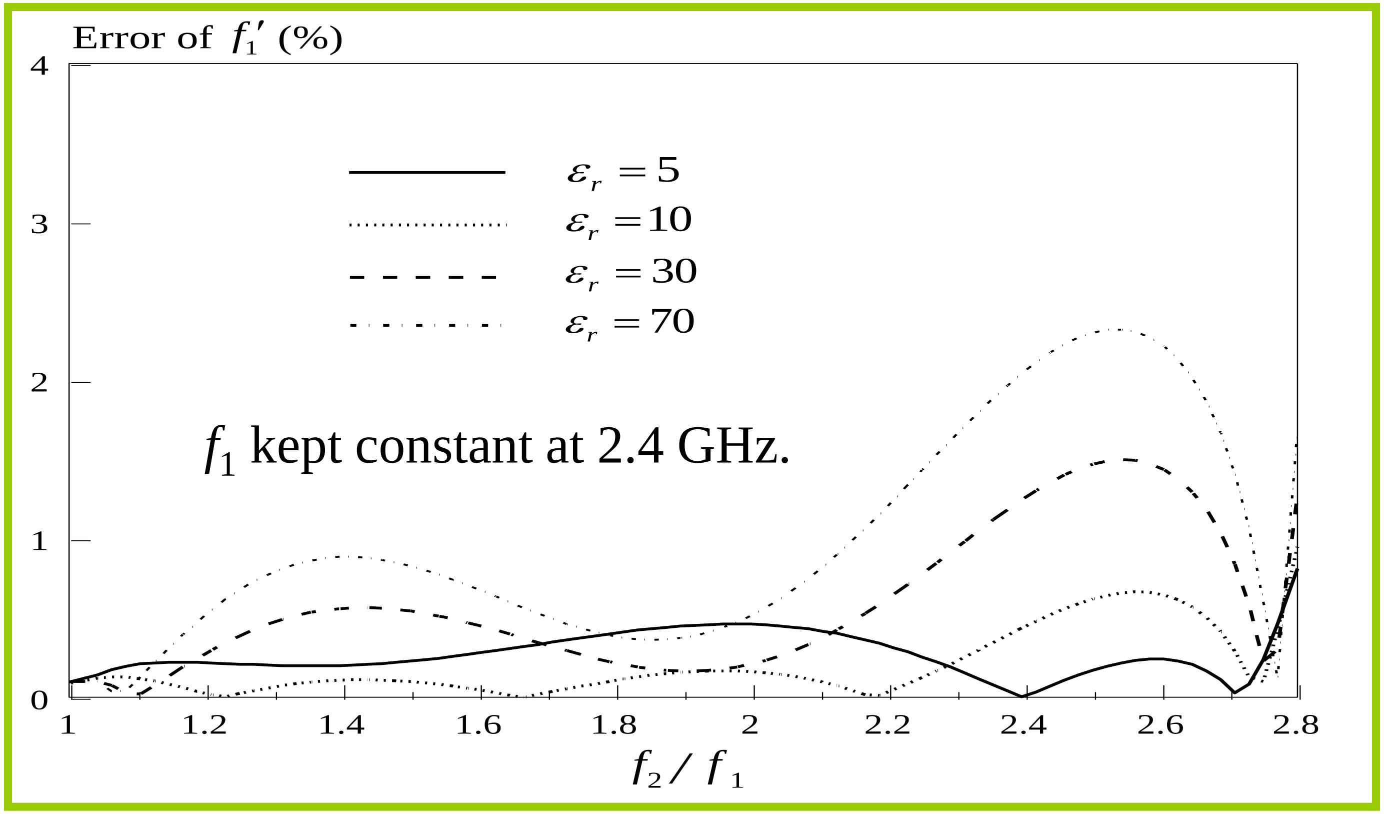

Compared with DWM results, errors of f_1, f_2 are both less than 2.5% for $1 < f_2/f_1 \leq 2.8$, $5 \leq \varepsilon_r \leq 70$.

A. Example for Dual-band Rectangular DRA Design

Given: f_1 = 3.47 GHz (WiMAX)

f_2 = 5.2 GHz (WLAN), ε_r=10

↓ Using dual-mode formulas

a = 20.8 mm, b = 10.5 mm, and d = 18.5 mm.

Configuration of the dualband DRA

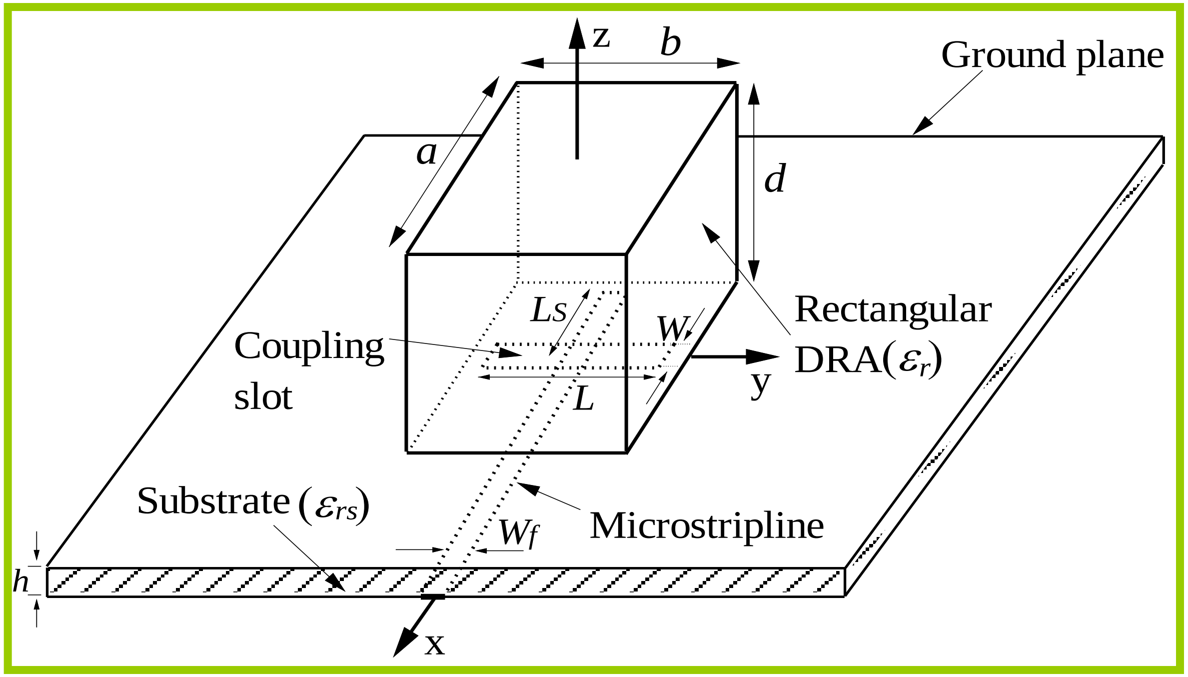

W = 2.6 mm, *L* =10.6 mm, *L*s=7.2 mm, W_f=1.94 mm, *h*=0.762mm, ε_{rs}= 2.93

Measured and simulated reflection coefficients

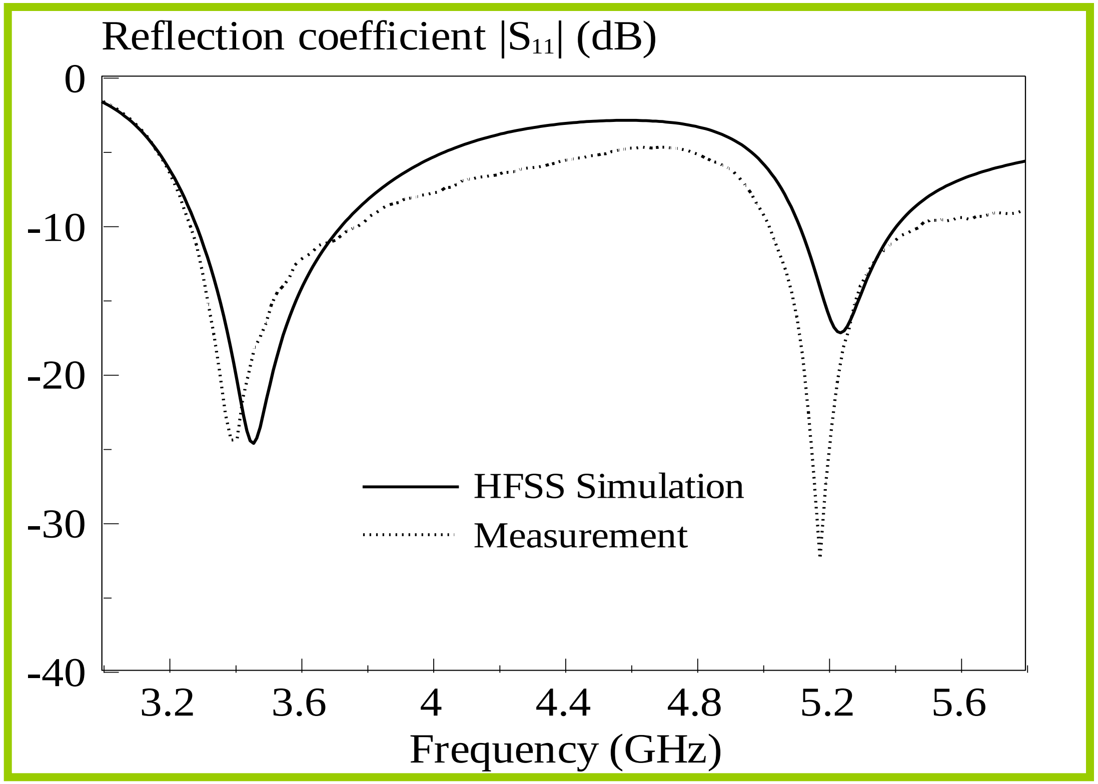

Measured bandwidths:

Lower band: 15% (3.25-3.78 GHz) covering WiMAX (3.4-3.7 GHz).

Upper band: 8.3% (5.03-5.47 GHz) covering WLAN (5.15-5.35 GHz).

COMPARISON OF DESIGN, SIMULATED, AND MEASURED RESONANCE FREQUENCIES OF TE_{111}^{y} AND TE_{113}^{y} MODES

Resonant Mode	Measured frequency (GHz)	Design frequency		Simulated HFSS frequency	
		$f_{1,2}$ (GHz)	Error (%)	f_{HFSS} (GHz)	Error (%)
TE_{111}^{y}	3.40	3.47	2.05	3.47	2.05
TE_{113}^{y}	5.18	5.30	2.32	5.24	1.15

Measured and simulated radiation patterns

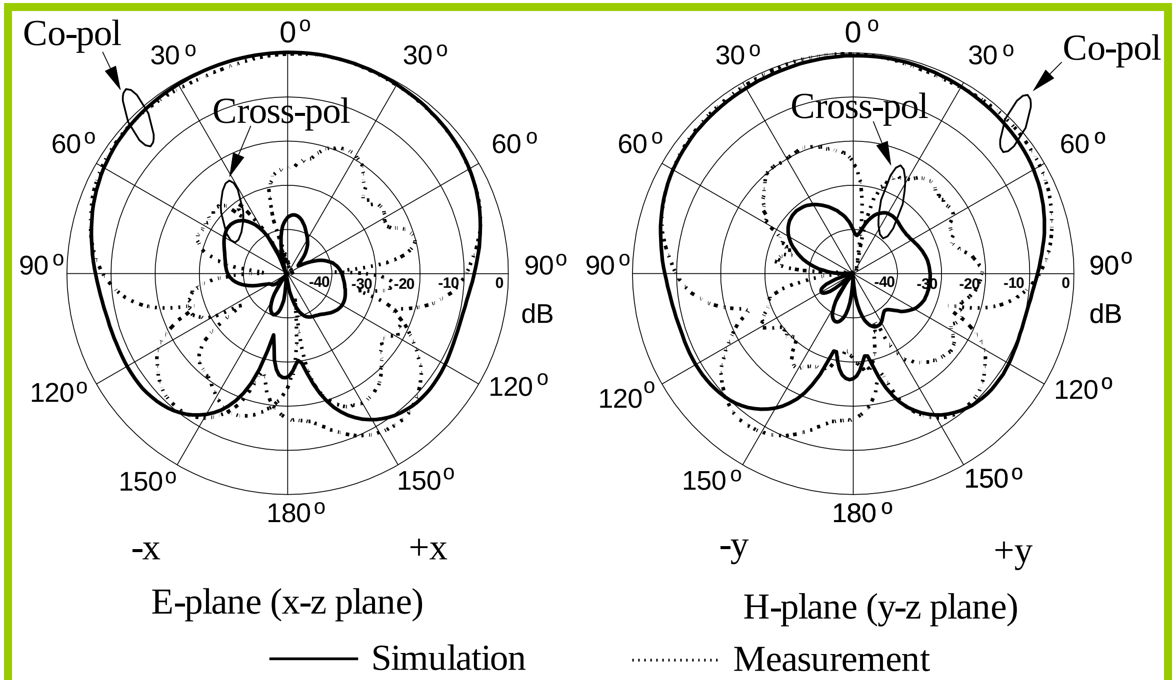

(a)

- TE_{111}^{y} mode: measured (3.40 GHz), simulated (3.47 GHz).
- Broadside radiation patterns are observed for both planes.
- Co-polarized fields > cross-polarized fields by more than 20 dB in the boresight direction.

Measured and simulated radiation patterns

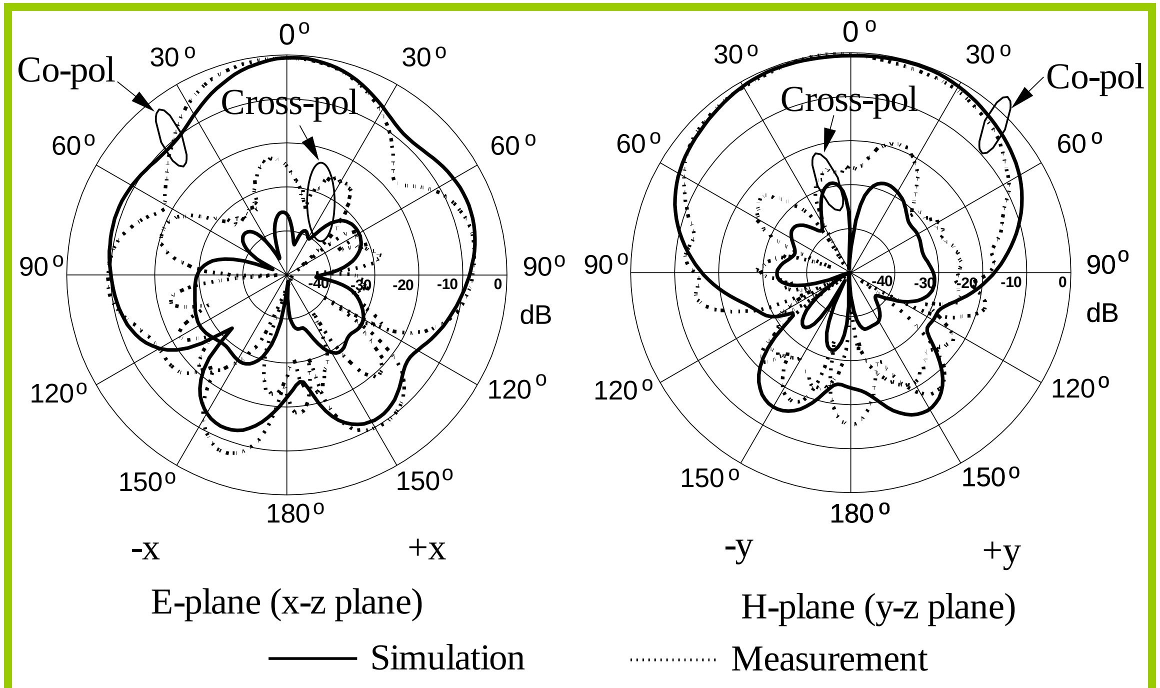

(b)

- TE_{113}^{y} mode: measured (5.18 GHz), simulated (5.24 GHz).
- Broadside radiation patterns are observed for both planes.
- Co-polarized fields > cross-polarized fields by more than 20 dB in the boresight direction.

Measured antenna gain

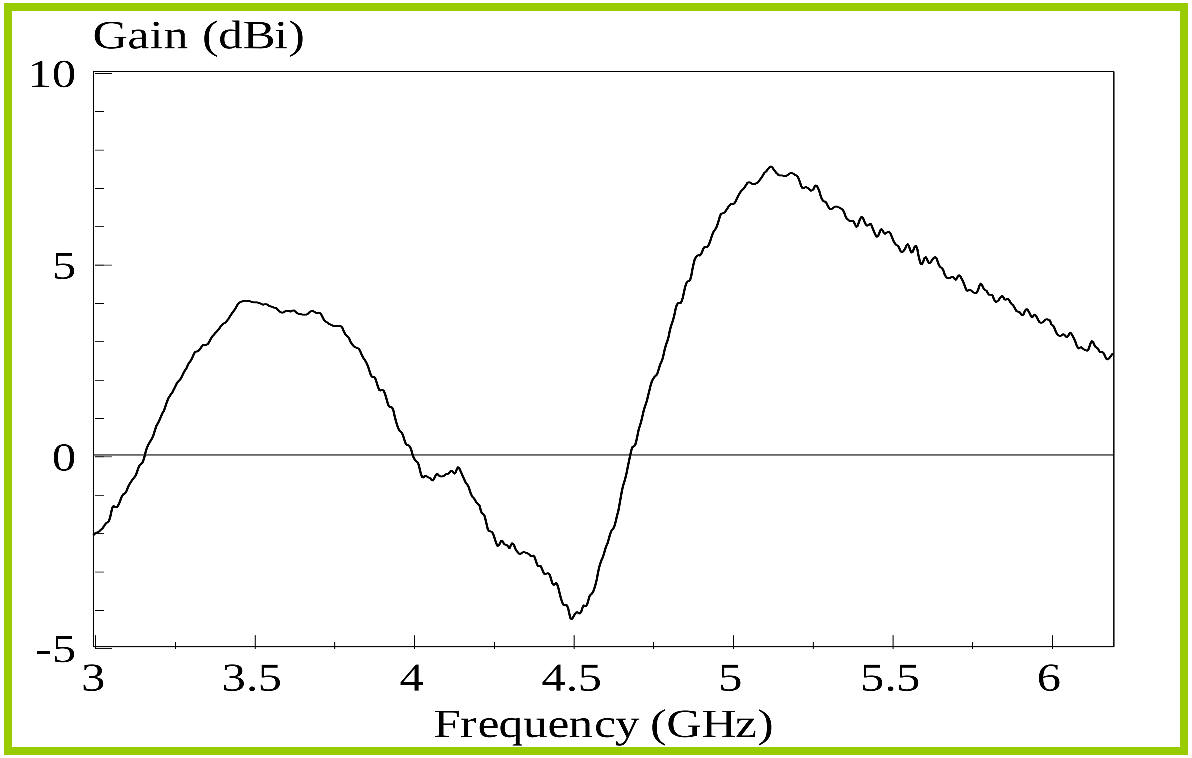

- TE_{111}^{y} mode: Maximum gain of 4.02 dBi at 3.48 GHz.
- TE_{113}^{y} mode: Maximum gain of 7.52 dBi at 5.13 GHz.
- Electrically larger antenna has a higher antenna gain.

B. Example for Wideband DRA Design

Given: f_1 = 1.98 GHz (PCS)

f_2 = 2.48 GHz (WLAN), ε_r=10

↓ Using formulas for dual-mode rectangular DRA

a = 30.7 mm, b = 24.7 mm, and d = 47.7 mm.

Configuration of the wideband DRA

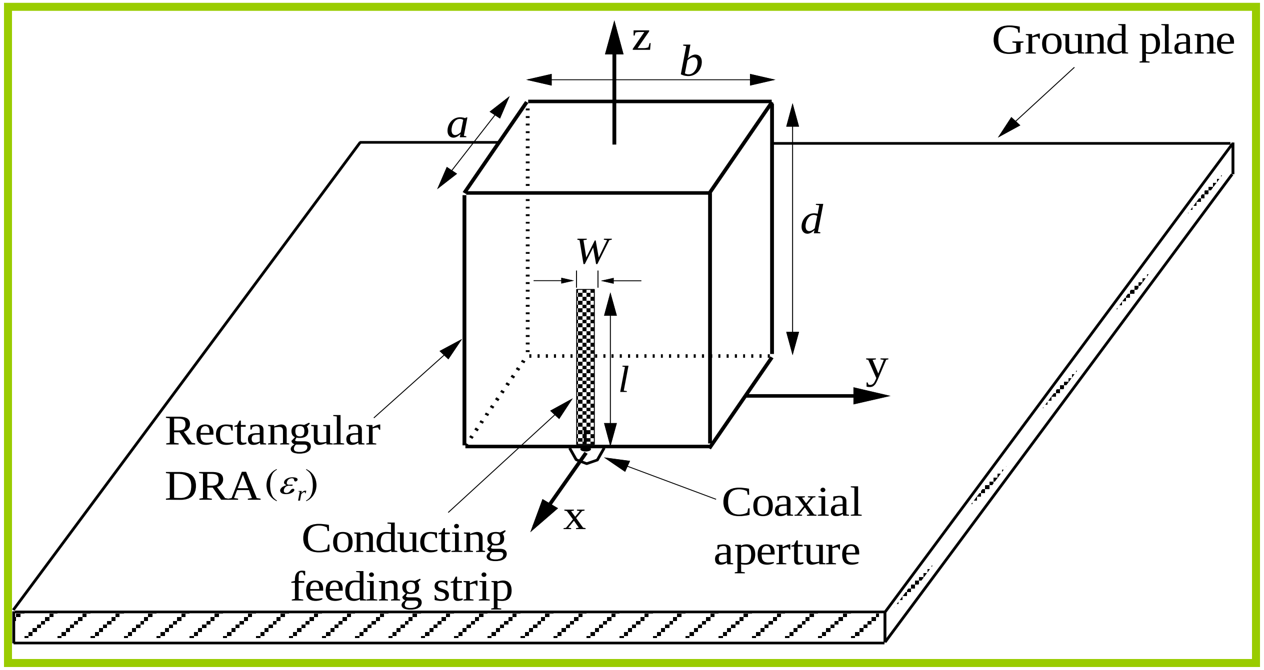

l = 17 mm, W = 1 mm

Measured and simulated reflection coefficients

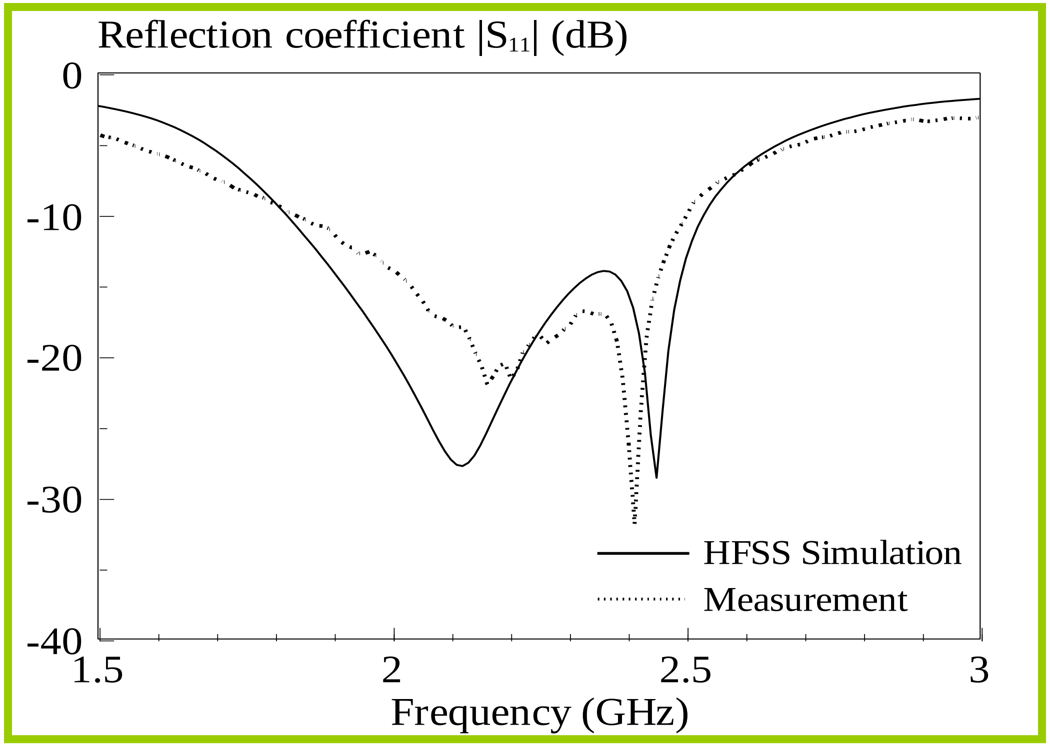

Measured bandwidths : 30.9% (1.83-2.50 GHz)

PCS (1.85-1.99 GHz), UMTS (1.99-2.20 GHz)
& WLAN (2.4-2.48 GHz)

Measured and simulated radiation patterns

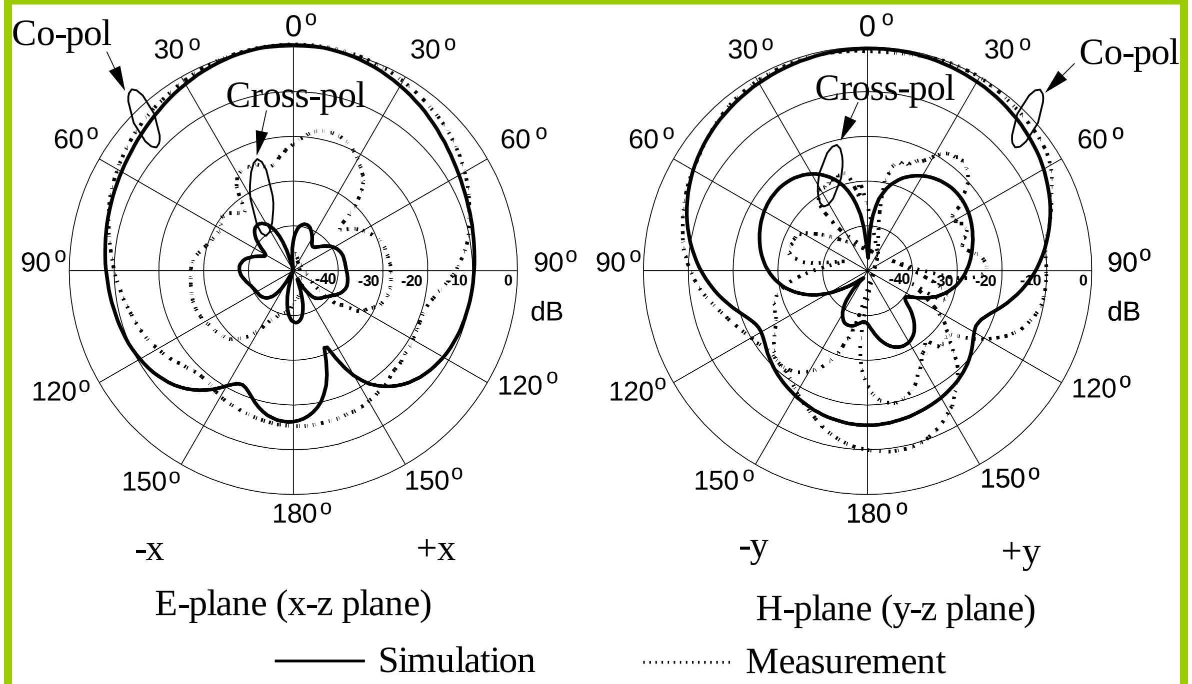

(a)

- Measured (2.16 GHz), simulated (2.11 GHz).
- Broadside radiation patterns are observed.
- Co-polarized fields > cross-polarized fields by more than 20 dB in the boresight direction.

Measured and simulated radiation patterns

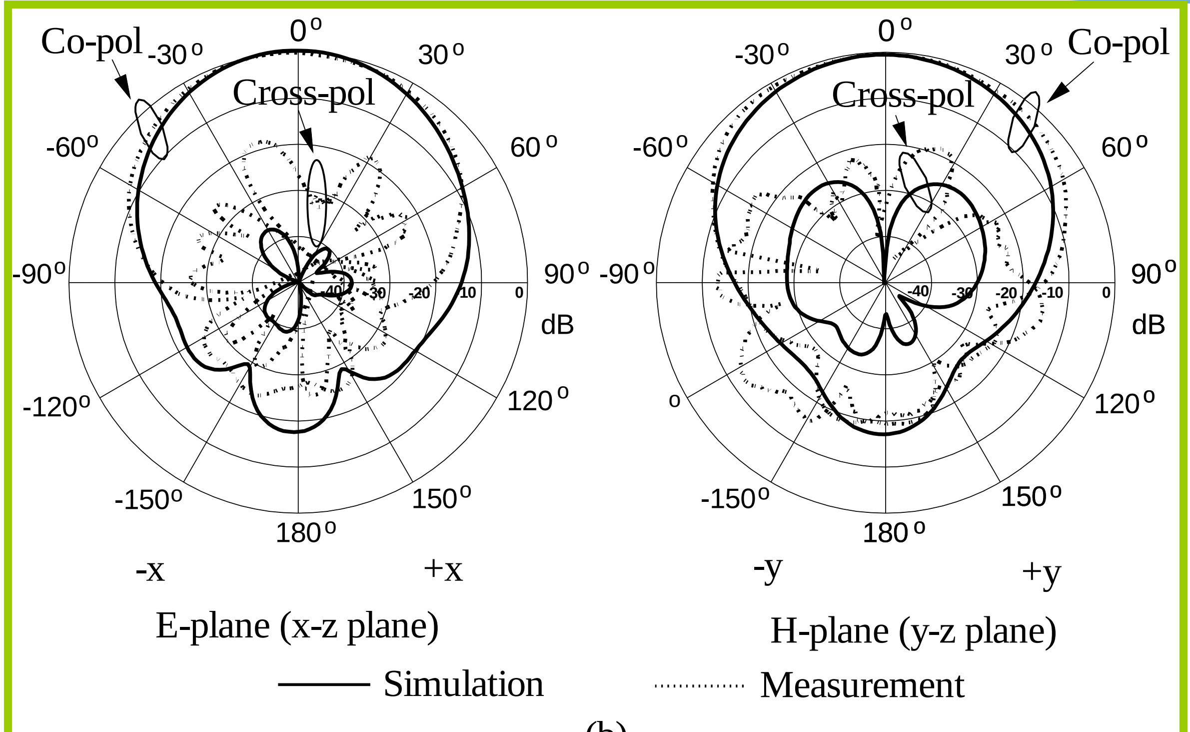

(b)

- Measured (2.41 GHz), simulated (2.46 GHz).
- Broadside radiation patterns are observed.
- Co-polarized fields > cross-polarized fields by more than 20 dB in the boresight direction.

Measured antenna gain

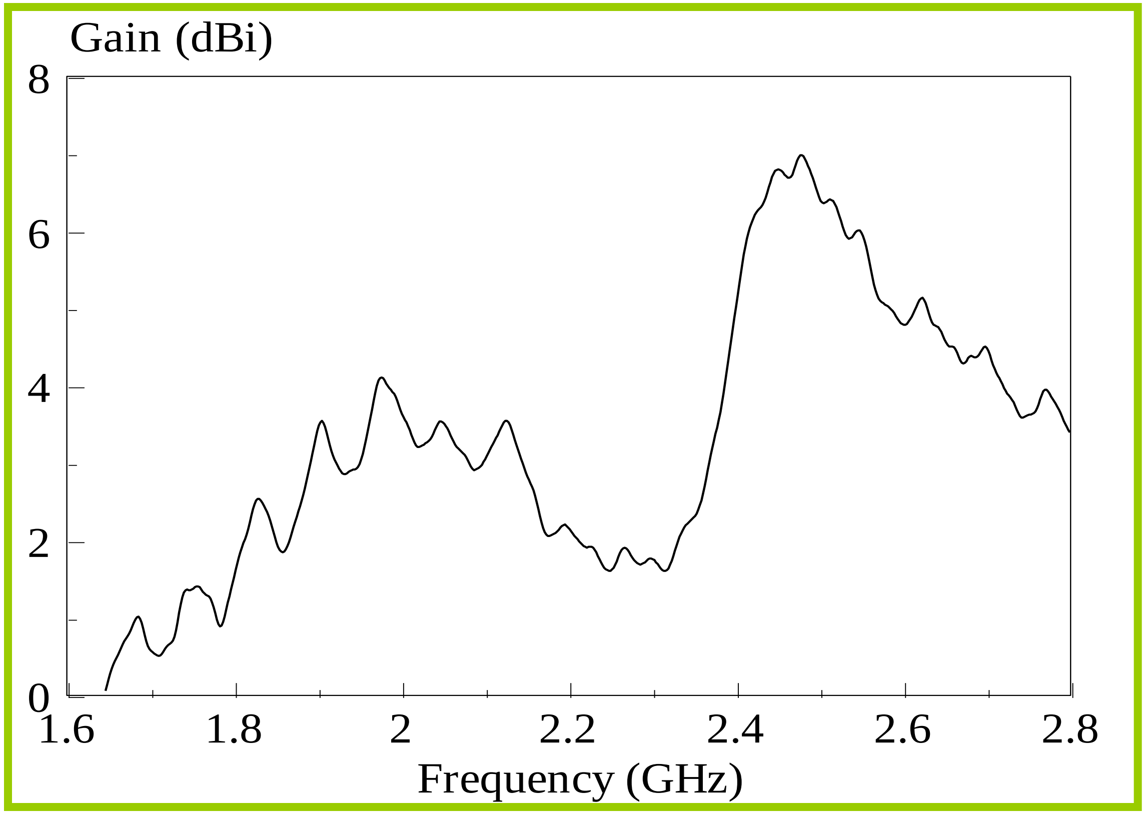

- The maximum gain of 6.98 dBi at 2.47GHz.
- TE_{113}^{y} -mode gain > TE_{111}^{y} -mode gain.

(ii) Cylindrical DRA

Resonance frequency of the HEM_{mnr} mode of the cylindrical DRA

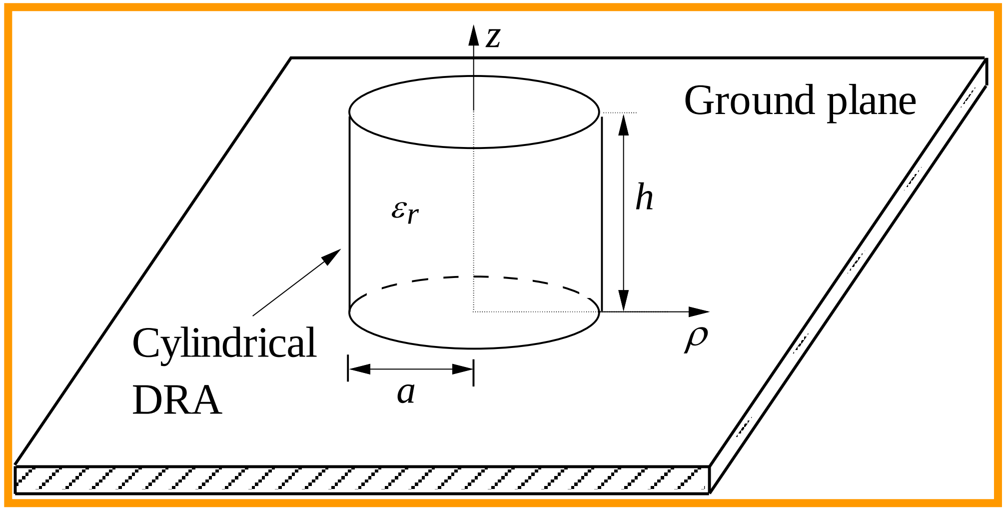

$$k_{\rho i}^2 + k_{zi}^2 = \varepsilon_r k_{0i}^2 \quad (1)$$

$i = 1, 2$ for f_1, f_2

f_1 : HEM_{111} mode frequency
f_2 : HEM_{113} mode frequency

- $k_{\rho i}$ & k_{zi} :dielectric wavenumbers along the ρ & z directions
- $k_{0i} = 2\pi f_i / c$: wavenumber in air

Resonance frequency of the HEM$_{mnr}$ mode of the cylindrical DRA

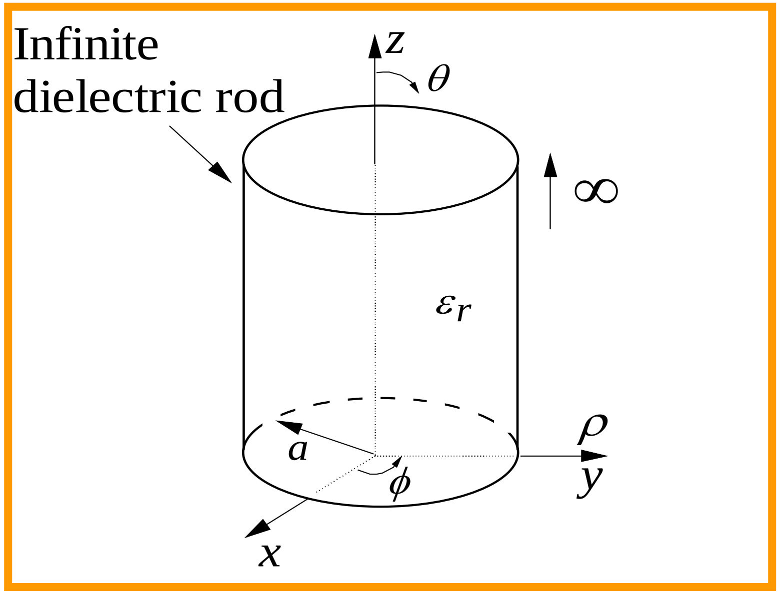

For k_ρ:

$$\left(\frac{1}{k_{\rho i}}\frac{J_m'(k_{\rho i}a)}{J_m(k_{\rho i}a)}+\frac{1}{k_{\rho i}'}\frac{K_m'(k_{\rho i}'a)}{K_m(k_{\rho i}'a)}\right)\cdot\left(\frac{\varepsilon_r}{k_{\rho i}}\frac{J_m'(k_{\rho i}a)}{J_m(k_{\rho i}a)}+\frac{1}{k_{\rho i}'}\frac{K_m'(k_{\rho i}'a)}{K_m(k_{\rho i}'a)}\right)=\frac{m^2(k_{\rho i}^{\,2}+k_{\rho i}'^{2})(k_{\rho i}^{\,2}+\varepsilon_r k_{\rho i}'^{2})}{(k_{\rho i}k_{\rho i}')^4a^2} \quad (2)$$

where

$$k_{\rho i}'=\sqrt{(\varepsilon_r-1)k_{0i}^2-k_{\rho i}^{\,2}} \quad (3)$$

is the radial wavenumber outside the dielectric rod

$J_m(x)$: Bessel function of the first kind
$K_m(x)$: modified Bessel function of the second kind.

D. Kajfez and P. Guillon, “Dielectric resonators,” Norwood, MA, Artech House, Inc., 1986.

Resonance frequency of cylindrical DRA

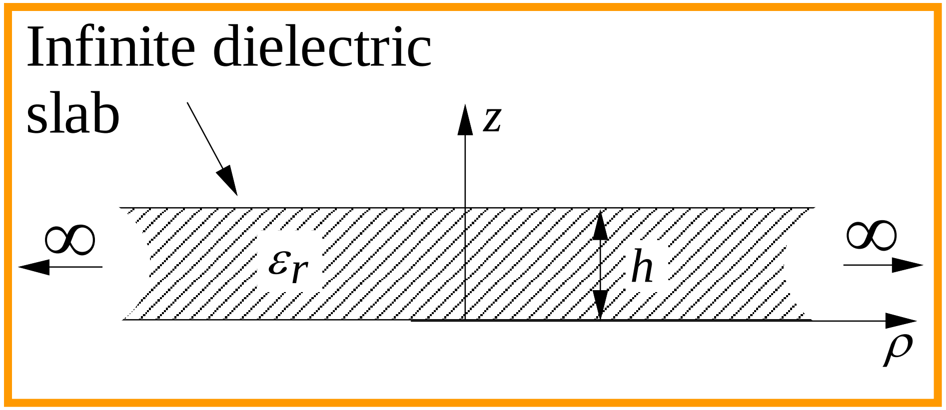

For k_z: approximated by the TM_{01}-mode wavenumber

$$\frac{hk_{zi}}{p_i} = \tan^{-1}\left(\frac{\varepsilon_r\sqrt{(\varepsilon_r - 1)k_{0i}^2 - k_{zi}^2}}{k_{zi}}\right)$$

$(i = 1, 2 \text{ for } f_1, f_2)$ (4)

where $p_1 = 1$ and $p_2 = 3$ correspond to the HEM_{111} and HEM_{113} modes, respectively.

R. K. Mongia and P. Bhartia, "Dielectric resonator antennas- a review and general design relations for resonant frequency bandwidth," *International Journal of Microwave and Millimeter-Wave Computer-Aided Engineering*, vol. 4, no. 3, pp 230-247, 1994.

Design formula of ratio *h*/*a* for given f_1, f_2, and ε_r

f_1 : HEM_{111} mode frequency (lower band)
f_2 : HEM_{113} mode frequency (upper band)

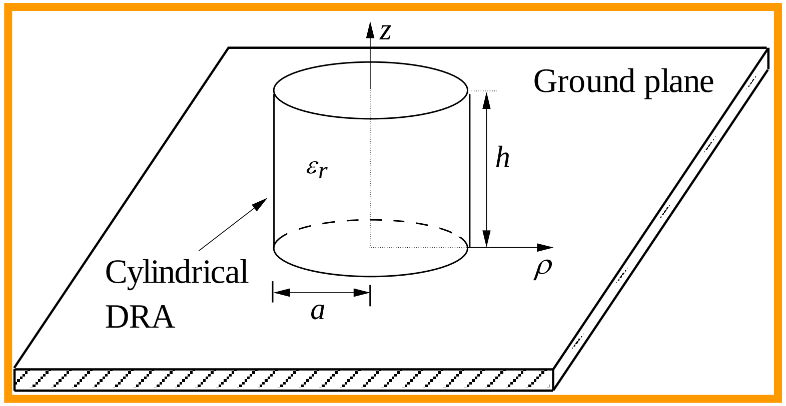

Using the covariance matrix adaptation evolutionary strategy again,

$$\frac{h}{a} = \frac{E_S}{\varepsilon_r^{\,4}} + \sum_{i=1}^{4} \frac{1}{\varepsilon_r^{\,4-i}} \left(\frac{A_i}{e^{\frac{B_i f_2}{f_1}} + C_i} + D_i \right) \qquad (1)$$

$$\begin{bmatrix} A_1 & B_1 & C_1 & D_1 & E_s \\ A_2 & B_2 & C_2 & D_2 & 0 \\ A_3 & B_3 & C_3 & D_3 & 0 \\ A_4 & B_4 & C_4 & D_4 & 0 \end{bmatrix} = \begin{bmatrix} 489.7 & 0.234 & -0.937 & -34800 & 116500 \\ 680.3 & -625.2 & -4.402 & 3682.7 & 0 \\ 36.15 & 1.511 & -4.713 & -160.2 & 0 \\ 19.23 & 1.162 & 3.982 & 1.996 & 0 \end{bmatrix}$$

Design formula of radius a

Radius a can be found by inserting h/a into (2) below:

$$a = \frac{\mathrm{c}}{2\pi\sqrt{\varepsilon_{\mathrm{r}}}\, f_1}\left[\frac{E_S}{\varepsilon_r^{\;4}} + \sum_{i=1}^{4}\frac{1}{\varepsilon_r^{\;4-i}}\left(\frac{A_i}{e^{\frac{B_i h}{a}} + C_i} + D_i\right)\right] \quad (2)$$

$$\begin{bmatrix} A_1 & B_1 & C_1 & D_1 & E_s \\ A_2 & B_2 & C_2 & D_2 & 0 \\ A_3 & B_3 & C_3 & D_3 & 0 \\ A_4 & B_4 & C_4 & D_4 & 0 \end{bmatrix} = \begin{bmatrix} 1.109 & -1.751 & 0.00152 & 3107.8 & -10932 \\ -0.0571 & -0.005 & -0.9973 & -304.1 & 0 \\ 0.152 & 0.0368 & -0.9764 & 17.814 & 0 \\ 4.429 & 5.659 & 6.114 & 0.057 & 0 \end{bmatrix}$$

After a is found, h can be determined from h/a.

Maximum error of a: 2.1% for $1 \le h/a \le 3.5$, $9 \le \varepsilon_{\mathrm{r}} \le 27$

Maximum error of h: 3.0% for $1.28 \le h/a \le 1.85$, $9 \le \varepsilon_{\mathrm{r}} \le 27$

A. Example for dualband cylindrical DRA design

Given: f_1 = 1.71 GHz (DCS:1.71- 1.88 GHz)

f_2 = 2.4 GHz (WLAN:2.4 - 2.48 GHz),

ε_r=9.4

↓ ← Using formulas (1) & (2)

a = 17.9 mm & h = 42.5 mm

Configuration of the dualband LP DRA

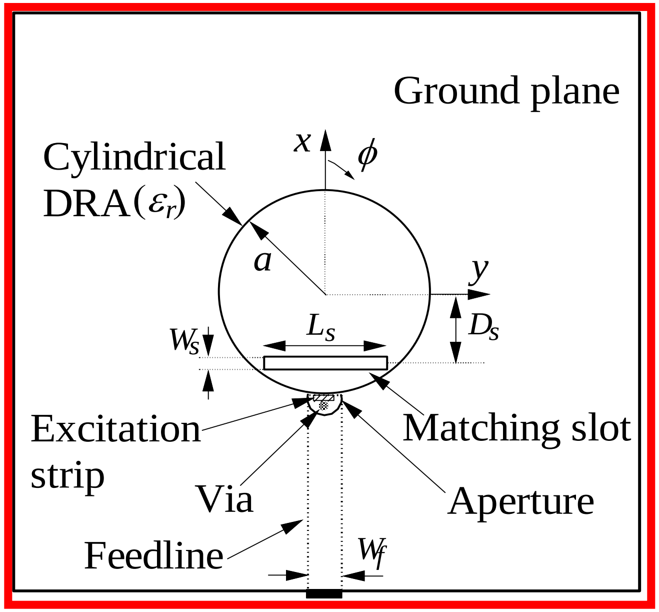

Top view

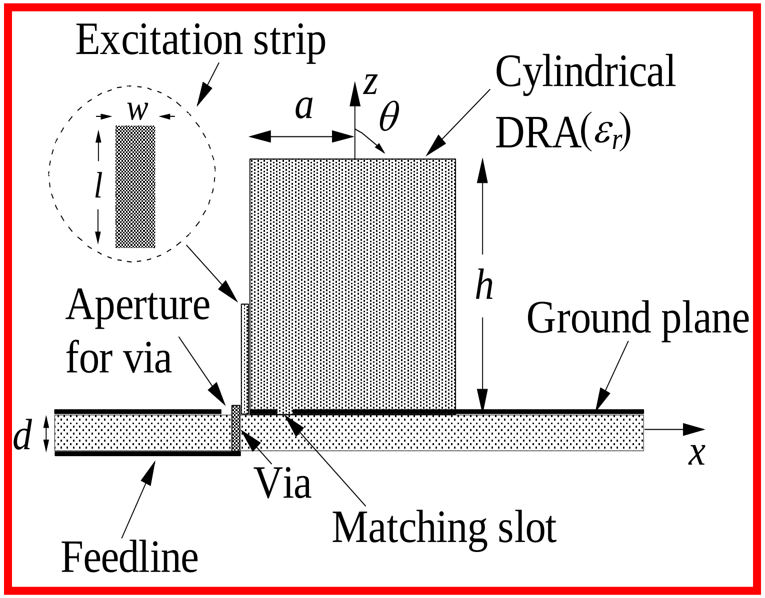

Side view

a = 18.7 mm, *h* = 42.5 mm, ε_r = 9.4, *l* = 12.5 mm, *w* = 1 mm, *Ls* = 20 mm, *Ws* = 1.5 mm, and *Ds* = 12.75 mm.

- Radius *a* has been slightly increased to reduce the merging effect

Measured and Simulated Reflection coefficients

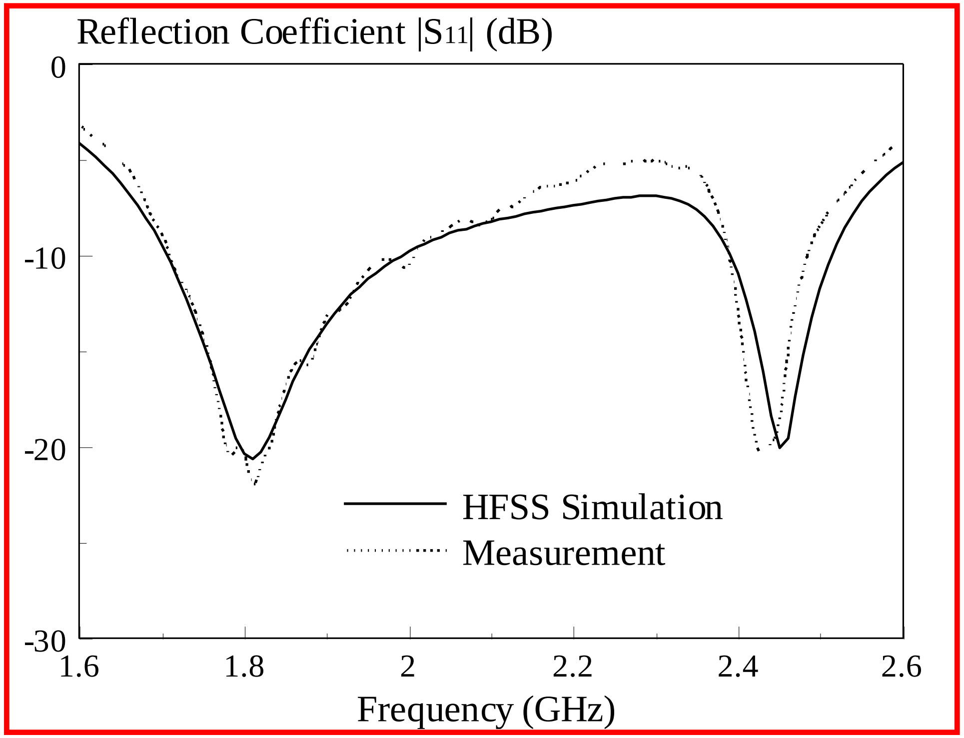

- Reasonable agreement
- Lower band impedance bandwidth: 15.5% (1.70-2.00 GHz)
- Upper band impedance bandwidth: 3.7% (2.39-2.48 GHz)

Measured and simulated radiation patterns

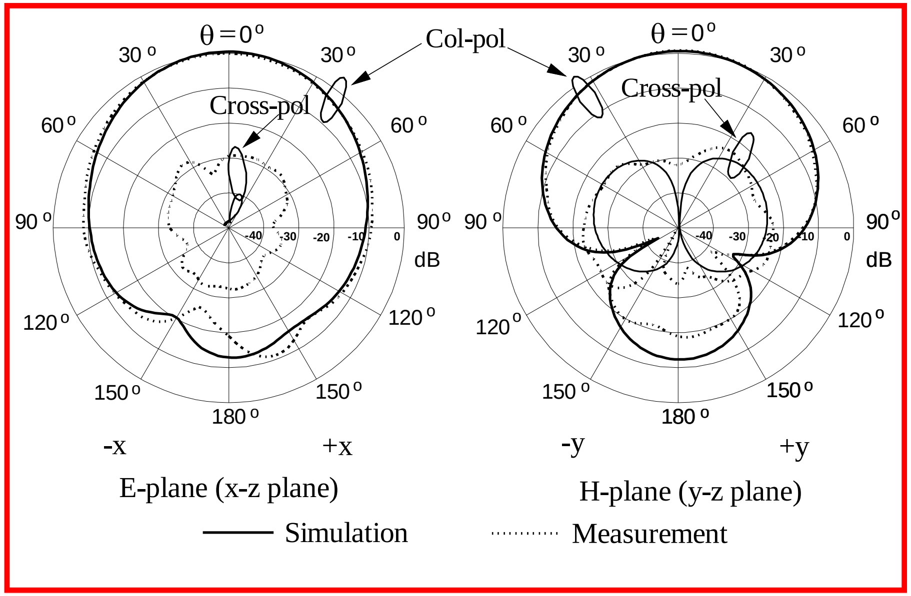

(a)

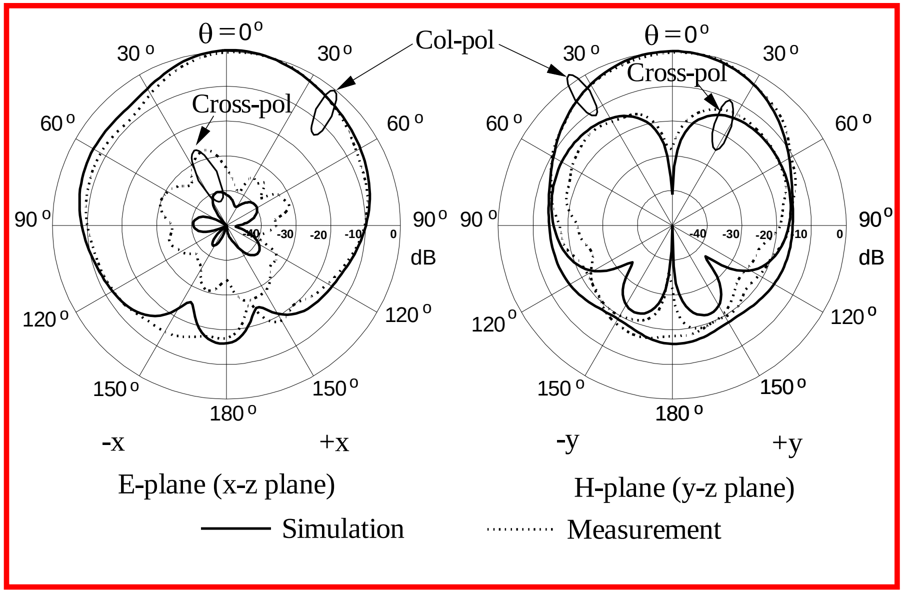

(b)

HEM_{111} mode: measured (1.8 GHz), simulated (1.8 GHz)
HEM_{113} mode: measured (2.42 GHz), simulated (2.45 GHz)

- Broadside radiation patterns are observed.
- Co-polarized fields > cross-polarized fields by more than 20 dB in the boresight direction.

Measured and simulated gain

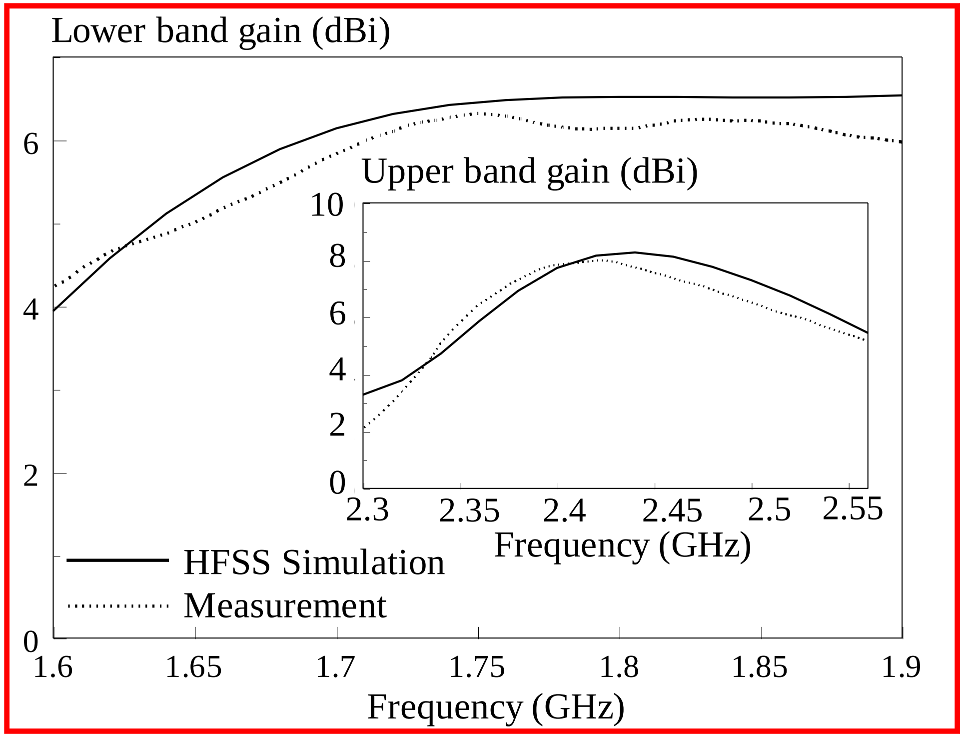

- HEM_{111} mode: Maximum measured gain of ~6 dBi (1.75 GHz)
- HEM_{113} mode: Maximum measured gain of ~ 8 dBi (2.43 GHz)

Dualband CP DRA

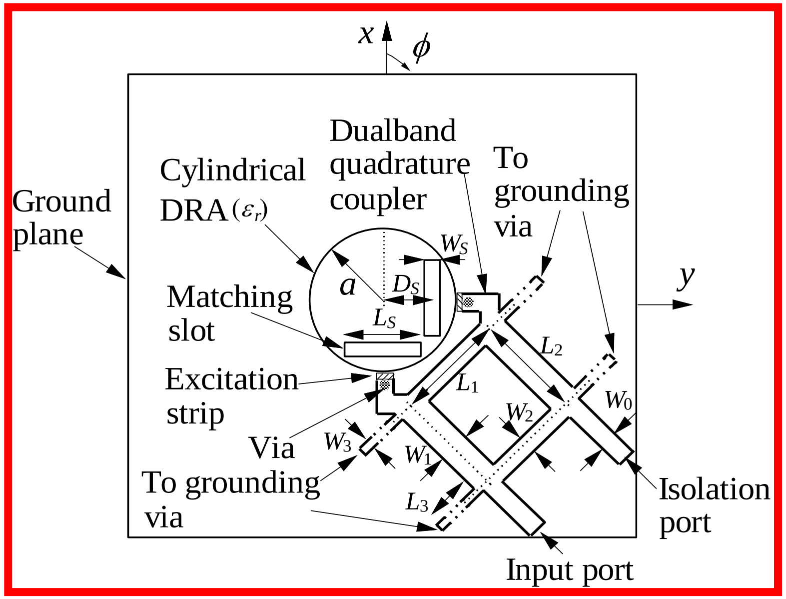

Top view

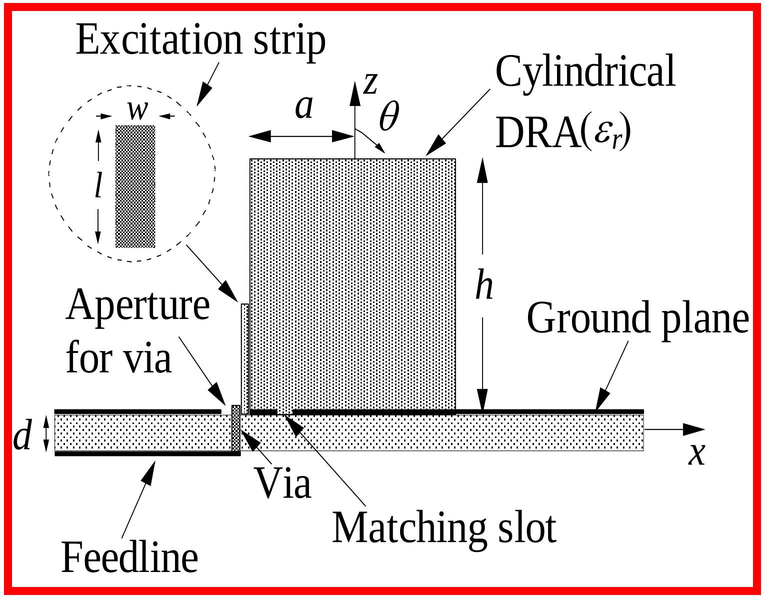

Side view

a = 18.7 mm, h = 42.5 mm, ε_r = 9.4, l = 12.5 mm, w = 1 mm, Ls = 21 mm, Ws = 1.5 mm, Ds = 12.75 mm, L_1 = 26.9 mm, L_2 =26.5 mm, L_3 = 56.65 mm, W_0 = 4.66 mm, W_1 = 7.3 mm, W_2 = 4.44 mm, and W_3 = 0.46 mm.

Measured and simulated reflection coefficients

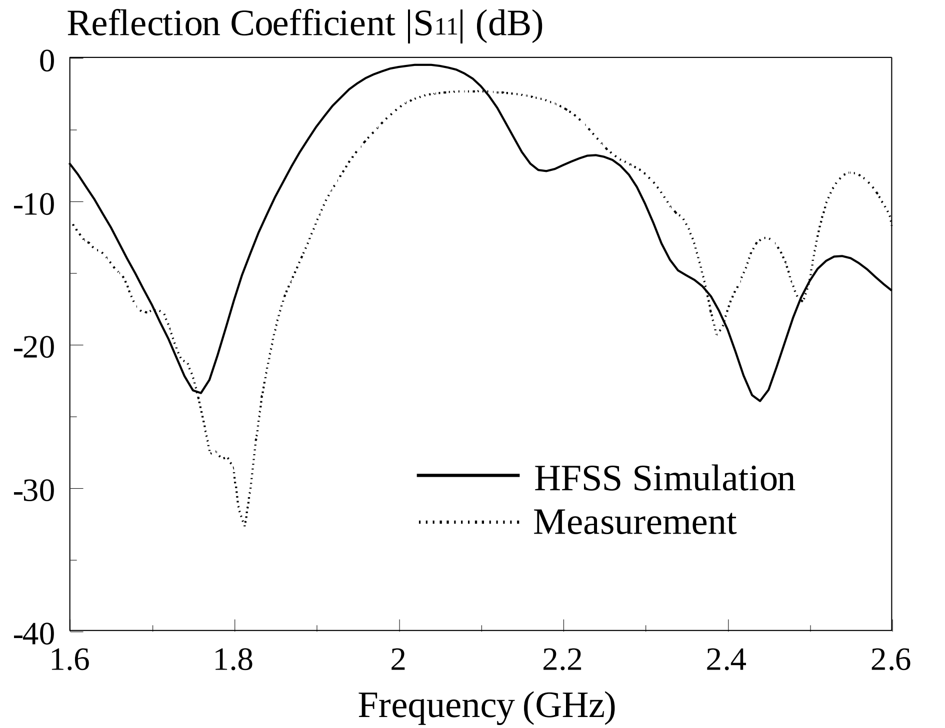

Reasonable agreement
Lower band bandwidth:18.9% (1.58-1.91 GHz).
Upper band bandwidth:7.8% (2.33-2.52 GHz).

Measured and simulated axial ratios (ARs)

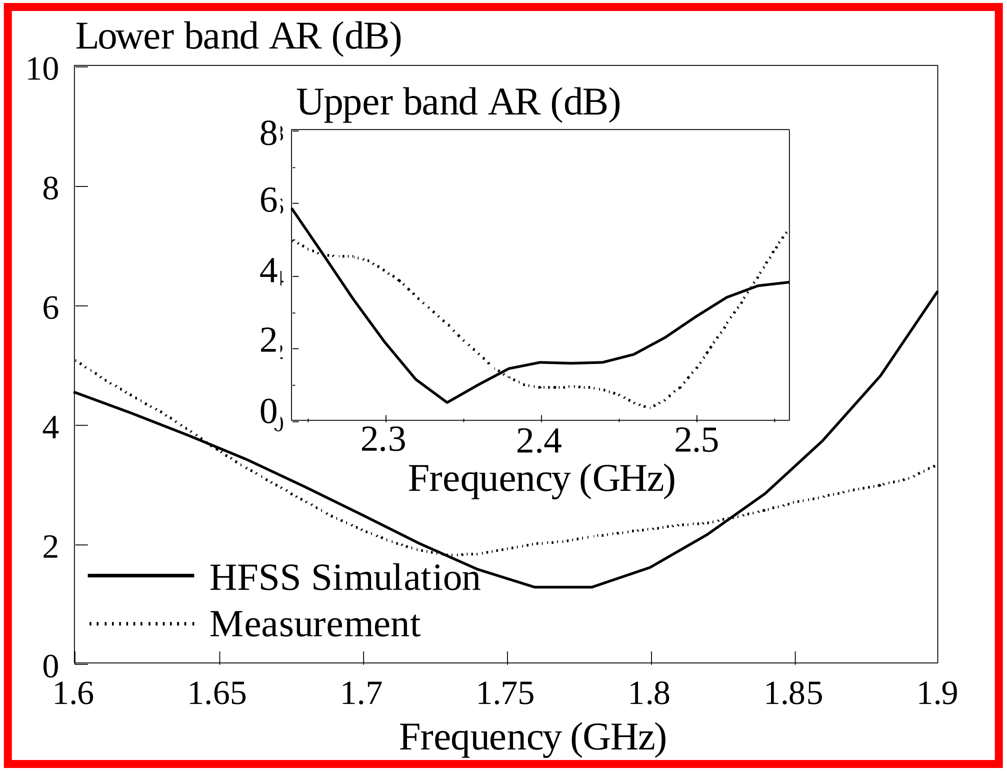

- Reasonable agreement
- Lower band AR bandwidth: 12.4% (1.67-1.89 GHz)
- Upper band AR bandwidth: 7.4% (2.34-2.52GHz)

Measured and simulated radiation patterns

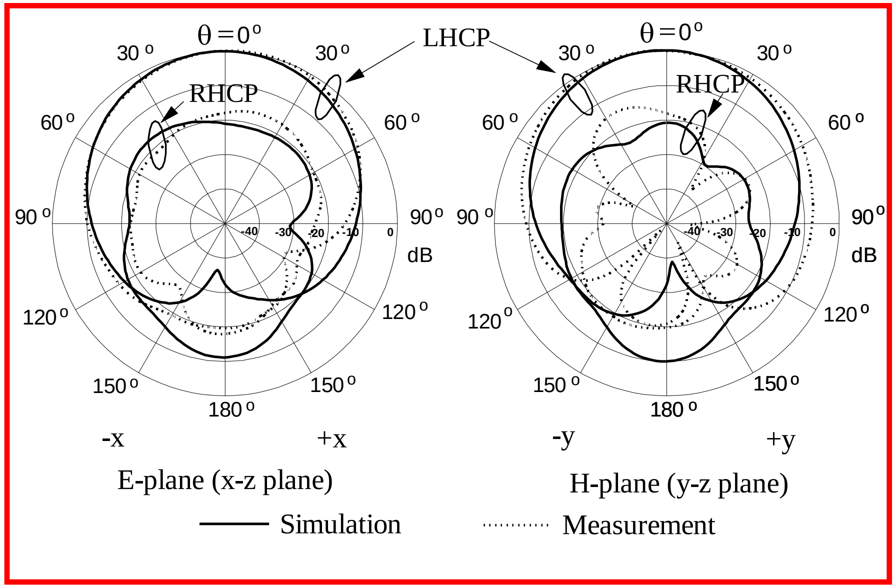

(a)

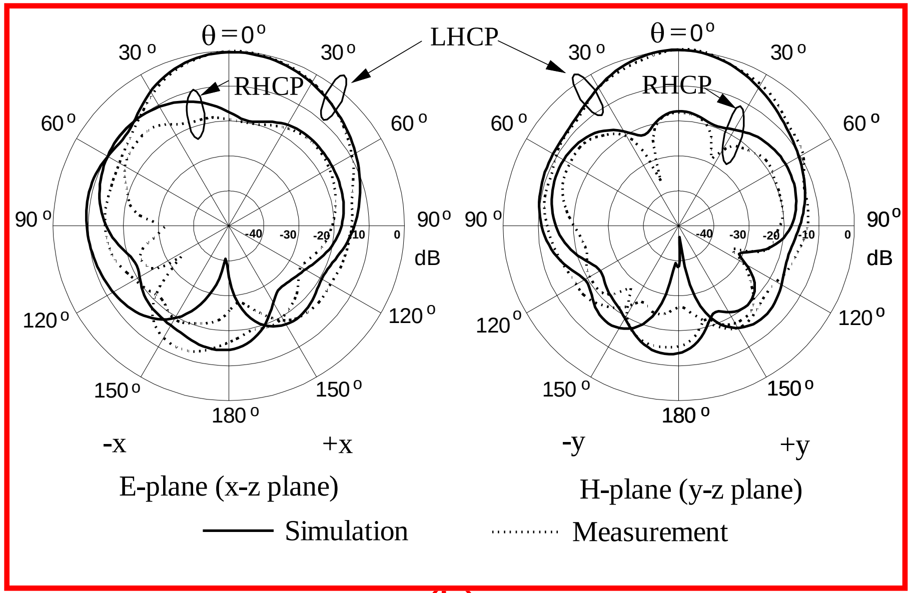

(b)

HEM_{111} mode: measured (1.8 GHz), simulated (1.8 GHz)

HEM_{113} mode: measured (2.42 GHz), simulated (2.45 GHz)

- Broadside radiation patterns are observed.
- LHCP fields > RHCP fields by ~20 dB in the boresight direction.

B. Example for wideband cylidnrical DRA design

Given: f_1 = 2.90 GHz, f_2 = 3.72 GHz, ε_r= 9.4

↓ ← Using formula (5) & (6)

a = 10.3 mm & h = 34.3 mm

Wideband LP cylindrical DRA

Configuration

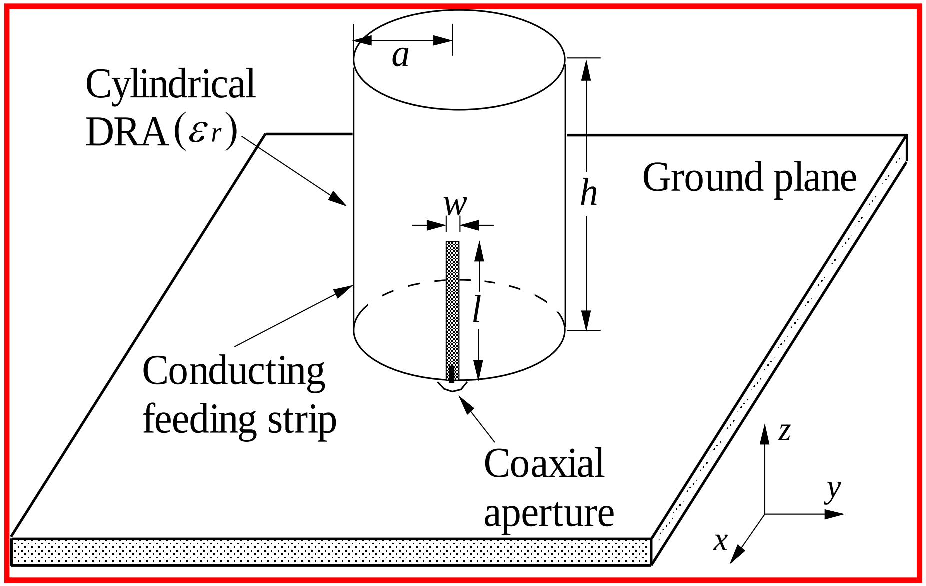

a = 10.3 mm, h = 34.3 mm, ε_r = 9.4, l = 12 mm, and w = 1 mm.

Reflection coefficient

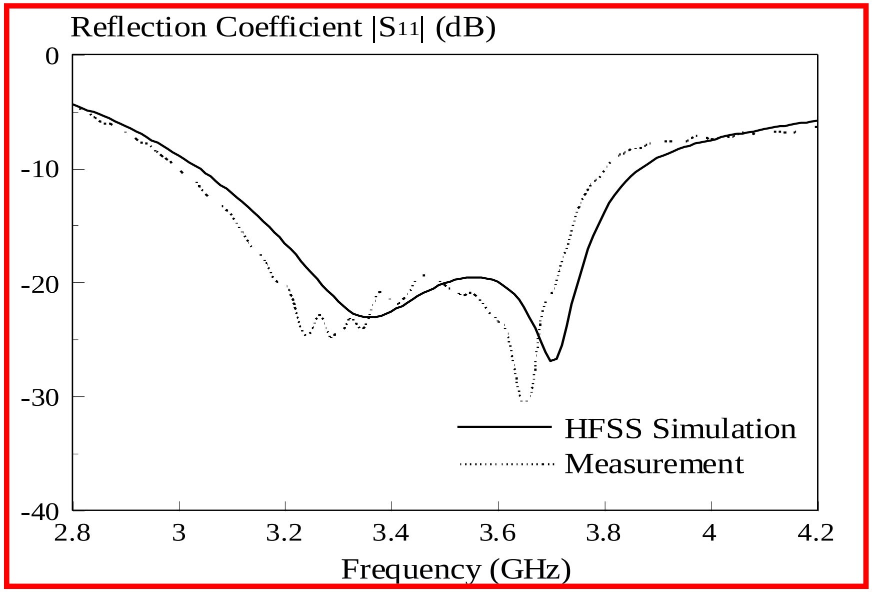

Good agreement

Measured impedance bandwidth: 23.5% (3-3.8 GHz)

Measured and simulated gain

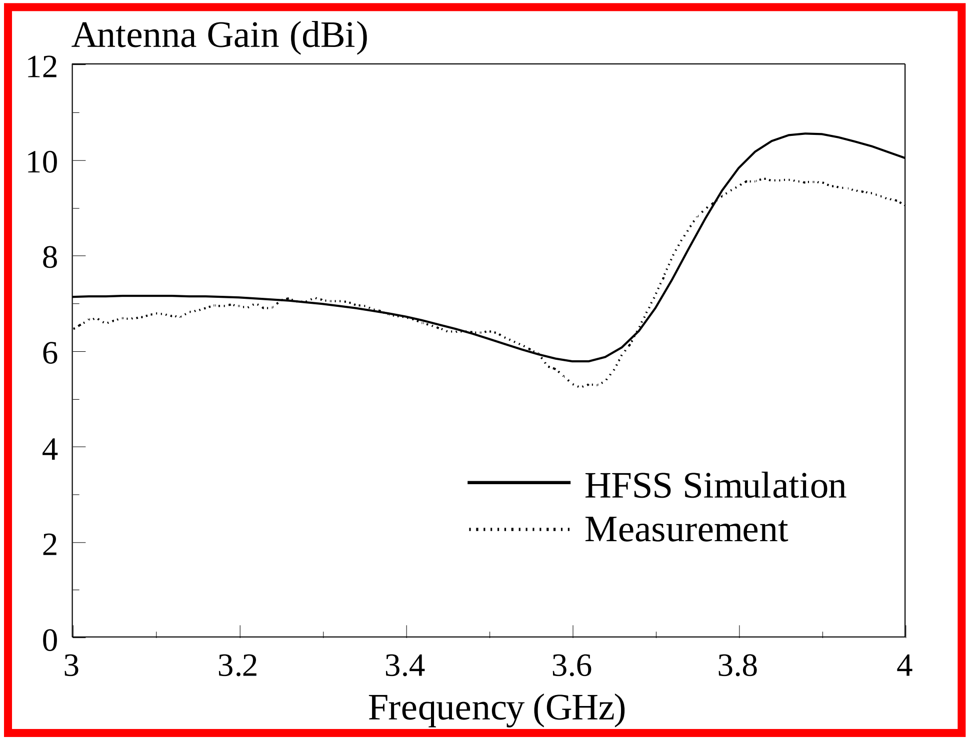

- HEM_{111} mode: Maximum measured gain of ~7 dBi (3.29 GHz)
- HEM_{113} mode: Maximum measured gain of ~10 dBi (3.83 GHz)

Wideband CP cylindrical DRA

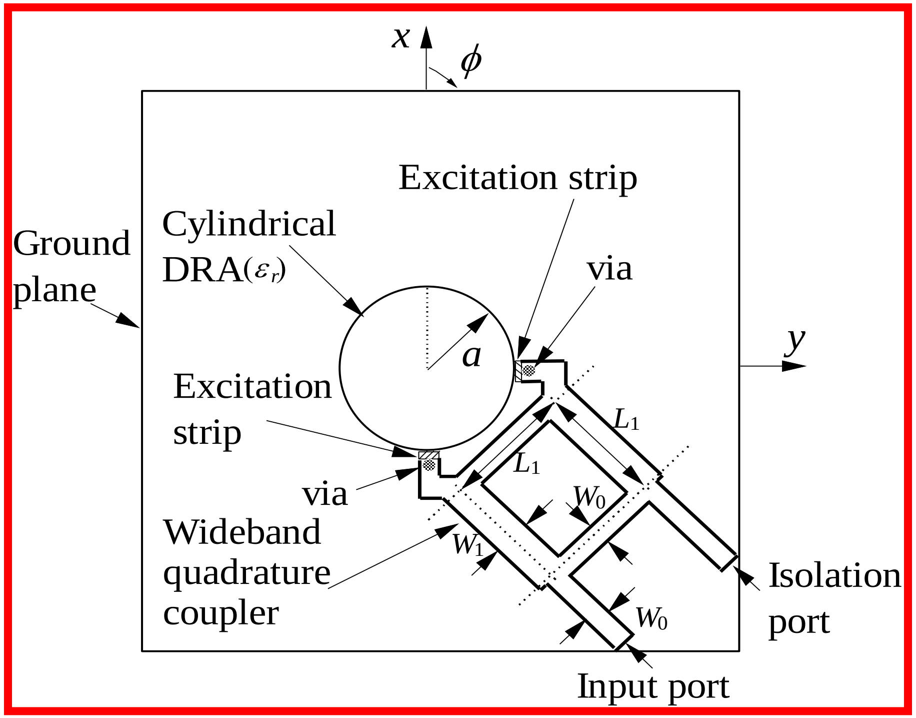

Top view

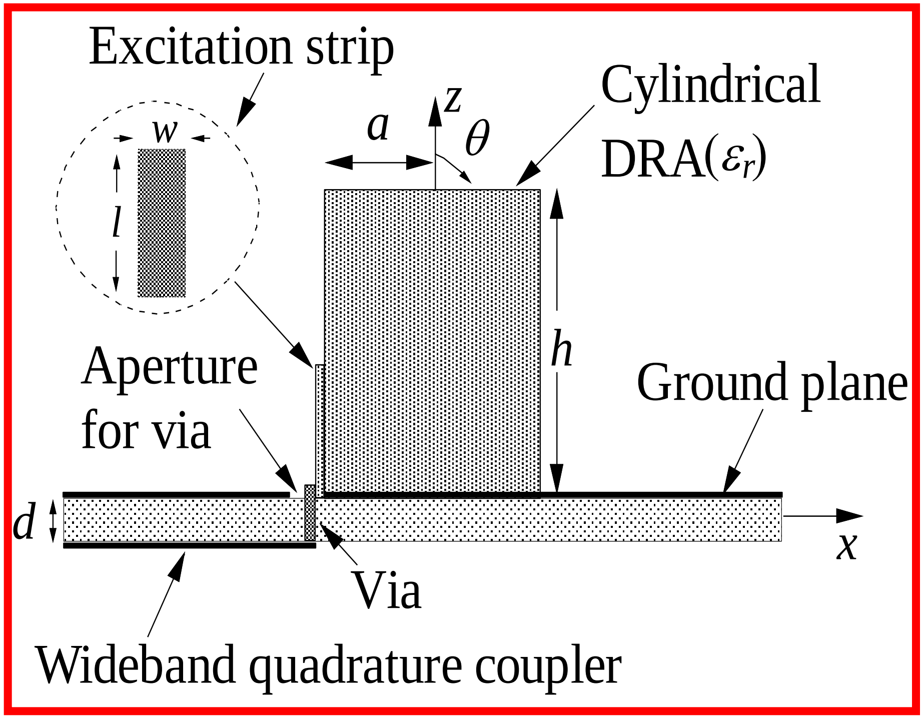

Side view

a = 10.3 mm, h = 34.3 mm, ε_r = 9.4, l = 11.5 mm, w = 1 mm, L_1 = 14.67 mm, W_0 = 1.94 mm, and W_1 = 3.21 mm.

Wideband CP DRA

Reflection coefficient

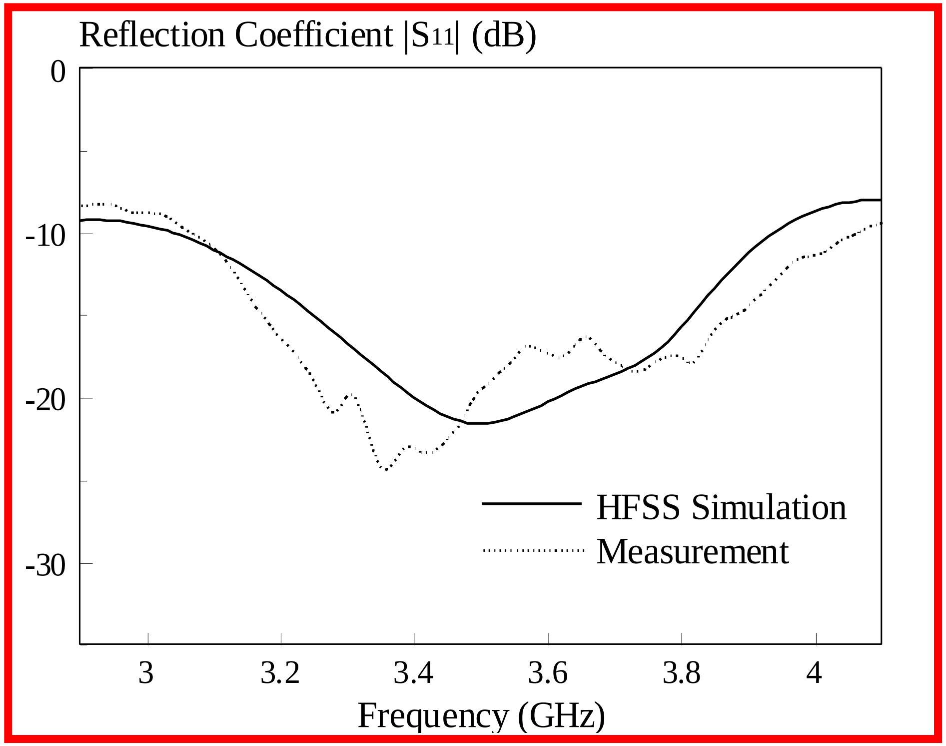

Axial ratio

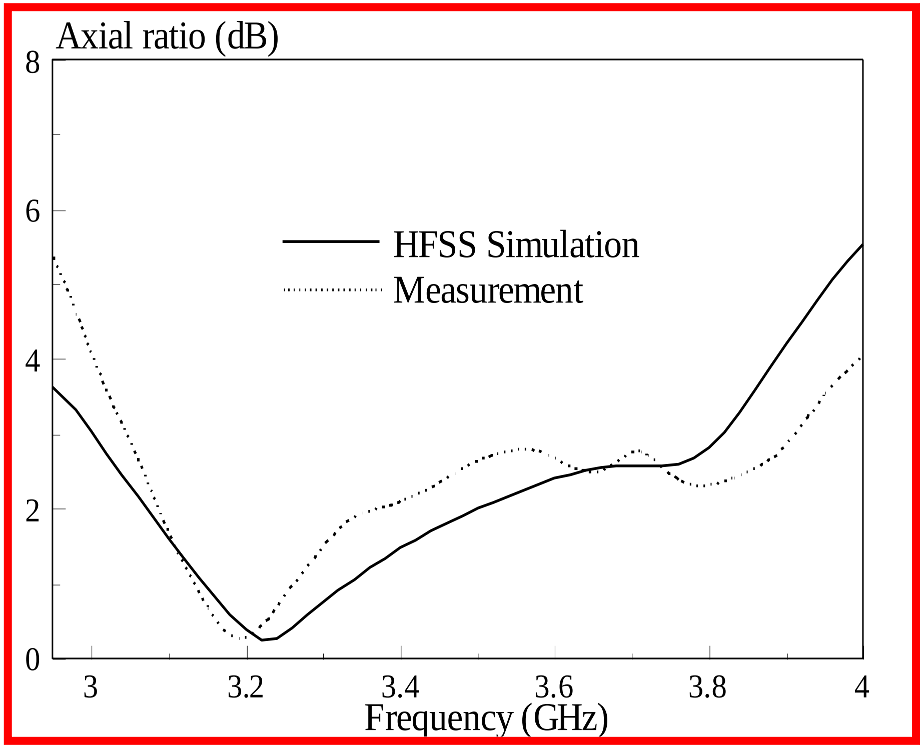

Measured impedance bandwidth: 25.5% (3.04-3.93 GHz).

Measured 3-dB AR bandwidth : 24.7% (3.05-3.91 GHz).

VI. Dualfunction DRAs

Advantage

System size and cost can be reduced by using dualfunction DRAs.

Additional functions

- Packaging cover
- Oscillator

Packaging Cover

Conventional

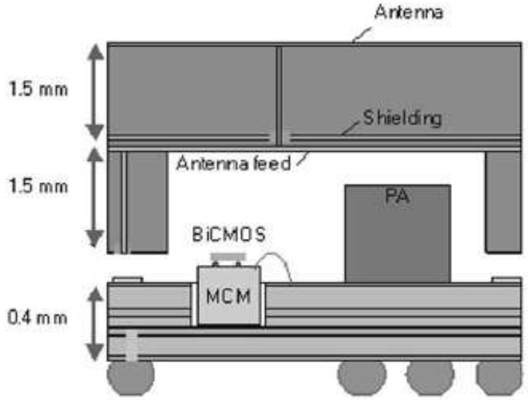

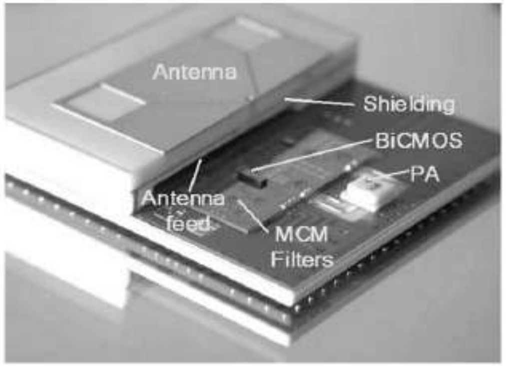

Proposal

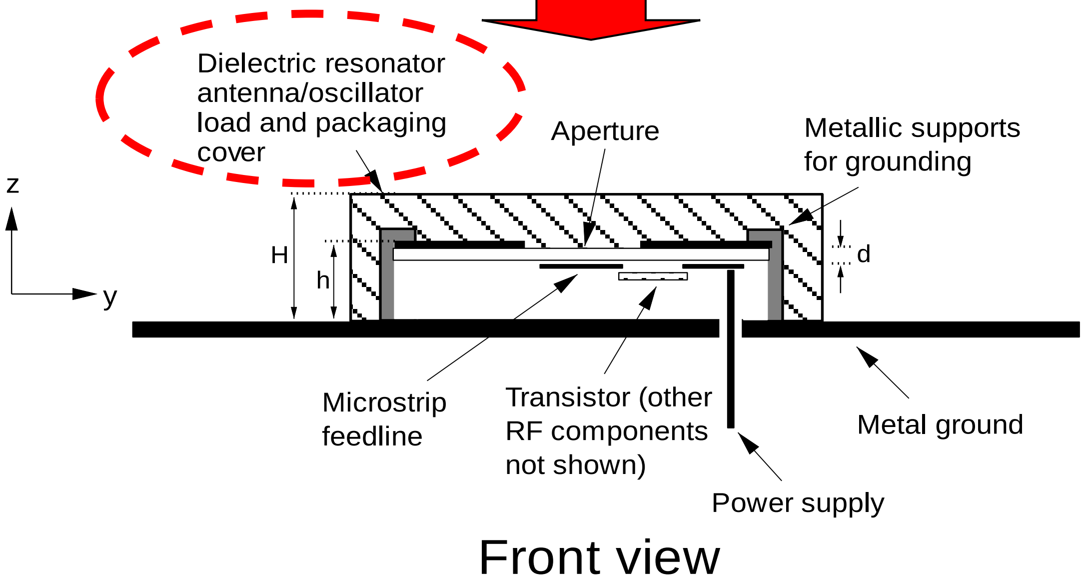

Antenna Configuration

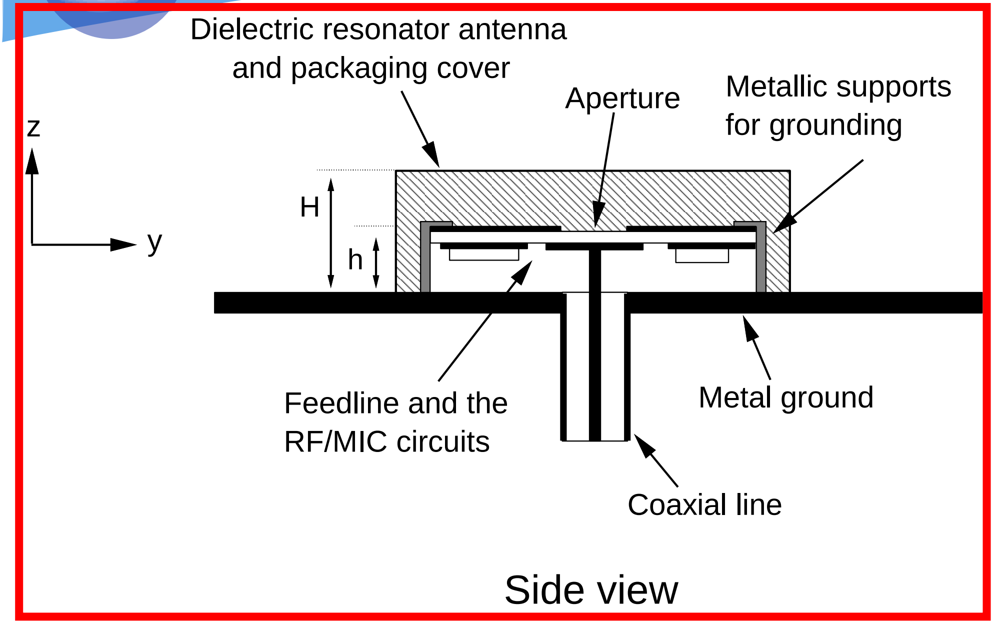

Side view

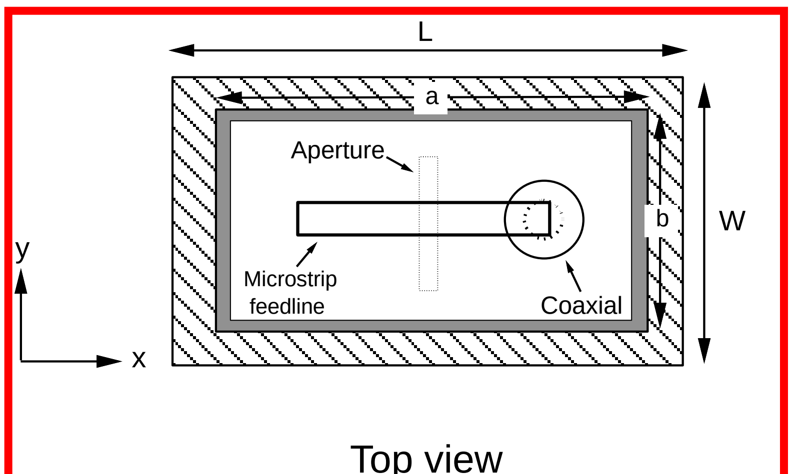

Top view

Resonant frequency

$f_0 = 2.4\text{GHz}$

Parameters:

- Hollow DRA:
  L=30mm, W=29mm,
  H=15mm, & ε_r =12
- Metallic Cavity:
  a = 15mm, b = 21.6mm, h = 5mm
  Top face : Duroid ε_r =2.94
  thickness 0.762mm
  Aperture: 0.2063 λ_e

Design Procedure (Simulation):

Step 1

Use the DWM to design a solid rectangular DRA at 2.4-GHz fundamental TE$_{111}$ Mode.

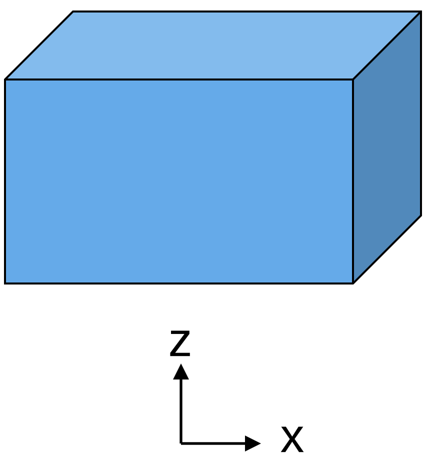

Step 2

Remove the lower center portion concentrically to form a notched DRA.
As a result, the resonant frequency >2.4GHz

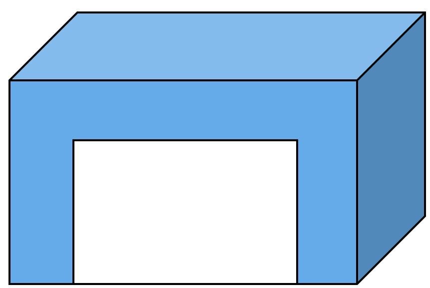

Step 3

Cover the two sides with the same material. Move the frequency back to 2.4GHz by increasing the thickness.
(thickness ↑ → f_0 ↓)

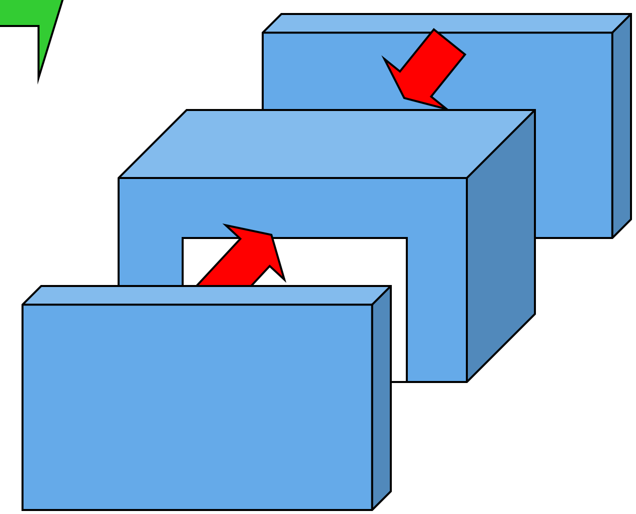

Experimental Verification:

- Hard-clad foam ($\varepsilon_r \approx 1$) is used to form the container.

- ECCOSTOCK HiK Powder of $\varepsilon_r = 12$ is used as the dielectric material.

Return Loss and Input Impedance (Passive hollow RDRA with a metallic cavity)

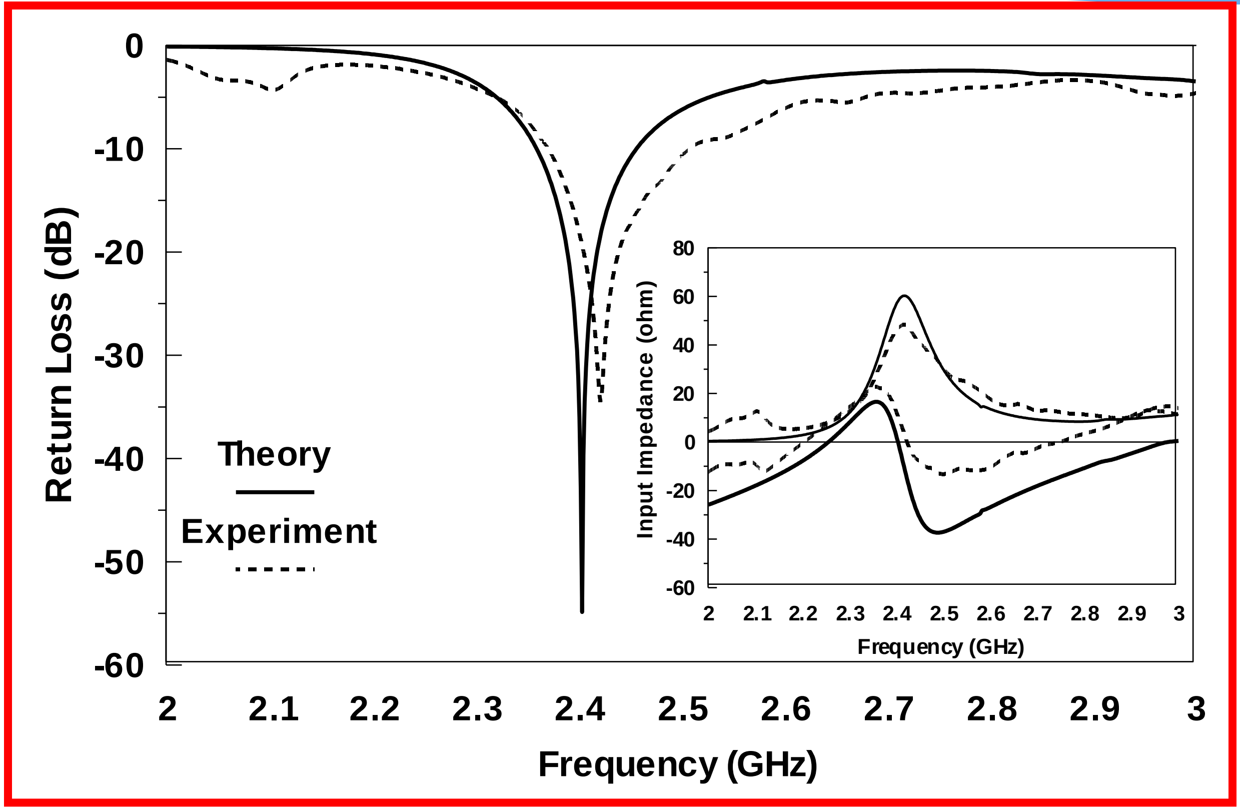

•Good agreement.

•Bandwidth ~ 5.6%.

• Measured resonance frequency: 2.42GHz (error < 0.83%)

Radiation Patterns
(Passive hollow DRA with a metallic cavity)

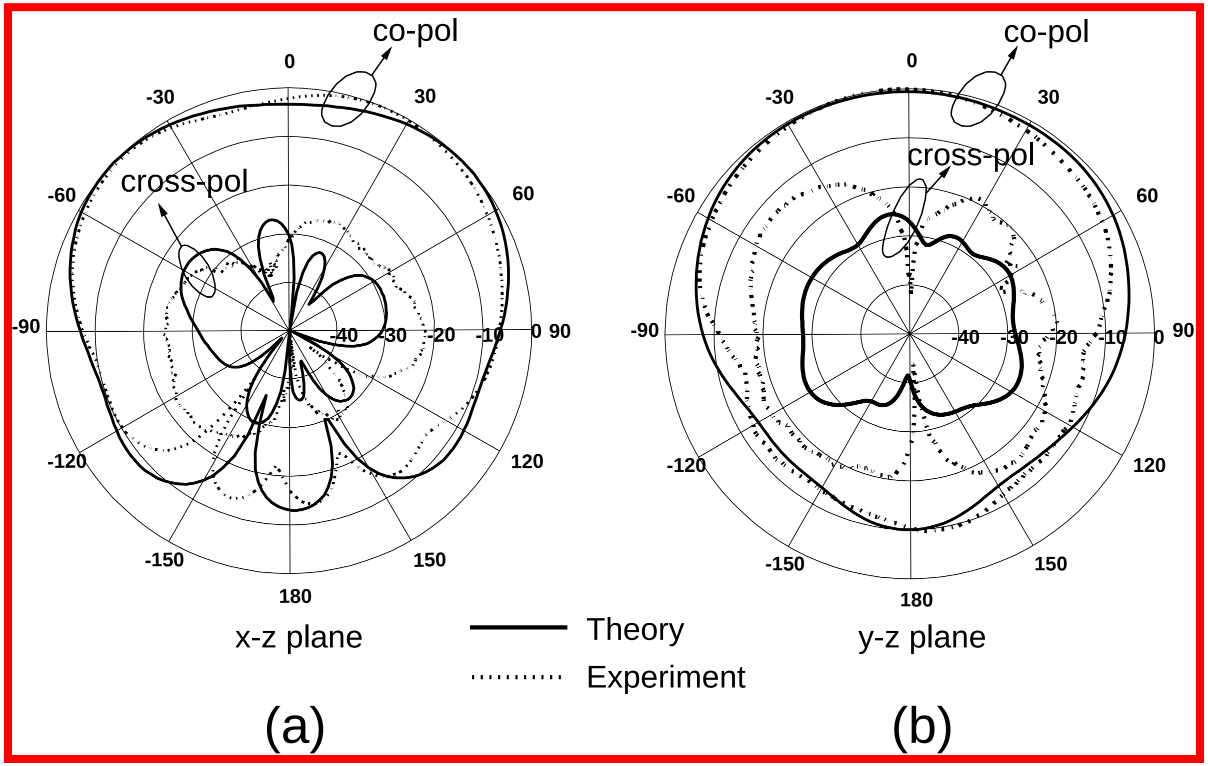

- Broadside TE_{111}^{y} mode is observed.
- Co-polarized fields generally stronger than the cross-polarized fields by 20dB in the boresight direction.

Return Loss of the Active Integrated Antenna

- Integrated with Agilent AG302-86 low noise amplifier (LNA) (gain of 13.6dB at 2.4GHz)
- LNA prematched to 50Ω at the input.
- A small hole is drilled on the ground plane to supply the DC bias to the LNA.

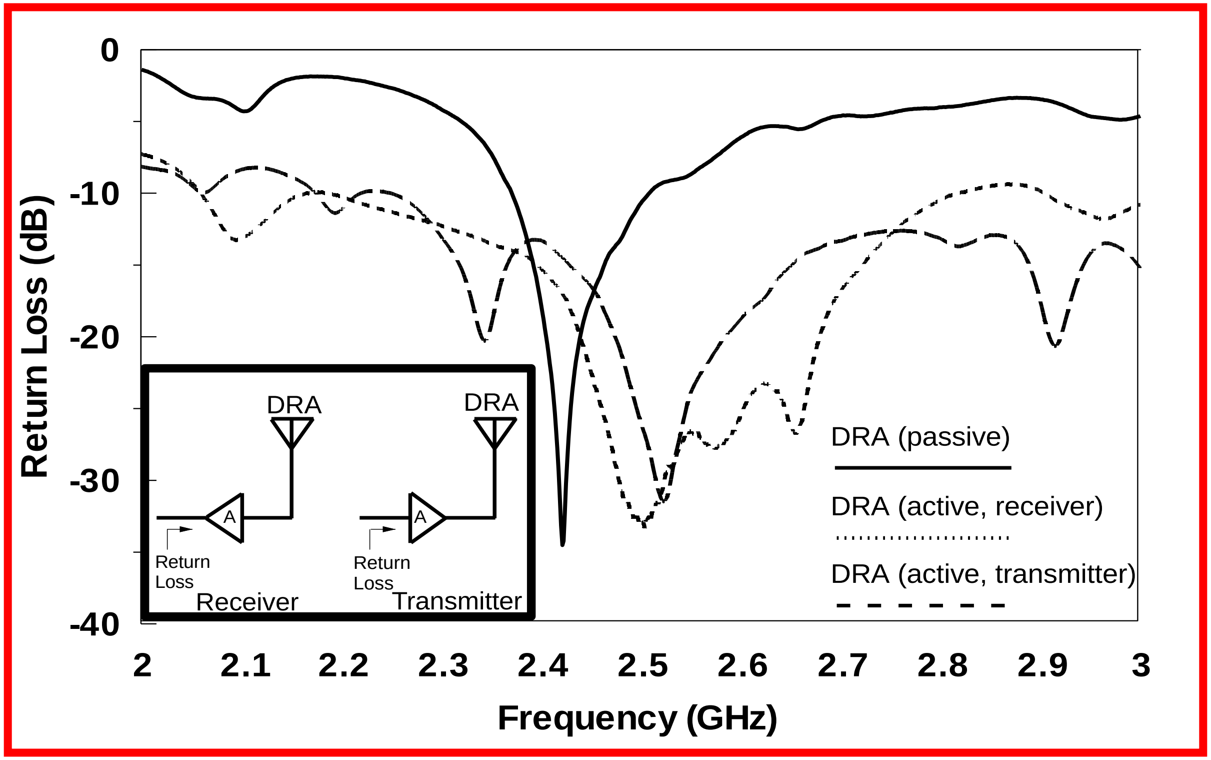

Amplified Radiation Pattern

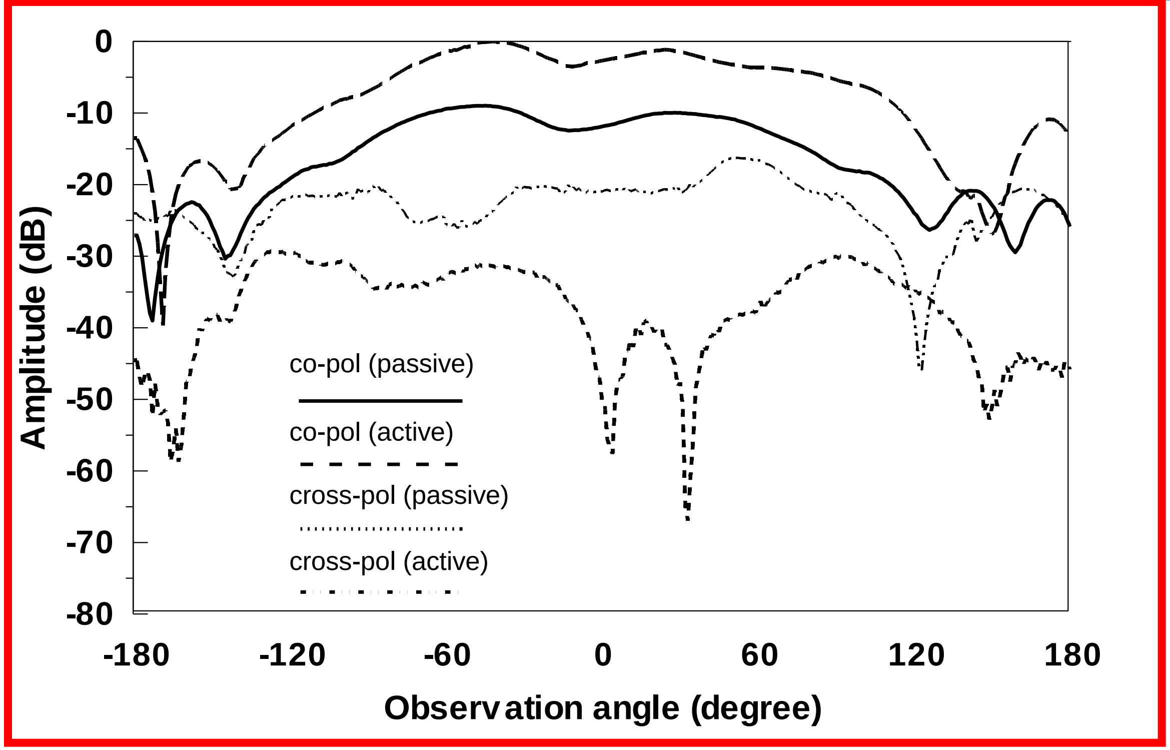

- Compared to the passive DRA, the active DRA has a gain of 7 - 12dB across the observation angle from -90° to 90°.
- The gain is less than the specification due to unavoidable impedance variations and imperfections in the measurement.

Dielectric Resonator Antenna Oscillator (DRAO)

Methodology

- The DRA is used as the oscillator load, named as DRAO.
- The reflection amplifier method is used to design the antenna oscillator.

DRAO Schematic Diagram

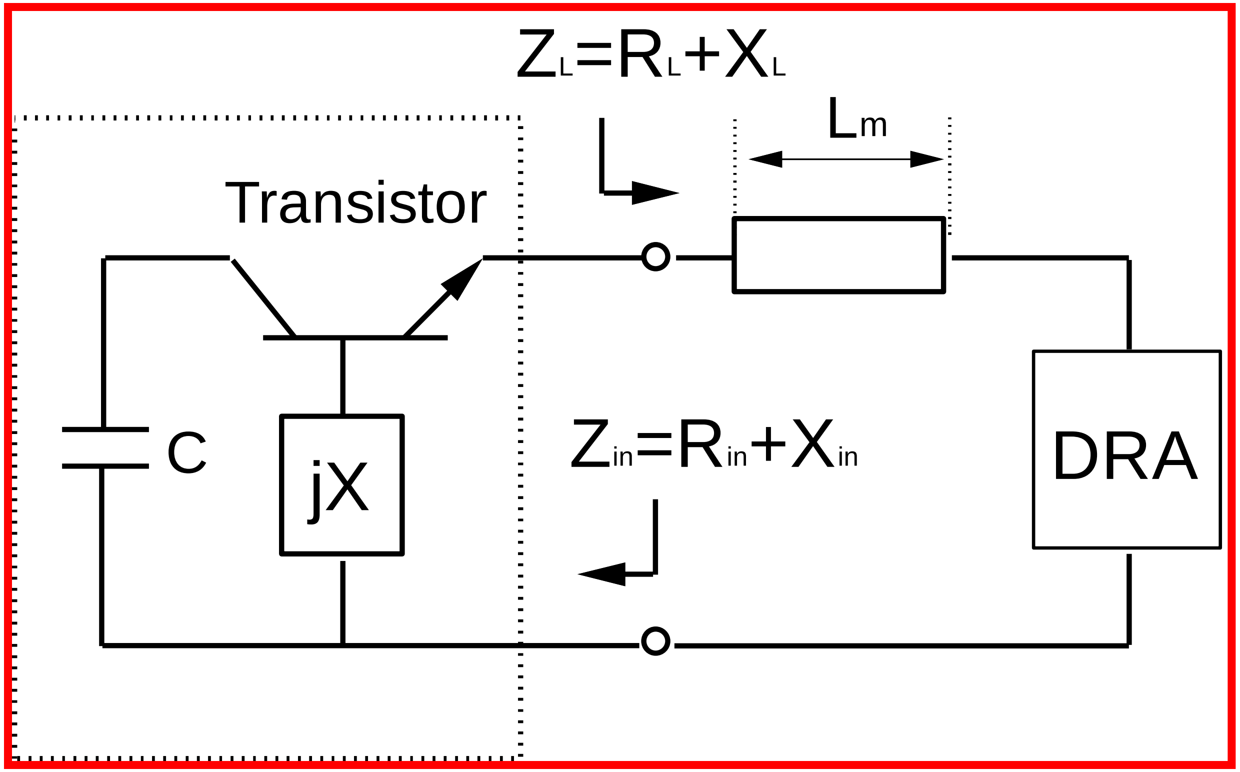

- Oscillate condition: $X_L+X_{in}=0$ & $R_L<|R_{in}|$
- DRA first replaced by a 50Ω load at 1.85GHz.

Antenna Configuration:

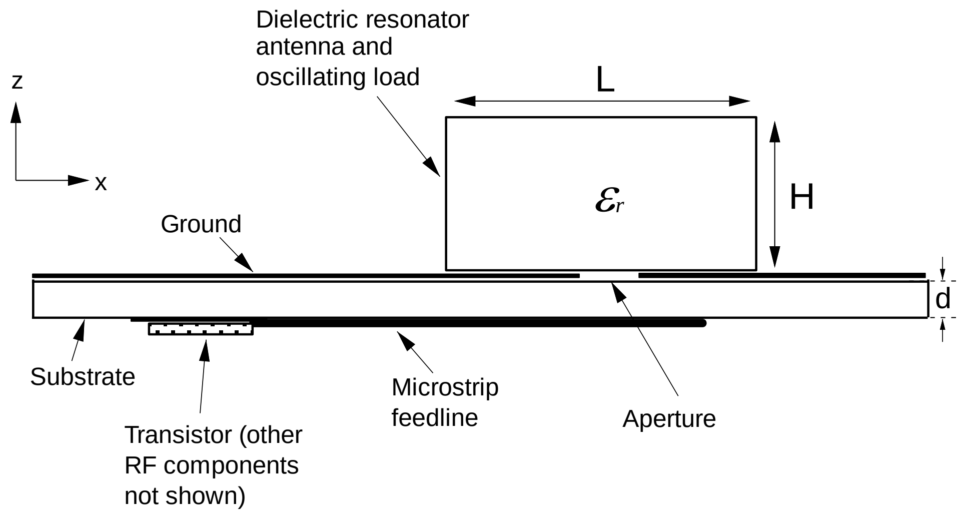

Side view

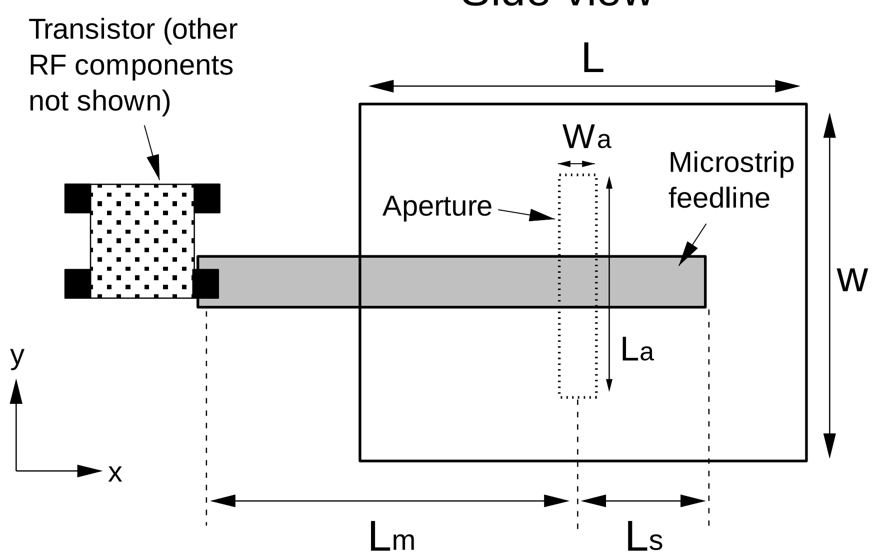

Top view

Resonance frequency

f_o = 1.85GHz at TE_{111}^{y}

Parameters:

DRA

L=52.2mm,

W=42.4mm,

H=26.1mm,

ε_r = 6.

Aperture

$L_a = 0.3561\lambda_e$, W_a = 2mm

L_s = 9.5 mm, L_m = 40 mm.

Duroid substrate

ε_{rs}=2.94, d=0.762mm

Return Loss and Input Impedance

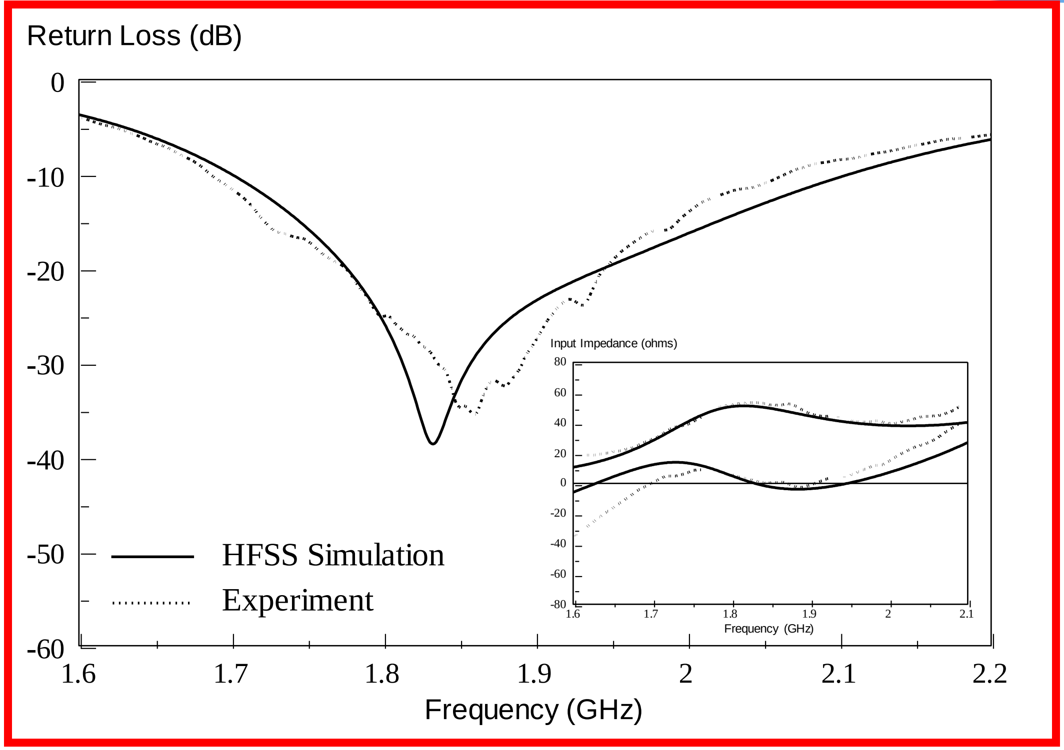

- Good agreement.
- Bandwidth ~ 22.14%.
- Resonance frequency: Measured 1.86GHz
  Simulated 1.83GHz (1.5% error).

Spectrum of the Free-running DRAO

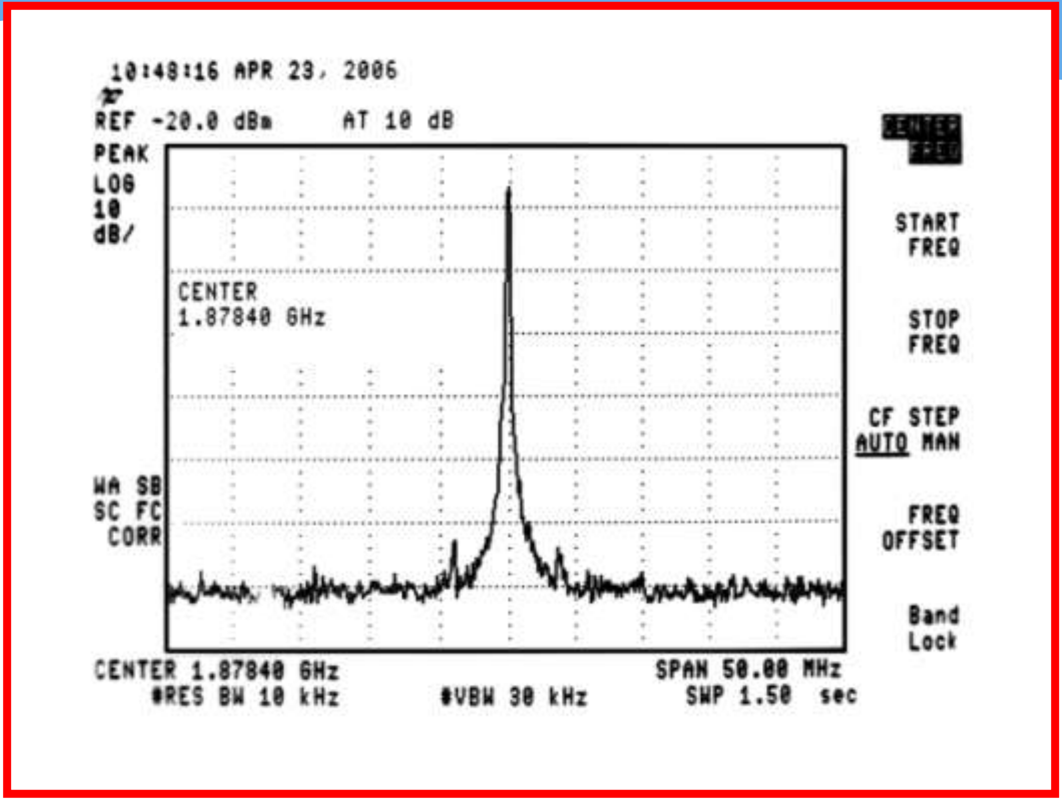

- Transmitting power P_t = 16.4dBm
- DC-RF efficiency: ~ 13% (2-25% in the literature).
- Phase noise: 103dBc/Hz at 5MHz offset
- Second harmonic < fundamental by 22dB

Radiation Pattern

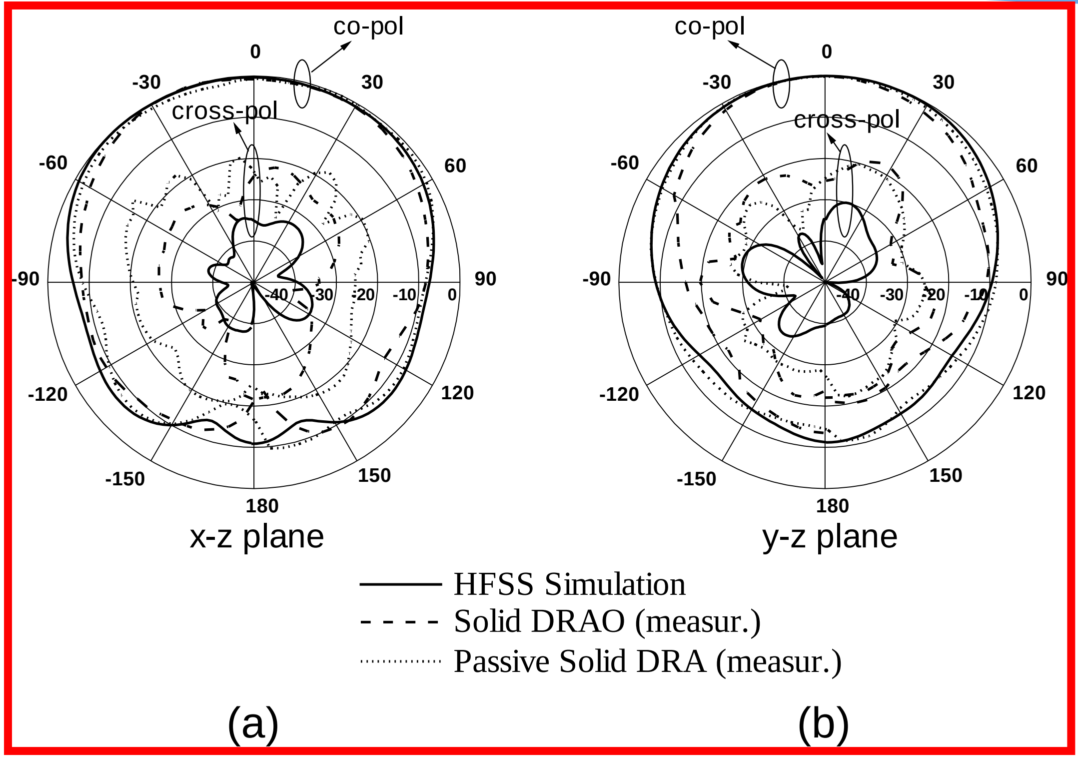

- Broadside TE_{111}^{y} is observed.
- Co-polarized fields are generally 20dB stronger than the cross-polarized fields in the boresight direction.

DRA can be of any shape. Can it be made like a swan?

Yes!

DRA is simple made of dielectric. Can glass be used for the dielectric?

Yes!

It leads to probably the most beautiful antenna in the world …….

Glass-Swan DRA

Distinguished Lecture

Transparent antennas: From 2D to 3D

Conclusion

- The DRA can be easily excited with various excitation schemes.

- Frequency tuning of the DRA can be achieved by using a loading-disk or parasitic slot.

- The dualband and wideband DRAs can be easily designed using higher-order modes.

- Compact omnidirectional CP DRAs have been presented

- Dualfuncton DRAs for packaging and oscillator designs have been demonstrated.

Thank you !

Q & A